https://www.mdc-berlin.de/de/veroeffentlichungstypen/clinical-journal-club

Als gemeinsame Einrichtung von MDC und Charité fördert das Experimental and Clinical Research Center die Zusammenarbeit zwischen Grundlagenwissenschaftlern und klinischen Forschern. Hier werden neue Ansätze für Diagnose, Prävention und Therapie von Herz-Kreislauf- und Stoffwechselerkrankungen, Krebs sowie neurologischen Erkrankungen entwickelt und zeitnah am Patienten eingesetzt. Sie sind eingeladen, um uns beizutreten. Bewerben Sie sich!

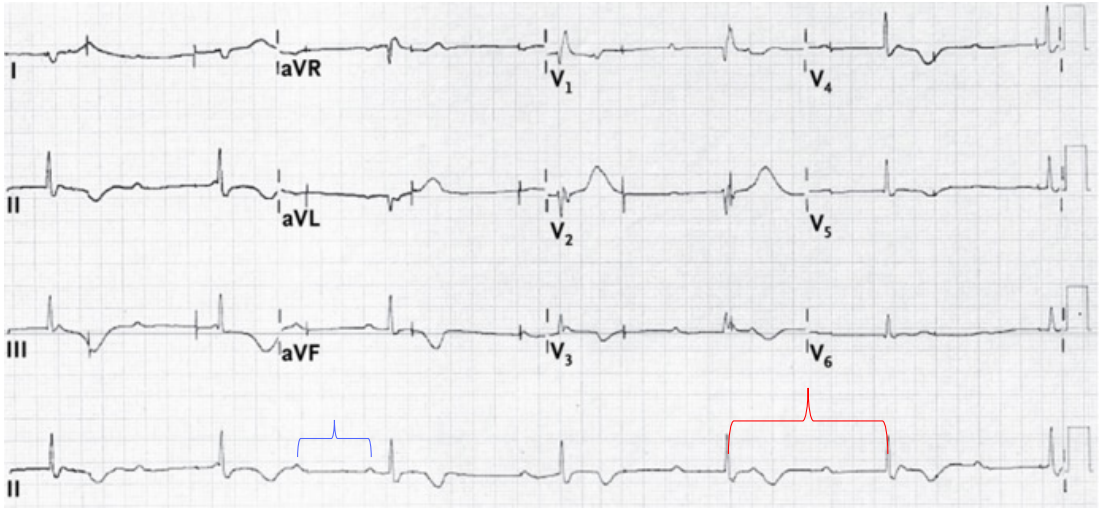

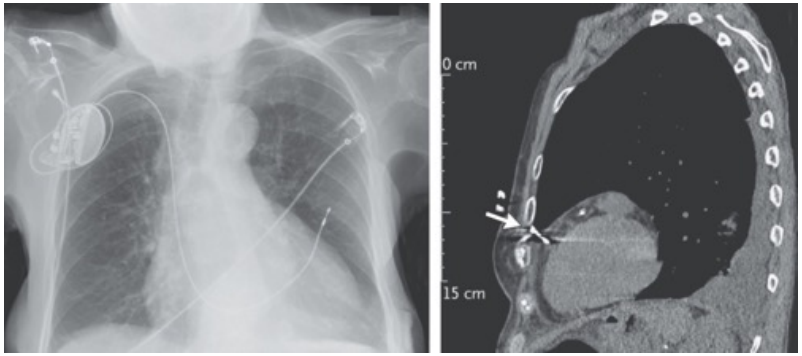

A 96-year-old woman presented to the emergency department with a 1-day history of pleuritic chest pain 4 days after a single-chamber transvenous pacemaker had been implanted. A chest radiograph and computed tomographic scan of the chest showed the tip of the right ventricular lead in the left pleural space. What rhythm does the electrocardiogram show?

Atrial fibrillation
Complete heart block ←
Second degree heart block
Ventricular-paced rhythm
Wandering atrial pacemaker

The electrocardiogram showed complete heart block with an atrial rate of 84 beats per minute, a junctional escape with a right bundle-branch block and a rate of 42 beats per minute, and pacing spikes without ventricular capture. A diagnosis of pacemaker-lead dislodgement with cardiac perforation was made. A percutaneous lead revision was performed urgently and the patient was discharged home 3 days after presentation.

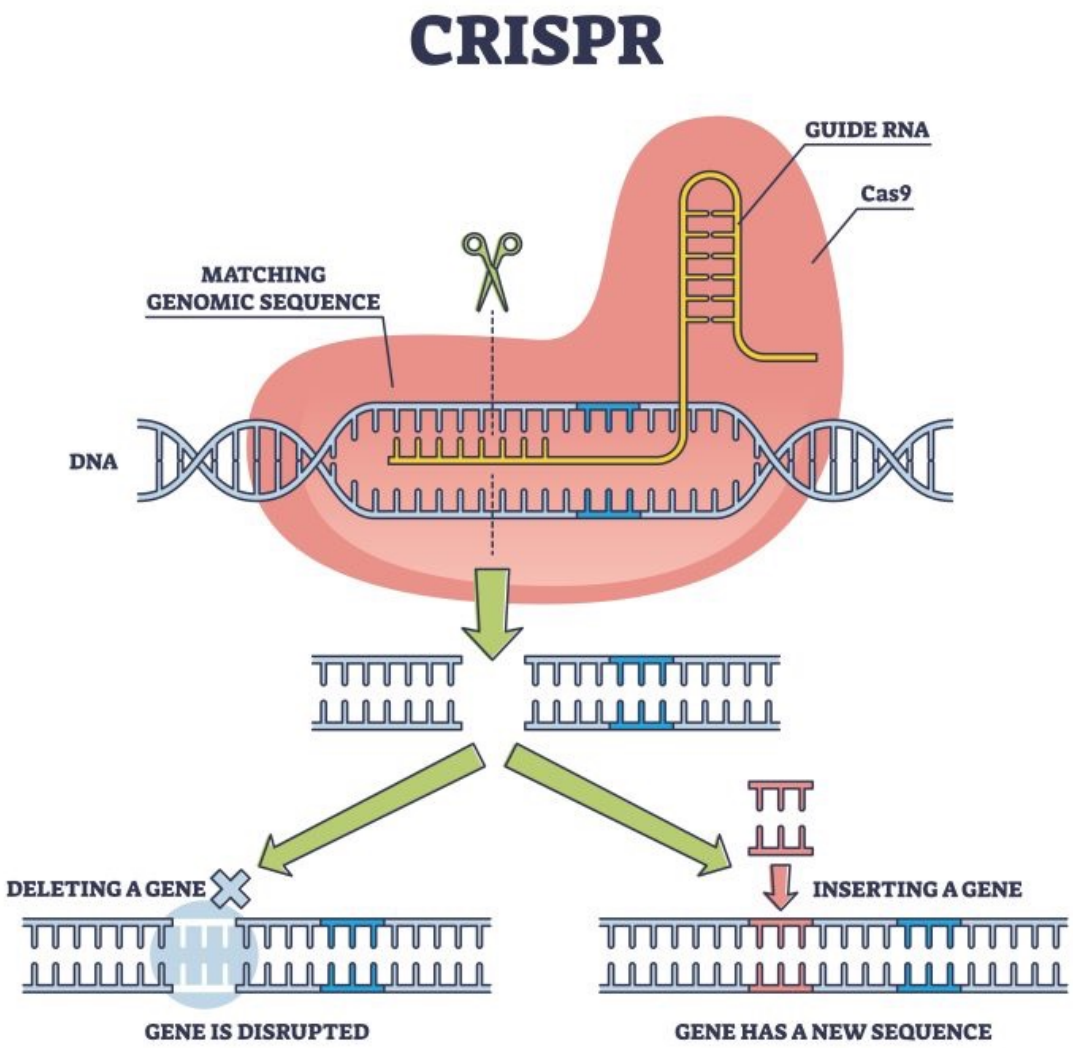

CRISPR gene editing standing for "Clustered Regularly Interspaced Short Palindromic Repeats" is a genetic engineering technique in molecular biology by which the genomes of living organisms may be modified. It is based on a simplified version of the bacterial CRISPR-Cas9 antiviral defense system. By delivering the Cas9 nuclease complexed with a synthetic guide RNA (gRNA) into a cell, the cell's genome can be cut at a desired location, allowing existing genes to be removed and/or new ones added.

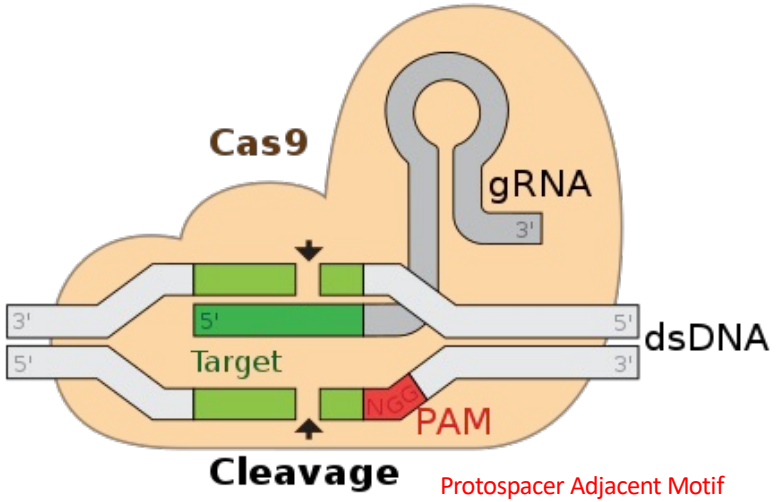

Protospacer Adjacent Motif

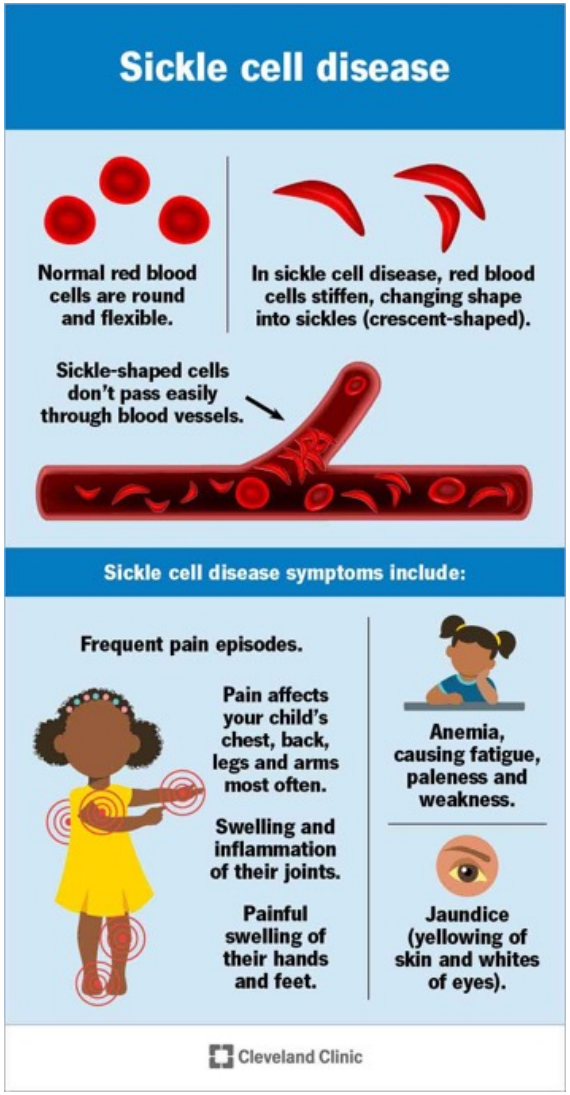
Sickle cell disease
Normal red blood cells are round and flexible.
In sickle cell disease, red blood cells stiffen, changing shape into sickles (crescent-shaped).
Sickle-shaped cells don't pass easily through blood vessels.
Sickle cell disease symptoms include:
Frequent pain episodes.
Pain affects your child's chest, back, legs and arms most often.
Swelling and inflammation of their joints.
Painful swelling of their hands and feet.
Anemia, causing fatigue, paleness and weakness.
Jaundice (yellowing of skin and whites of eyes).
Cleveland Clinic

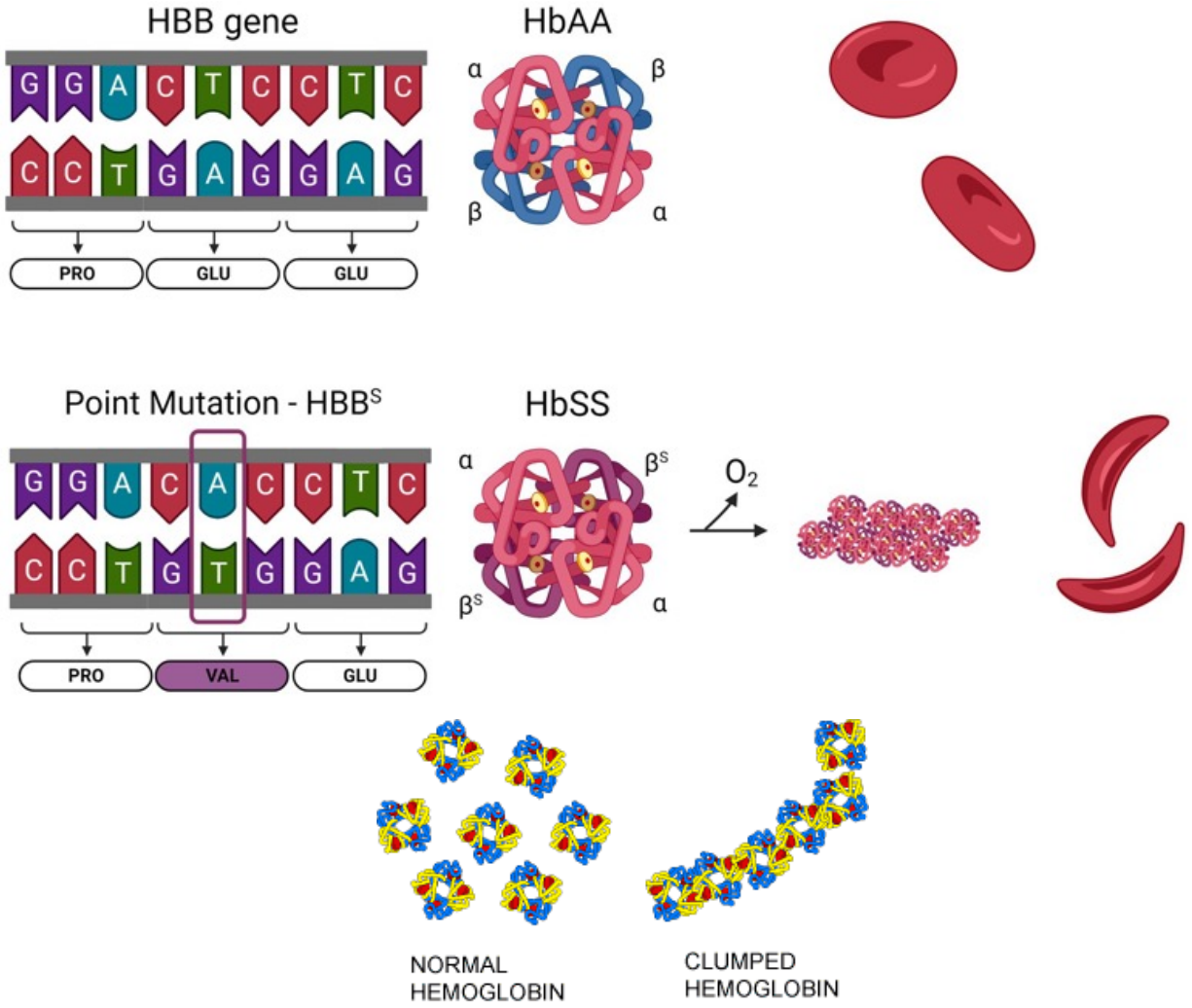
HBB gene
G G A C T C C T C
C C T G A G G A G
PRO GLU GLU
HbAA
α β β α
Point Mutation - HBB^S
G G A C A C C T C
C C T G T G G A G
PRO VAL GLU
HbSS
α β^S β^S α
O_2
NORMAL HEMOGLOBIN
CLUMPED HEMOGLOBIN

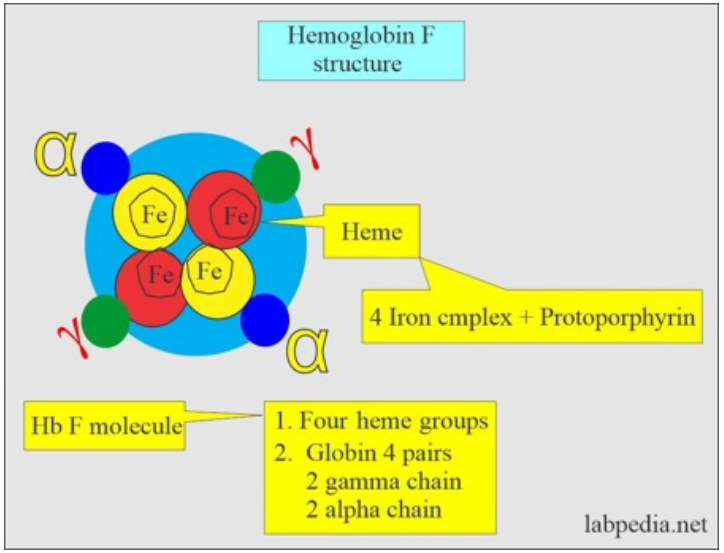

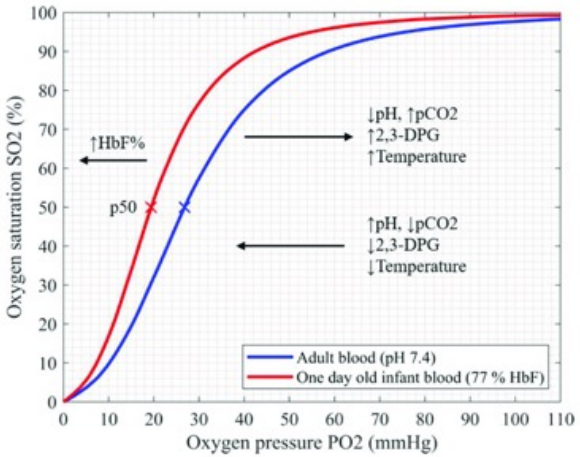

BCL11A ist ein Transkriptionsfaktor, der die Expression von Gamma-Globin, einem Bestandteil des fetalen Hämoglobins, hemmt. Die Bildung von fetalem Hämoglobin hört normalerweise nach der Geburt auf. Durch die Abschaltung von BCL11A soll es reaktiviert werden.

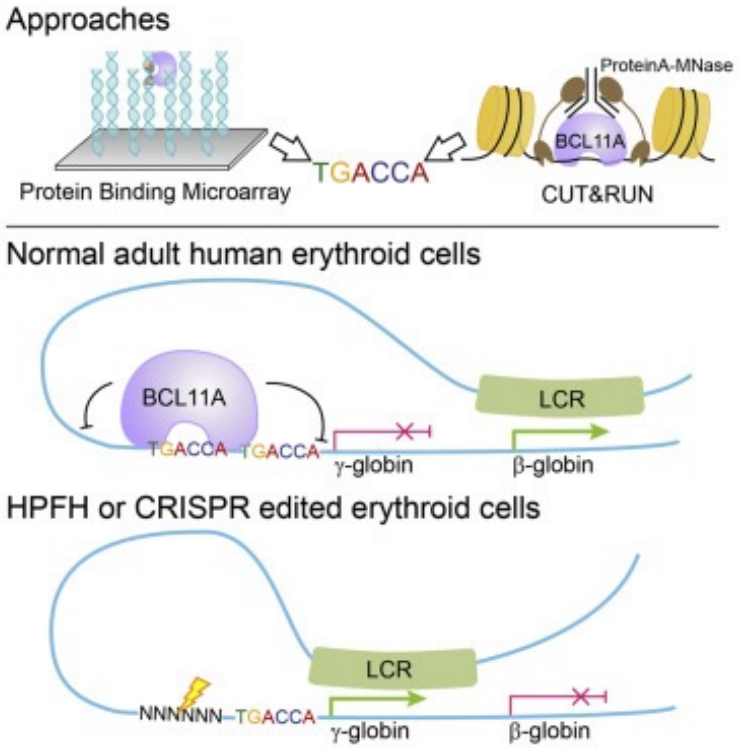

Exagamglogene Autotemcel for Severe Sickle Cell Disease

Exagamglogene autotemcel (exa-cel) is a nonviral cell therapy designed to reactivate fetal hemoglobin synthesis by means of ex vivo clustered regularly interspaced short palindromic repeats (CRISPR)–Cas9 gene editing of autologous CD34+ hematopoietic stem and progenitor cells (HSPCs) at the erythroid-specific enhancer region of *BCL11A*. We conducted a phase 3, single-group, open-label study of exa-cel in patients 12 to 35 years of age with sickle cell disease who had had at least two severe vaso-occlusive crises in each of the 2 years before screening. CD34+ HSPCs were edited with the use of CRISPR-Cas9. Before the exa-cel infusion, patients underwent myeloablative conditioning with pharmacokinetically dose-adjusted busulfan. The primary end point was freedom from severe vaso-occlusive crises for at least 12 consecutive months. A key secondary end point was freedom from inpatient hospitalization for severe vaso-occlusive crises for at least 12 consecutive months. The safety of exa-cel was also assessed.

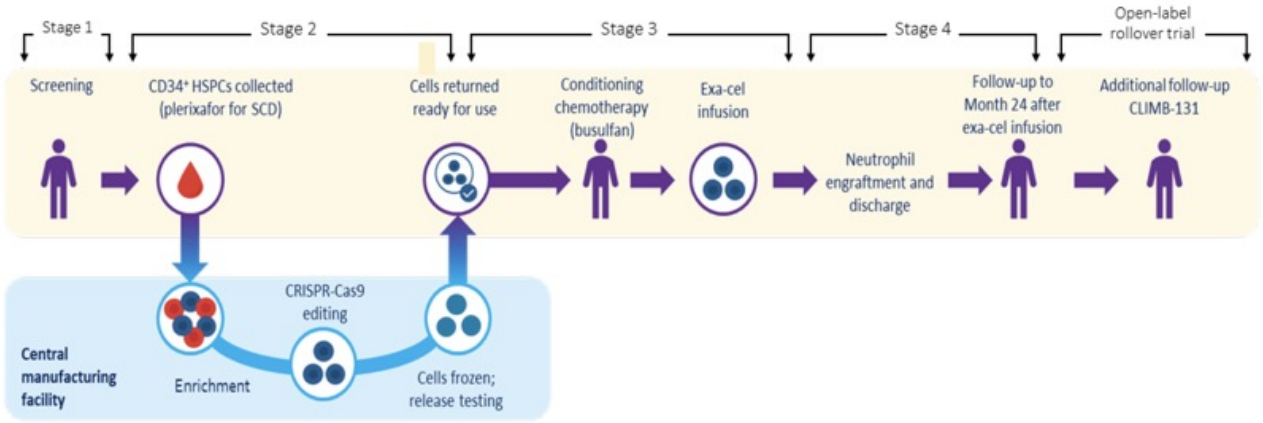

CRISPR-Cas9, clustered regularly interspaced short palindromic repeats-associated 9 nuclease; **exa-cel,** exagamglogene autotemcel; **HSPC,** hematopoietic stem and progenitor cell; **M24,** month 24.

Methods

Patients, Study Design, and Oversight

We are conducting this ongoing phase 3, open-label, single-dose, 2-year study of exa-cel (CLIMB SCD-121) at 16 sites in Belgium, Canada, France, Germany, Italy, the United Kingdom, and the United States. Patients 12 to 35 years of age with a confirmed diagnosis of severe sickle cell disease and a history of at least two vaso-occlusive episodes per year during the 2 years before screening were eligible.

Autologous CD34+ HSPCs were obtained after plerixafor mobilization of HSPCs, followed by apheresis for up to 3 consecutive days for each episode in which the cells were obtained. Exa-cel was manufactured from these CD34+ cells with the use of CRISPR-Cas9, with a single-guide RNA molecule selectively targeting the *BCL11A* erythroid-specific enhancer.[23] Before the exa-cel infusion, patients received myeloablative conditioning with pharmacokinetically adjusted single-agent busulfan for 4 days.

Exa-cel was administered intravenously through a central venous catheter at least 48 hours, but no more than 7 days, after the completion of the busulfan infusion. Additional details about study eligibility, mobilization of HSPCs, the myeloablative busulfan conditioning regimen, and exa-cel manufacturing are provided.

The study was designed by Vertex Pharmaceuticals and CRISPR Therapeutics in collaboration with the steering committee. Each patient or the patient's legal guardian provided written informed consent, with assent obtained when appropriate. An independent data monitoring committee is reviewing safety data throughout the study.

End-Point Measures

The primary end point was freedom from any severe vaso-occlusive crises for at least 12 consecutive months. A severe vaso-occlusive crisis was defined as an event of acute pain that led to a visit to a medical facility and the administration of pain medications (opioids or intravenous nonsteroidal antiinflammatory drugs) or red-cell transfusion, acute chest syndrome, priapism that lasted for more than 2 hours

Results

Evaluation of Off-Target Editing

Preclinically, the precision of CRISPR-Cas9 gene editing at the *BCL11A* locus was assessed by means of orthogonal off-target evaluation methods. Yen et al. found no evidence of off-target editing in CD34+ HSPCs of eight healthy donors and three donors with sickle cell disease.

Population and Engraftment Characteristics

Enrollment has now been completed, with 63 patients enrolled. The first patient was enrolled on November 27, 2018. As of June 14, 2023, a total of 58 patients had started mobilization, 44 of whom had completed myeloablative busulfan conditioning and received exa-cel (full analysis population). A total of 40 patients (91%) had the β^S/β^S genotype, 3 (7%) had the β^S/β^0 genotype, and 1 (2%) had the β^S/β^+ genotype. Twelve patients (27%) were 12 to 17 years of age

Characteristic	Full Analysis Population (N=44)	Primary Efficacy Population (N=30)
Sex — no. (%)		
Male	24 (55)	16 (53)
Female	20 (45)	14 (47)
Age at screening		
Mean — yr	21.2±6.1	22.1±6.0
Distribution — no. (%)		
12 to <18 yr	12 (27)	6 (20)
18 to 35 yr	32 (73)	24 (80)
Race — no. (%)†		
White	3 (7)	1 (3)
Black	38 (86)	26 (87)
Other	3 (7)	3 (10)
Genotype — no. (%)		
β^S/β^S	40 (91)	29 (97)
Non-β^S/β^S		
β^S/β^0	3 (7)	1 (3)
β^S/β^+	1 (2)	0
Annualized rate of severe vaso-occlusive crises‡		
No. of severe vaso-occlusive crises/yr	4.1±3.0	3.9±2.1
Distribution — no. (%)		
≥3 vaso-occlusive crises/yr	26 (59)	17 (57)
<3 vaso-occlusive crises/yr	18 (41)	13 (43)
Total hemoglobin — g/dl§	9.1±1.6	9.0±1.6
Total fetal hemoglobin — %§	5.4±3.9	5.2±3.8
Median no. of mobilization cycles (range)	2 (1–6)	2 (1–5)
Median exa-cel dose (range) — CD34+ cells/kg	4.0×10^6 (2.9×10^6–14.4×10^6)	4.0×10^6 (2.9×10^6–14.4×10^6)

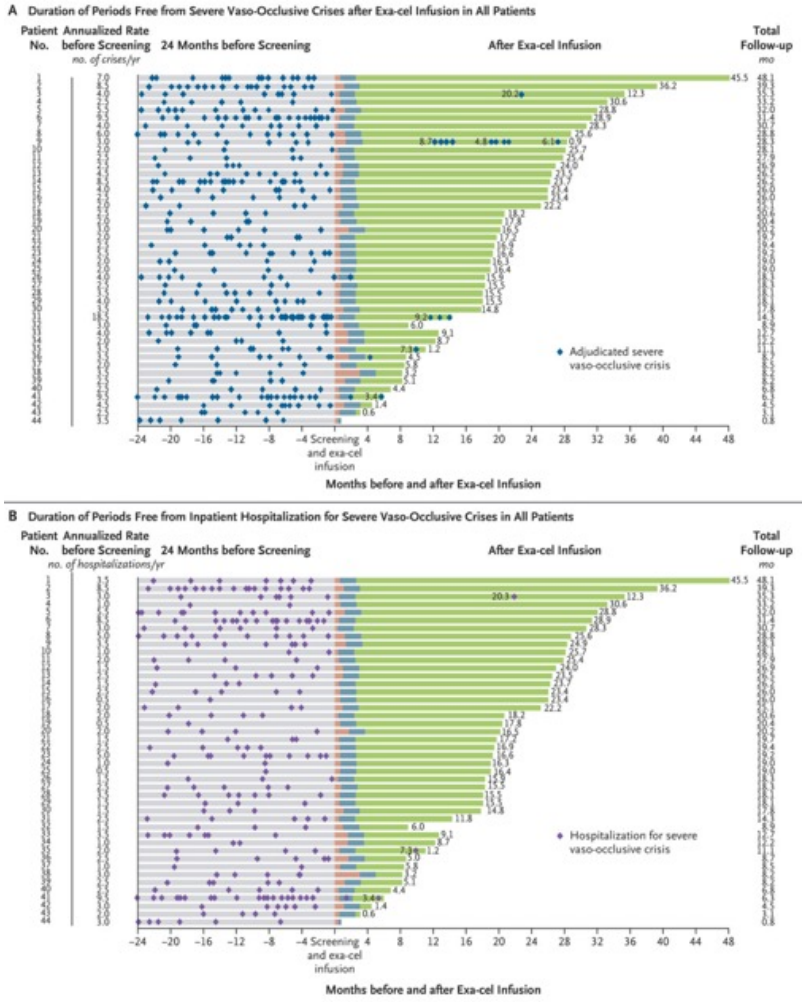

Primary and Key Secondary Efficacy Results in Patients in the Primary Efficacy Population and the Early Efficacy Population.

End Point	Value
Primary end point	
Freedom from severe vaso-occlusive crises for ≥12 mo	
No. of patients who met end-point criteria/total no.	29/30
Percentage of patients (95% CI)	97 (83–100)
P value	<0.001
Key secondary efficacy end points	
Freedom from inpatient hospitalization for severe vaso-occlusive crises for ≥12 mo	
No. of patients who met end-point criteria/total no.	30/30
Percentage of patients (95% CI)	100 (88–100)
P value	<0.001
Freedom from vaso-occlusive crises for ≥9 mo	
No. of patients who met end-point criteria/total no.	31/32
Percentage of patients (95% CI)	97 (84–100)
P value	<0.001

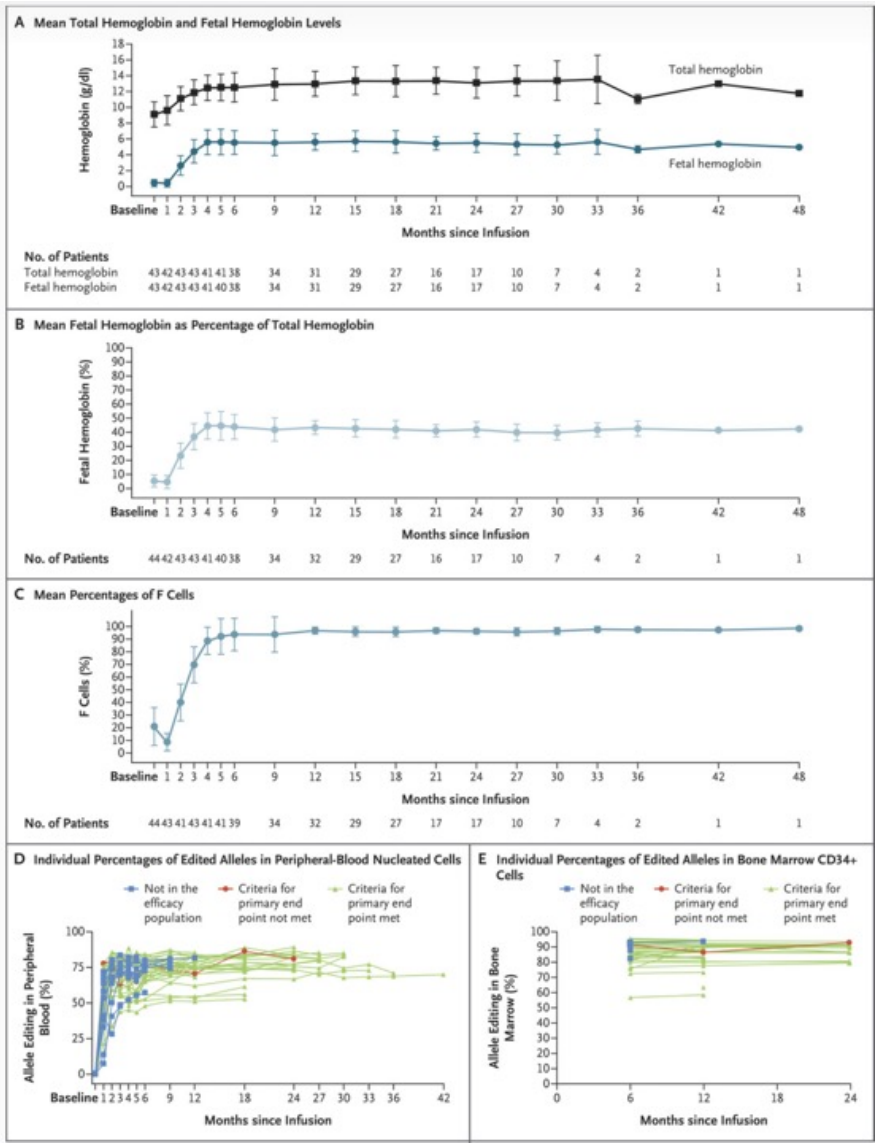

Grade 3 or 4 Adverse Events after Exa-Cel Infusion.

Event	Full Analysis Population (N=44)
	no. of patients (%)
Grade 3 or 4 adverse event	42 (95)
Grade 3 or 4 adverse event occurring in ≥5% of patients*	
Stomatitis	24 (55)
Febrile neutropenia	21 (48)
Platelet count decrease	21 (48)
Appetite decrease	18 (41)
Neutrophil count decrease	17 (39)
Mucosal inflammation	14 (32)
Anemia	11 (25)
Thrombocytopenia	11 (25)
Neutropenia	10 (23)
White-cell count decrease	6 (14)
Abdominal pain	5 (11)
CD4 lymphocyte count decrease	5 (11)
Cholelithiasis	5 (11)
Pruritus	5 (11)
Constipation	4 (9)
Headache	4 (9)
Nausea	4 (9)
Noncardiac chest pain	4 (9)
Pneumonia	4 (9)
Upper abdominal pain	3 (7)
Arthralgia	3 (7)
Back pain	3 (7)
Deep-vein thrombosis	3 (7)
Oropharyngeal pain	3 (7)
Pain	3 (7)
Weight decreased	3 (7)

Discussion

This phase 3, single-group study of exa-cel met the primary end point and both key secondary end points: 97% of patients with sickle cell disease were free from vaso-occlusive crises for at least 12 months, 100% were free from inpatient hospitalization for severe vaso-occlusive crises for at least 12 months, and 97% were free from vaso-occlusive crises for at least 9 months. Patients were free from vaso-occlusive crises for a mean duration of 22.4 months (range, 14.8 to 45.5). Patients had early and sustained increases in total and fetal hemoglobin levels, with a mean total hemoglobin level of 11.9±1.5 g per deciliter at month 3 and 12.5±1.8 g per deciliter at month 6, and normal or near-normal levels (normal range, 12.1 to 17.2 g per deciliter) were maintained thereafter. Improvements were seen in all markers of hemolysis evaluated, including normalization of lactate dehydrogenase and detectable haptoglobin levels, findings that indicated resolution of intravascular hemolysis. Patients also had clinically meaningful improvements in quality of life. These results show that a one-time treatment with nonviral ex vivo CRISPR-Cas9 editing of the erythroid-specific enhancer region of *BCL11A* reactivated fetal hemoglobin production in erythrocytes to levels previously shown to be protective in persons with hereditary persistence of fetal hemoglobin and sickle cell disease (>20% fetal hemoglobin in pancellular distribution) and resulted in a clinical benefit. Although all the patients had adverse events, in most patients these events were considered by the investigators to be related to the busulfan-based conditioning.

Als Beta-Thalassämie bezeichnet man eine autosomal-rezessiv vererbbare Synthesestörung der β-Ketten des Proteinanteils (Globin) im Hämoglobin. Die Erkrankung gehört zu den Hämoglobinopathien.
Ursächlich ist eine Mutation im β-Globin-Gen (HBB), das auf dem kurzen Arm von Chromosom 11 lokalisiert ist. Es existieren mehr als 200 unterschiedliche genetische Varianten, von denen die meisten Punktmutationen sind. Deletionen kommen nur selten vor. Weiterhin existieren thalassämische Hämoglobinvarianten, die phänotypisch das Bild einer Thalassämie hervorrufen können (z.B. Hämoglobin Lepore, HbE-Krankheit).
Je nach den Auswirkungen der Mutation auf die Produktion von β-Globin-Ketten unterscheidet man drei Klassen von Mutationen:

- β^0: keine Produktion von β-Globin-Ketten
- β^+: deutlich verringerte Produktion von β-Globin-Ketten
- β^{++}: moderat verringerte Produktion von β-Globin-Ketten

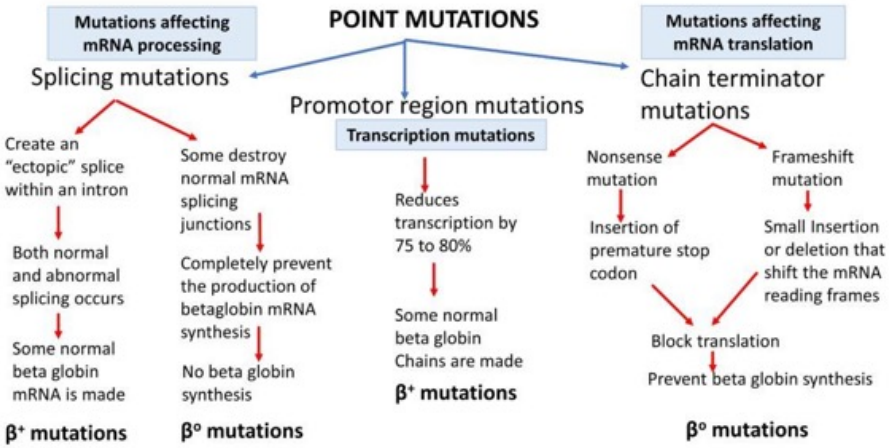

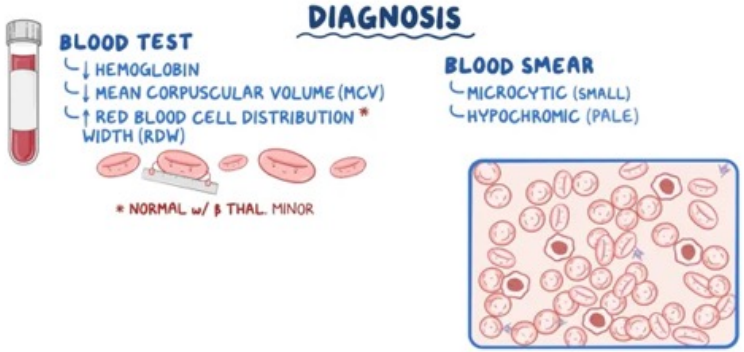

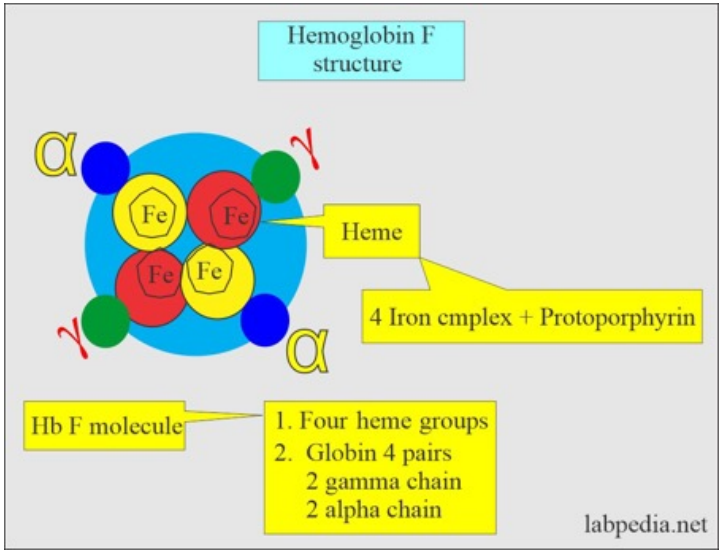

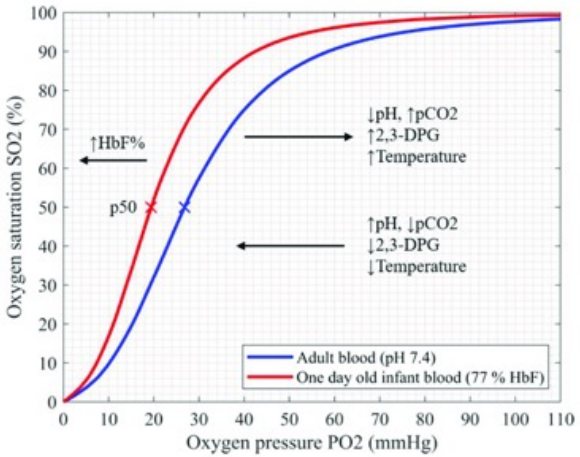

BCL11A ist ein Transkriptionsfaktor, der die Expression von Gamma-Globin, einem Bestandteil des fetalen Hämoglobins, hemmt. Die Bildung von fetalem Hämoglobin hört normalerweise nach der Geburt auf. Durch die Abschaltung von BCL11A soll es reaktiviert werden.

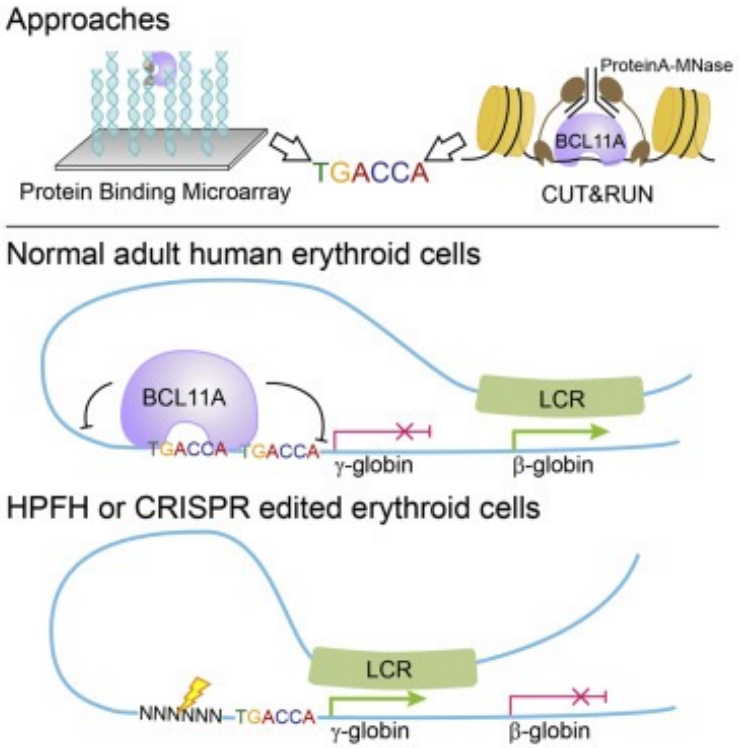

Exagamglogene Autotemcel for Transfusion-Dependent β-Thalassemia

Exagamglogene autotemcel (exa-cel) is a nonviral cell therapy designed to reactivate fetal hemoglobin synthesis through ex vivo clustered regularly interspaced short palindromic repeats (CRISPR)–Cas9 gene editing of the erythroid-specific enhancer region of *BCL11A* in autologous CD34+ hematopoietic stem and progenitor cells (HSPCs). We conducted an open-label, single-group, phase 3 study of exa-cel in patients 12 to 35 years of age with transfusion-dependent β-thalassemia and a β^0/β^0, β^0/β^0-like, or non–β^0/β^0-like genotype. CD34+ HSPCs were edited by means of CRISPR-Cas9 with a guide mRNA. Before the exa-cel infusion, patients underwent myeloablative conditioning with pharmacokinetically dose-adjusted busulfan. The primary end point was transfusion independence, defined as a weighted average hemoglobin level of 9 g per deciliter or higher without red-cell transfusion for at least 12 consecutive months. Total and fetal hemoglobin concentrations and safety were also assessed.

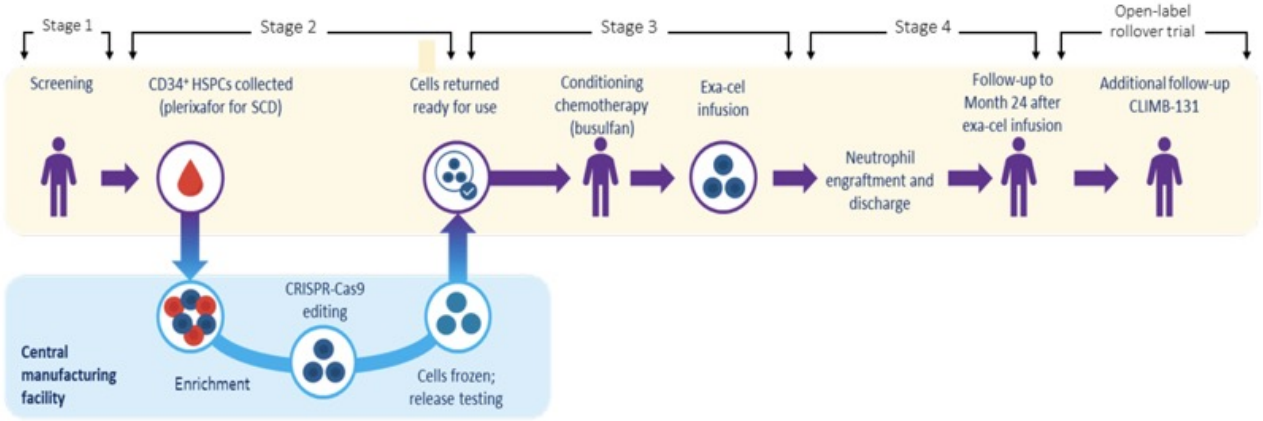

CRISPR-Cas9, clustered regularly interspaced short palindromic repeats-associated 9 nuclease; **exa-cel,** exagamglogene autotemcel; **HSPC,** hematopoietic stem and progenitor cell; **M24,** month 24.

Methods

Study Design, Patients, and Oversight

We are conducting this ongoing phase 3, open-label, single-dose study of exa-cel (CLIMB THAL-111) at 13 sites in Canada, Germany, Italy, the United Kingdom, and the United States. Patients 12 to 35 years of age were eligible if they had a confirmed diagnosis of transfusion-dependent β-thalassemia and a transfusion history of at least 100 ml of packed red cells per kilogram of body weight per year or 10 units of packed red cells per year for 2 years before screening. Patients received a combination of granulocyte-colony stimulating factor (G-CSF) and plerixafor for HSPC mobilization followed by apheresis for up to 3 consecutive days to collect CD34+ HSPCs. Exa-cel was manufactured from CD34+ cells with the use of CRISPR-Cas9 and a single guide RNA molecule. Before the exa-cel infusion, patients received a myeloablative, pharmacokinetically adjusted busulfan conditioning regimen for 4 days. Exa-cel was infused intravenously through a central venous catheter at least 48 hours but no more than 7 days after completion of the busulfan infusion. Neutrophil engraftment was considered to have occurred on the first of 3 different days on which three consecutive measurements of the absolute neutrophil count were 500 per microliter or higher.

End-Point Measures

The primary end point was transfusion independence, defined as a weighted average hemoglobin level of at least 9 g per deciliter without red-cell transfusion for at least 12 consecutive months. The key secondary end point was a weighted average hemoglobin level of at least 9 g per deciliter without red-cell transfusion for at least 6 months. Evaluation of these two end points started 60 days after the last red-cell transfusion.

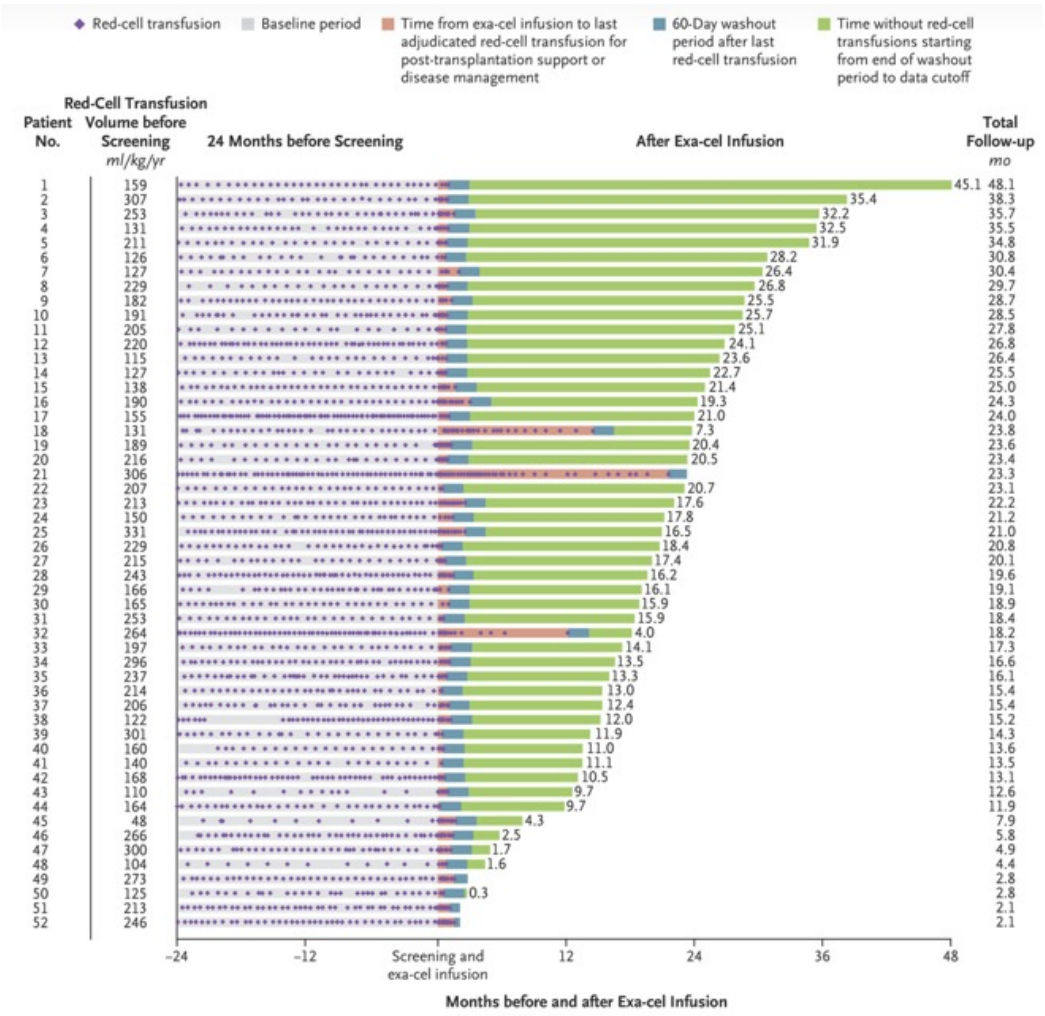

Characteristic	Full Analysis Population (N = 52)	Primary Efficacy Population (N = 35)
Sex — no. (%)		
Male	27 (52)	18 (51)
Female	25 (48)	17 (49)
Age at screening		
Mean — yr	21.5±6.7	21.1±6.1
Distribution — no. (%)		
12 to <18 yr	18 (35)	11 (31)
≥18 to 35 yr	34 (65)	24 (69)
Race or ethnic group — no. (%)†		
White	18 (35)	15 (43)
Asian	22 (42)	13 (37)
Data not collected per local regulations	7 (13)	4 (11)
Other	2 (4)	0
Multiracial	3 (6)	3 (9)
Genotype — no. (%)		
β^0/β^0-like	31 (60)	20 (57)
β^0/β^0	19 (37)	10 (29)
β^0/IVS-I-110	9 (17)	7 (20)
IVS-I-110/IVS-I-110	3 (6)	3 (9)
Non–β^0/β^0-like	21 (40)	15 (43)
β^+/β^+	4 (8)	3 (9)
β^+/β^0	12 (23)	8 (23)
β^E/β^0	5 (10)	4 (11)
Annualized volume of red-cell transfusions — ml/kg		
Mean	196.8±63.0	202.0±57.1
Median (range)	201.0 (48.3–330.9)	205.2 (115.2–330.9)
Median annualized red-cell transfusions (range) — units	35.0 (11.0–71.0)	35.0 (20.5–71.0)
Total hemoglobin concentration — g/dl	10.4±2.0	10.4±1.9
Total fetal hemoglobin concentration — g/dl	0.6±1.0	0.5±0.6
Spleen intact — no. (%)	36 (69)	26 (74)
Iron status		
Median liver iron concentration (range) — mg/g	3.5 (1.2–14.0)	4.0 (1.4–14.0)
Median cardiac iron content by T2*-weighted MRI (range) — msec	34.0 (12.4–61.1)	34.8 (19.6–61.1)
Median serum ferritin concentration (range) — pmol/liter	2891.9 (584.2–10,837.3)	2653.7 (674.1–10,740.7)
Median no. of mobilization cycles (range)	1 (1–4)	1 (1–2)
Median exa-cel dose (range) — CD34+ cells/kg	7.5×10^6 (3.0×10^6–19.7×10^6)	6.4×10^6 (3.0×10^6–19.7×10^6)

End Point	Primary Efficacy Population (N=35)
Primary end point: weighted average hemoglobin level of ≥9 g/dl without red-cell transfusion for ≥12 consecutive months	
No. of patients	32
Percentage of patients (95% CI)*	91 (77–98)
P value	<0.001
Key secondary end point: weighted average hemoglobin level of ≥9 g/dl without red-cell transfusion for ≥6 consecutive months	
No. of patients	32
Percentage of patients (95% CI)*	91 (77–98)
P value	<0.001

Adverse Event	Full Analysis Population (N=52)
	no. of patients (%)
Any grade 3 or 4 event	46 (88)
Grade 3 or 4 events occurring in ≥5% of patients*	
Febrile neutropenia	28 (54)
Stomatitis	21 (40)
Anemia	20 (38)
Platelet count decrease	18 (35)
Thrombocytopenia	18 (35)
Mucosal inflammation	17 (33)
Neutrophil count decrease	14 (27)
Decrease in appetite	12 (23)
Epistaxis	7 (13)
Neutropenia	7 (13)
White-cell count decrease	7 (13)
Veno-occlusive liver disease	5 (10)
Blood bilirubin increase	4 (8)
Hypokalemia	4 (8)
Hypophosphatemia	4 (8)
Iron overload	4 (8)
Nausea	4 (8)
Vomiting	4 (8)
CD4 lymphocyte count decrease	3 (6)
Hematuria	3 (6)
Headache	3 (6)
Hypoxia	3 (6)

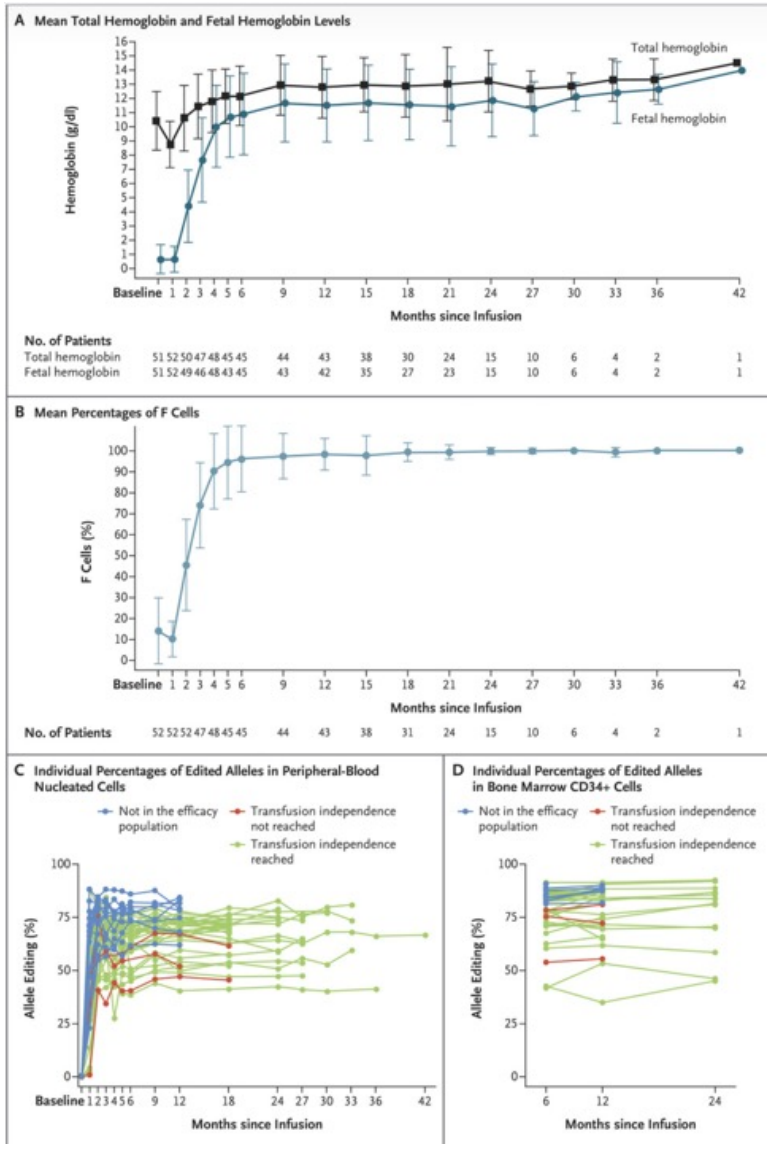

Discussion

In this phase 3 study of exa-cel, we enrolled patients with transfusion-dependent β-thalassemia who had a high burden of red-cell transfusions and impaired quality of life. The study met the primary end point: 91% of the patients had transfusion independence and mean total hemoglobin levels within the normal range. Patients stopped transfusions approximately 1 month after the exa-cel infusion, and transfusion independence was durable, with a mean duration of 22.5 months (range, 13.3 to 45.1). The majority of hemoglobin was fetal hemoglobin, which had a pancellular distribution. These results confirm that CRISPR-Cas9–edited erythroid-specific enhancer region of *BCL11A* in the exa-cel product effectively reactivates fetal hemoglobin production to levels that are known to be protective in persons with hereditary persistence of fetal hemoglobin and that are observed during the neonatal period, which confers a transformational benefit in patients with transfusion-dependent β-thalassemia. The increases in total and fetal hemoglobin levels were consistent among patients with various genotypes, including those with the most severe β^0/β^0 genotype (who produce no endogenous hemoglobin A), a finding consistent with a normalization of hemoglobin levels by exa-cel independent of genotype.

Large hemispheric infarction (LHI) is a severe form of ischemic stroke affecting the majority of or complete middle cerebral artery (MCA) distribution area with or without anterior cerebral artery and posterior cerebral artery involvement and characterized by the development of life-threatening cerebral edema.

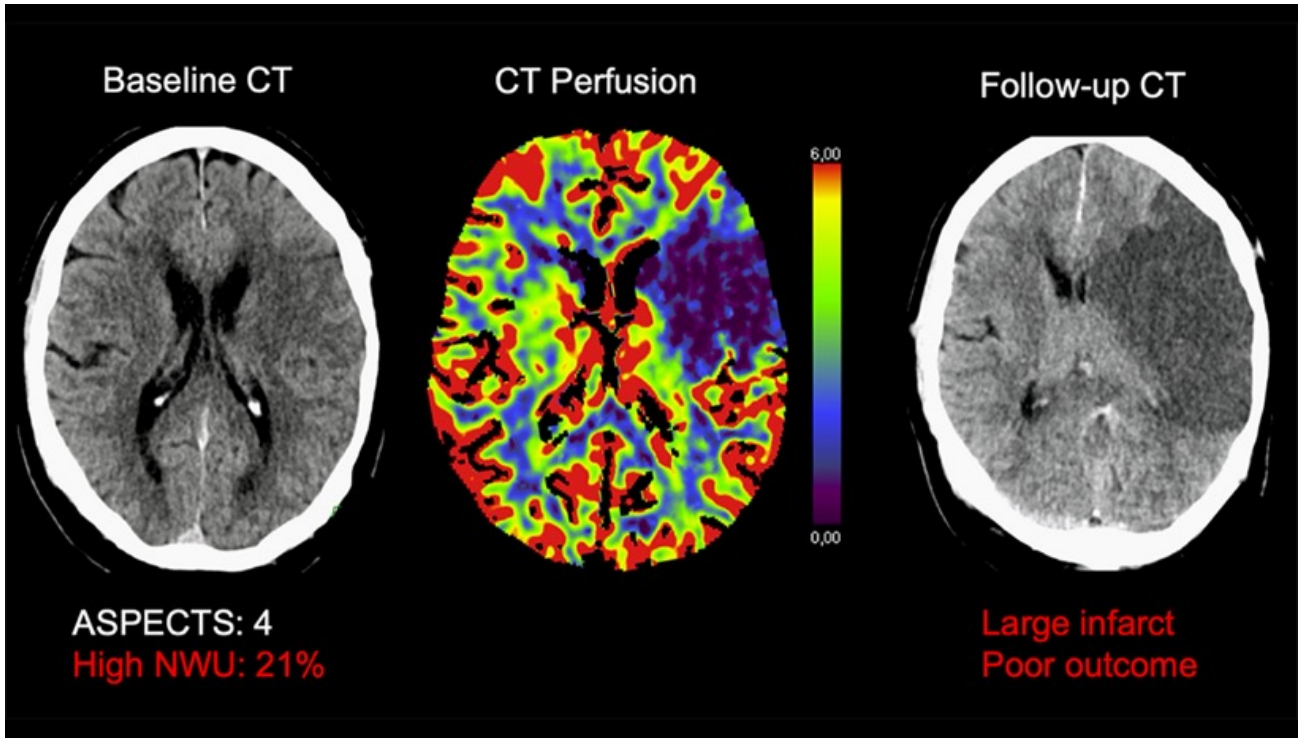

Trial of Thrombectomy for Stroke with a Large Infarct of Unrestricted Size

The use of thrombectomy in patients with acute stroke and a large infarct of unrestricted size has not been well studied. We assigned, in a 1:1 ratio, patients with proximal cerebral vessel occlusion in the anterior circulation and a large infarct (as defined by an Alberta Stroke Program Early Computed Tomographic Score of ≤5; values range from 0 to 10) detected on magnetic resonance imaging or computed tomography within 6.5 hours after symptom onset to undergo endovascular thrombectomy and receive medical care (thrombectomy group) or to receive medical care alone (control group). The primary outcome was the score on the modified Rankin scale at 90 days (scores range from 0 to 6, with higher scores indicating greater disability). The primary safety outcome was death from any cause at 90 days, and an ancillary safety outcome was symptomatic intracerebral hemorrhage.

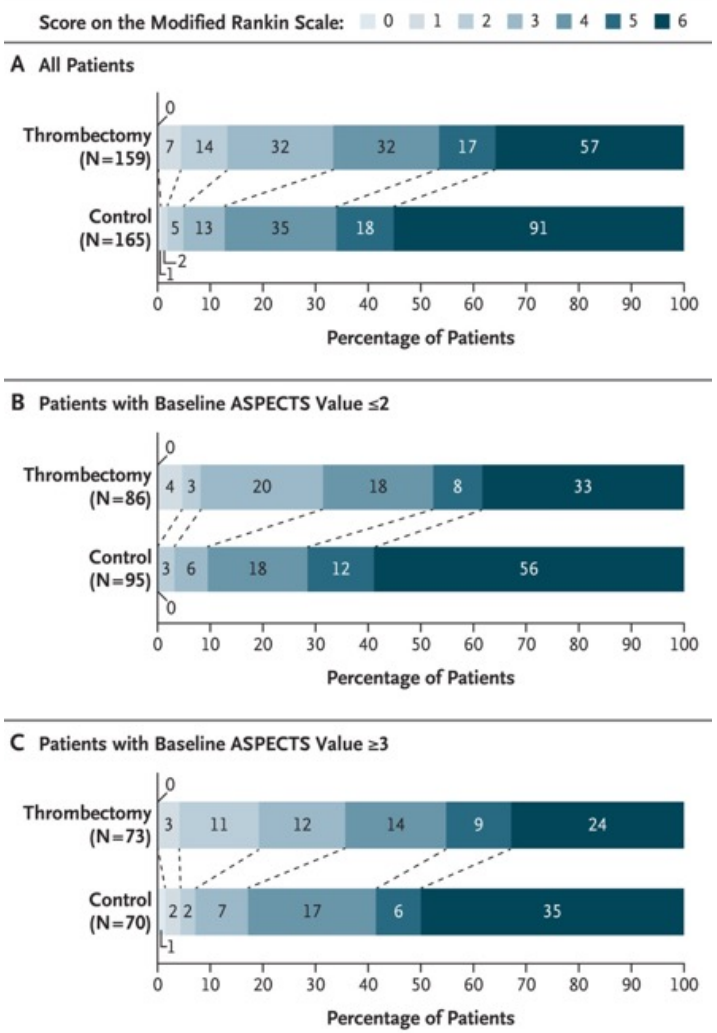

Randomized trials have shown the benefit of endovascular thrombectomy in patients with acute stroke due to large-artery occlusion in the anterior circulation and a large baseline infarct (core). In the early stages of ischemia, the infarct is visible as a hypodense lesion on noncontrast computed tomography (CT) scans and as a hyperintense lesion on diffusion-weighted magnetic resonance imaging (MRI) scans. The size of the infarct can be assessed on CT and MRI scans with the use of the semiquantitative Alberta Stroke Program Early Computed Tomography Score (ASPECTS; values range from 0 to 10, with lower values indicating larger infarcts). In these trials, a large core was defined by an ASPECTS value of 5 or less, but because of concerns about the deleterious effects associated with the reperfusion of large infarcts, patients with the largest infarcts (ASPECTS value, 0 or 1) were excluded from enrollment. However, the benefit of thrombectomy did not diminish with increasing infarct size, suggesting that thrombectomy may be beneficial even in patients with the largest baseline infarcts.

Patients

Patients were eligible for inclusion in the trial if they were older than 18 years of age; had an ASPECTS value of 5 or less on CT or MRI, except for patients older than 80 years of age, who were eligible if they had a baseline ASPECTS value of 4 or 5 (the method for determining the ASPECTS value is described.

Trial Design

Patients were randomly assigned in a 1:1 ratio to undergo endovascular thrombectomy and receive medical care (thrombectomy group) or to receive medical care alone (control group).

Trial Outcomes

The primary outcome was the modified Rankin scale score at 90 days after randomization, with scores of 5 and 6 combined into one score.

Characteristic	Thrombectomy (N=159)	Control (N=165)
Age		
Median (IQR) — yr	73 (66–79)	74 (65–80)
>80 yr — no. (%)	34 (21.4)	38 (23.0)
Male sex — no. (%)	82 (51.6)	88 (53.3)
Transferred to thrombectomy-capable center	89 (56.0)	94 (57.0)
Modified Rankin scale score before stroke — no. (%)†		
0	130 (81.8)	129 (78.2)
1	27 (17.0)	34 (20.6)
>1	2 (1.3)	2 (1.2)
Median NIHSS score on admission (IQR)‡	21 (18–24)	21 (18–24)
Qualifying imaging method — no. (%)		
Computed tomography	28 (17.6)	25 (15.2)
Magnetic resonance imaging	131 (82.4)	140 (84.8)
ASPECTS value§		
Median (IQR)	2 (1–3)	2 (1–3)
≤2	86 (54.1)	95 (57.6)
≥3	73 (45.9)	70 (42.4)
Median infarct volume at baseline (IQR) — ml¶	132 (104–185)	137 (106–187)
Occlusion site — no. (%)‖		
Intracranial segment of the internal carotid artery	69 (43.4)	74 (44.8)
Proximal, or M1, segment of the middle cerebral artery	88 (55.3)	91 (55.2)
Other	2 (1.3)	0
Intravenous thrombolysis therapy — no. (%)	55 (34.6)	58 (35.2)
Unknown time of symptom onset — no. (%)	48 (30.2)	47 (28.5)
Time from symptom onset to randomization — min**		
Median (IQR)	271 (199–351)	268 (207–336)
Mean	335	316
Time from symptom onset to qualifying imaging — min**		
Median (IQR)	170 (112–301)	169 (115–273)
Mean	261	242

Outcome	Thrombectomy (N=159)	Control (N=165)	Treatment Effect (95% CI)
Primary outcome			
Median modified Rankin scale score at 90 days (IQR)†	4 (3–6)	6 (4–6)	1.63 (1.29 to 2.06)‡
Secondary outcomes			
Modified Rankin scale score at 90 days — no./total no. (%)			
0 to 2	21/158 (13.3)	8/164 (4.9)	2.39 (1.18 to 6.22)§
0 to 3	53/158 (33.5)	20/164 (12.2)	2.62 (1.72 to 4.36)§
Modified Rankin scale score at 180 days			
Median (IQR)	4 (3–6)	6 (4–6)	1.71 (1.35 to 2.18)‡
0 to 2 — no./total no. (%)	29/157 (18.5)	8/162 (4.9)	3.26 (1.67 to 8.46)§
0 to 3 — no./total no. (%)	58/157 (36.9)	21/162 (13.0)	2.67 (1.79 to 4.41)§
Utility-weighted modified Rankin scale score			
At 90 days	0.30±0.32	0.16±0.25	0.144 (0.08 to 0.20)¶
At 180 days	0.33±0.34	0.17±0.26	0.164 (0.10 to 0.23)¶
EQ-5D-5L utility index‖			
At 90 days	0.30±0.43	0.10±0.32	0.51 (0.26 to 0.75)**
At 180 days	0.32±0.41	0.14±0.34	0.51 (0.28 to 0.75)**
Decompressive craniectomy within 7 days — no. (%)	14 (8.8)	19 (11.5)	0.81 (0.37 to 1.74)††
Early neurologic improvement — no./total no. (%)‡‡	47/153 (30.7)	18/158 (11.4)	2.62 (1.70 to 4.56)§
Mean change in infarct volume from baseline at 24 hr (95% CI) — ml	51.6 (39.9 to 63.2)	119.5 (107.9 to 131.1)	−67.9 (−84.1 to −51.6)¶
Safety outcomes			
Death from any cause at 90 days — no./total no. (%)	57/158 (36.1)	91/164 (55.5)	0.65 (0.50 to 0.84)§
Symptomatic intracerebral hemorrhage within 24 hr — no./total no. (%)§§			
According to the Heidelberg bleeding classification	15/157 (9.6)	9/157 (5.7)	1.73 (0.78 to 4.68)§
According to the SITS-MOST criteria	5/157 (3.2)	4/157 (2.5)	1.29 (0.21 to 16.39)§
Early neurologic worsening — no./total no. (%)¶¶	49/153 (32.0)	57/158 (36.1)	0.89 (0.64 to 1.21)§
Adverse event related to the procedure or device — no. (%)‖‖			
Embolization in a previously uninvolved territory	1 (0.6)	NA	—
Arterial dissection	2 (1.3)	NA	—
Arterial perforation	2 (1.3)	NA	—
Other	6 (3.8)	NA	—

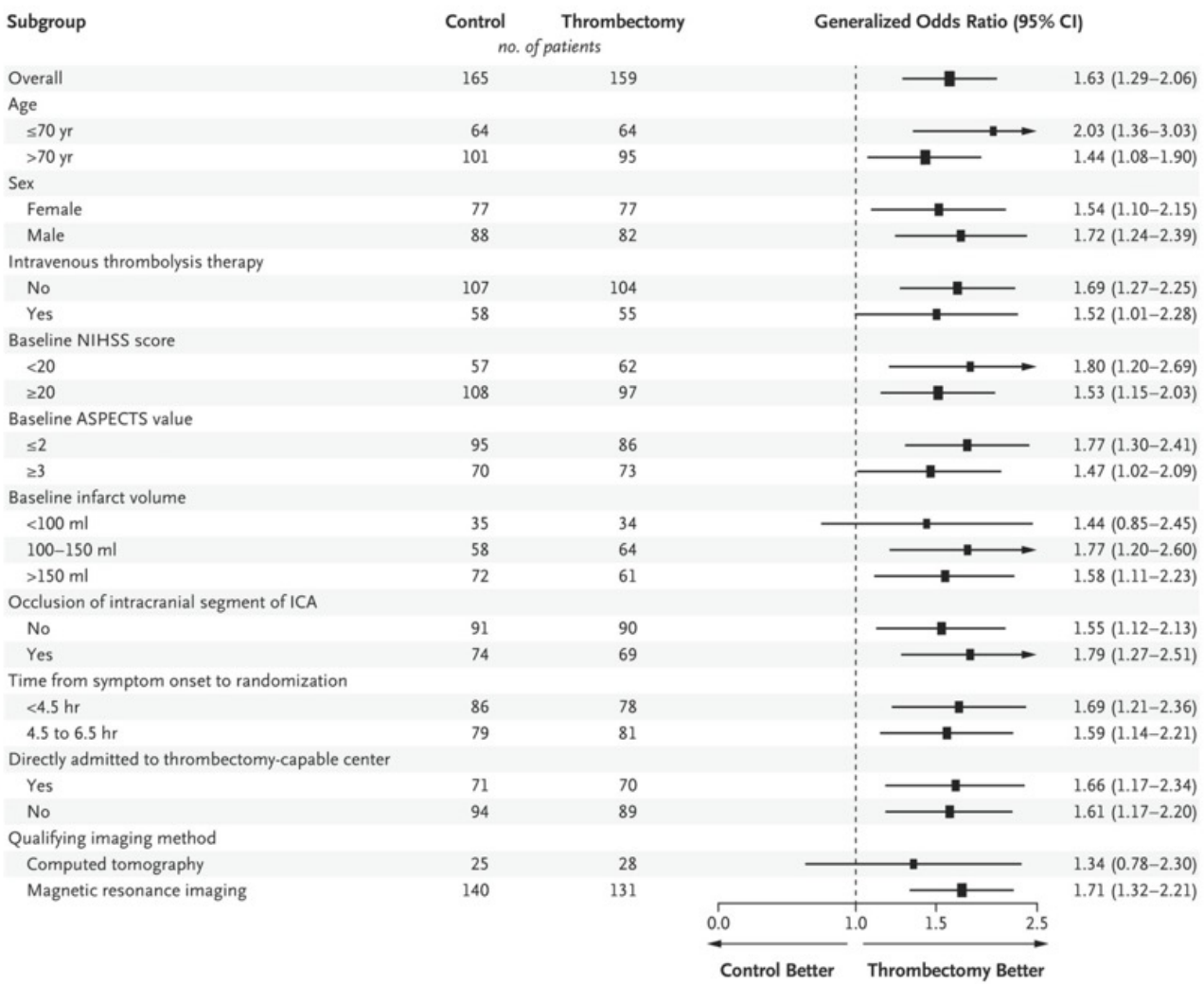
Subgroup
Control
Thrombectomy
no. of patients
Generalized Odds Ratio (95% CI)
Overall 165 159 1.63 (1.29–2.06)
Age
≤70 yr 64 64 2.03 (1.36–3.03)
>70 yr 101 95 1.44 (1.08–1.90)
Sex
Female 77 77 1.54 (1.10–2.15)
Male 88 82 1.72 (1.24–2.39)
Intravenous thrombolysis therapy
No 107 104 1.69 (1.27–2.25)
Yes 58 55 1.52 (1.01–2.28)
Baseline NIHSS score
<20 57 62 1.80 (1.20–2.69)
≥20 108 97 1.53 (1.15–2.03)
Baseline ASPECTS value
≤2 95 86 1.77 (1.30–2.41)
≥3 70 73 1.47 (1.02–2.09)
Baseline infarct volume
<100 ml 35 34 1.44 (0.85–2.45)
100–150 ml 58 64 1.77 (1.20–2.60)
>150 ml 72 61 1.58 (1.11–2.23)
Occlusion of intracranial segment of ICA
No 91 90 1.55 (1.12–2.13)
Yes 74 69 1.79 (1.27–2.51)
Time from symptom onset to randomization
<4.5 hr 86 78 1.69 (1.21–2.36)
4.5 to 6.5 hr 79 81 1.59 (1.14–2.21)
Directly admitted to thrombectomy-capable center
Yes 71 70 1.66 (1.17–2.34)
No 94 89 1.61 (1.17–2.20)
Qualifying imaging method
Computed tomography 25 28 1.34 (0.78–2.30)
Magnetic resonance imaging 140 131 1.71 (1.32–2.21)
0.0
1.0
1.5
2.5
Control Better
Thrombectomy Better

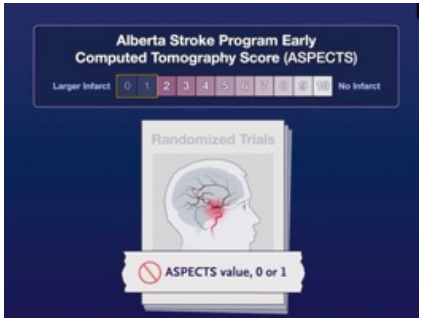
Alberta Stroke Program Early
Computed Tomography Score (ASPECTS)
Larger Infarct
0 1 2 3 4 5 6 7 8 9 10
No Infarct
Randomized Trials
ASPECTS value, 0 or 1


Thrombectomy
N=166
Control
N=167
Endovascular Thrombectomy
+ Medical Care
Medical Care Alone

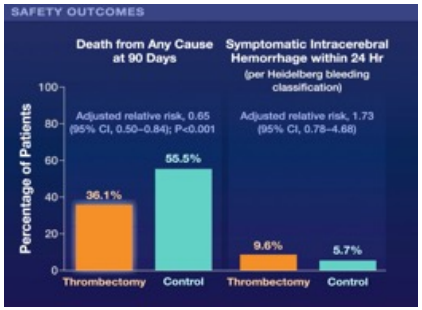
SAFETY OUTCOMES
Death from Any Cause
at 90 Days
Symptomatic Intracerebral
Hemorrhage within 24 Hr
(per Heidelberg bleeding
classification)
Adjusted relative risk, 0.65
(95% CI, 0.50–0.84); P<0.001
Adjusted relative risk, 1.73
(95% CI, 0.78–4.68)
Percentage of Patients
100
80
60
40
20
0
36.1%
55.5%
9.6%
5.7%
Thrombectomy
Control
Thrombectomy
Control

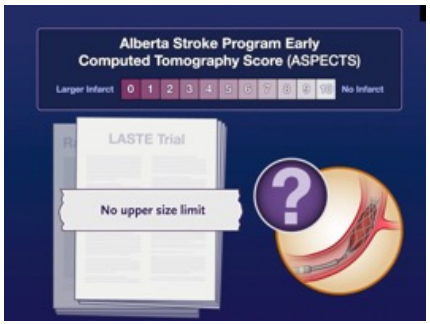
Alberta Stroke Program Early
Computed Tomography Score (ASPECTS)
Larger Infarct
0 1 2 3 4 5 6 7 8 9 10
No Infarct
LASTE Trial
No upper size limit

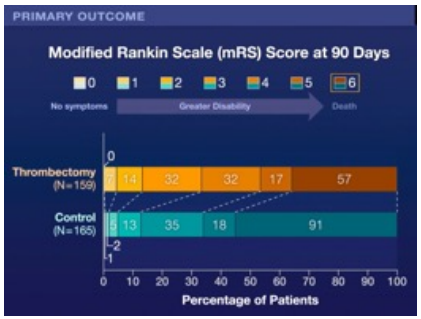
PRIMARY OUTCOME
Modified Rankin Scale (mRS) Score at 90 Days
0 1 2 3 4 5 6
No symptoms
Greater Disability
Death
Thrombectomy
(N=159)
7 14 32 32 17 57
Control
(N=165)
13 35 18 91
0 10 20 30 40 50 60 70 80 90 100
Percentage of Patients

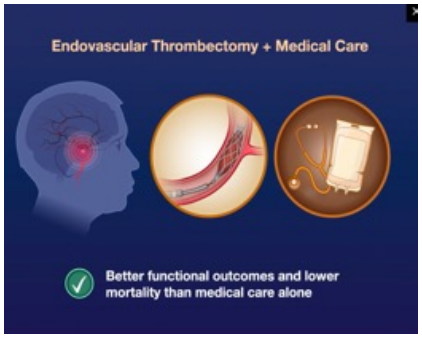
Endovascular Thrombectomy + Medical Care
Better functional outcomes and lower
mortality than medical care alone

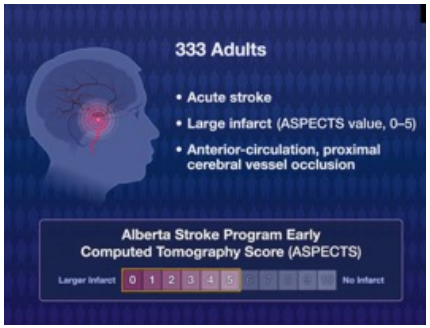
333 Adults
• Acute stroke
• Large infarct (ASPECTS value, 0–5)
• Anterior-circulation, proximal
cerebral vessel occlusion
Alberta Stroke Program Early
Computed Tomography Score (ASPECTS)
Larger Infarct
0 1 2 3 4 5
No Infarct

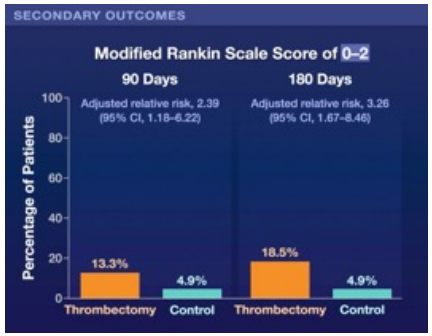
SECONDARY OUTCOMES
Modified Rankin Scale Score of 0–2
90 Days
180 Days
Adjusted relative risk, 2.39
(95% CI, 1.18–6.22)
Adjusted relative risk, 3.26
(95% CI, 1.67–8.46)
Percentage of Patients
100
80
60
40
20
0
13.3%
4.9%
18.5%
4.9%
Thrombectomy
Control
Thrombectomy
Control

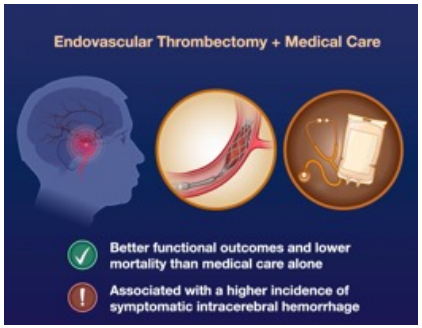
Endovascular Thrombectomy + Medical Care
Better functional outcomes and lower
mortality than medical care alone
Associated with a higher incidence of
symptomatic intracerebral hemorrhage

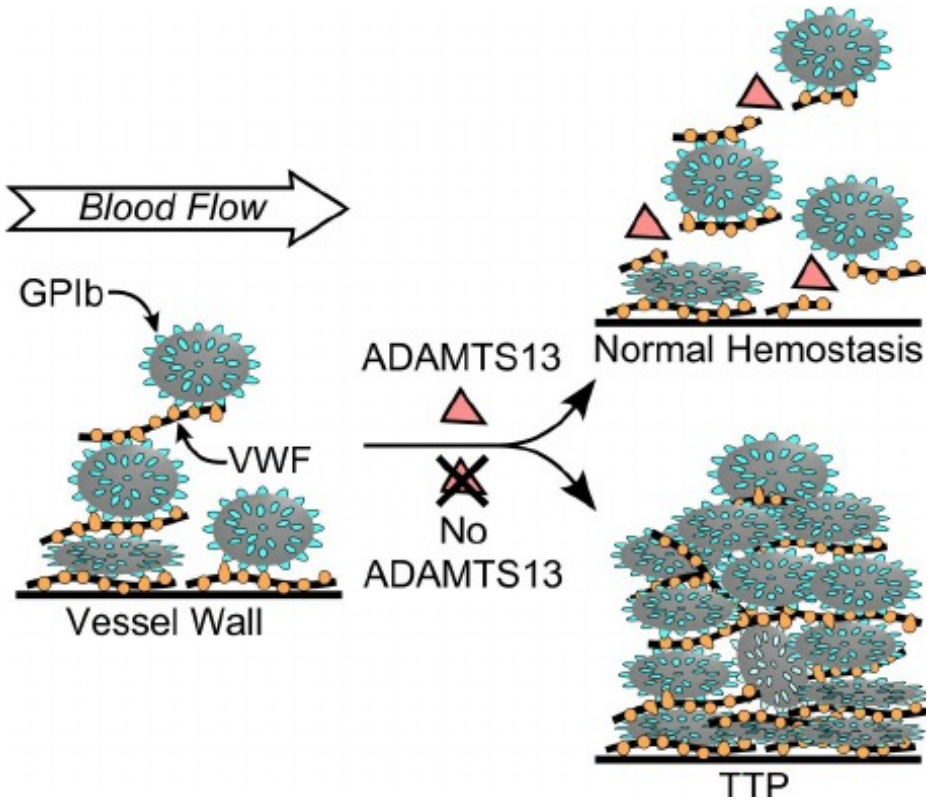
Blood Flow
GPIb
VWF
Vessel Wall
ADAMTS13
No
ADAMTS13
Normal Hemostasis
TTP

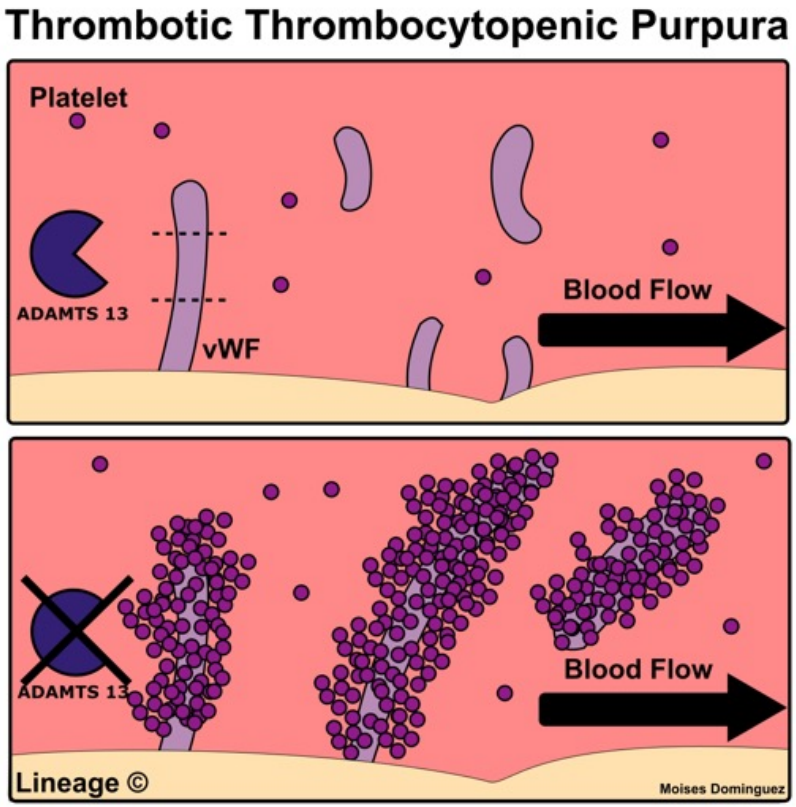
Thrombotic Thrombocytopenic Purpura
Platelet
ADAMTS 13
vWF
Blood Flow
ADAMTS 13
Blood Flow
Lineage ©
Moises Dominguez

Recombinant ADAMTS13 for Immune Thrombotic Thrombocytopenic Purpura

Summary

In patients with immune thrombotic thrombocytopenic purpura (iTTP), autoantibodies against the metalloprotease ADAMTS13 lead to catastrophic microvascular thrombosis. However, the potential benefits of recombinant human ADAMTS13 (rADAMTS13) in patients with iTTP remain unknown. Here, we report the clinical use of rADAMTS13, which resulted in the rapid suppression of disease activity and complete recovery in a critically ill patient whose condition had proved to be refractory to all available treatments. We also show that rADAMTS13 causes immune complex formation, which saturates the autoantibody and may promote its clearance. Our data support the role of rADAMTS13 as a novel adjunctive therapy in patients with iTTP.

Immune thrombotic thrombocytopenic purpura (iTTP) is an acute hematologic disorder characterized by thrombotic microangiopathy, end-organ damage, and death if left untreated. In patients with iTTP, autoantibodies inhibit the von Willebrand factor–cleaving metalloprotease ADAMTS13 or induce its clearance, leading to the accumulation of ultra-large multimers of von Willebrand factor and the formation of platelet-rich microvascular thrombi. The disease occurs more commonly in women of color, and patients have few if any effective options when standard treatment fails.

The mainstay of therapy for iTTP is plasma exchange, which removes the inhibitor and provides exogenous ADAMTS13. Plasma exchange induces a clinical response in most patients, despite at best repleting only approximately half of normal ADAMTS13 activity levels. By contrast, recombinant human ADAMTS13 (rADAMTS13) offers the possibility of greatly increased ADAMTS13 delivery and enhanced autoantibody clearance through the formation of ADAMTS13-containing immune complexes. However, the benefits of rADAMTS13 in iTTP remain theoretical. We describe the clinical use of rADAMTS13 in a patient with iTTP.

Case Report

A 28-year-old Black woman with a history of one pregnancy and one delivery presented 101 days post partum with fatigue and vaginal bleeding. Laboratory studies revealed anemia (hemoglobin level, 6.9 g per deciliter), an elevated lactate dehydrogenase level (2089 IU per liter), and profound thrombocytopenia (platelet count, 9×10^9 per liter).

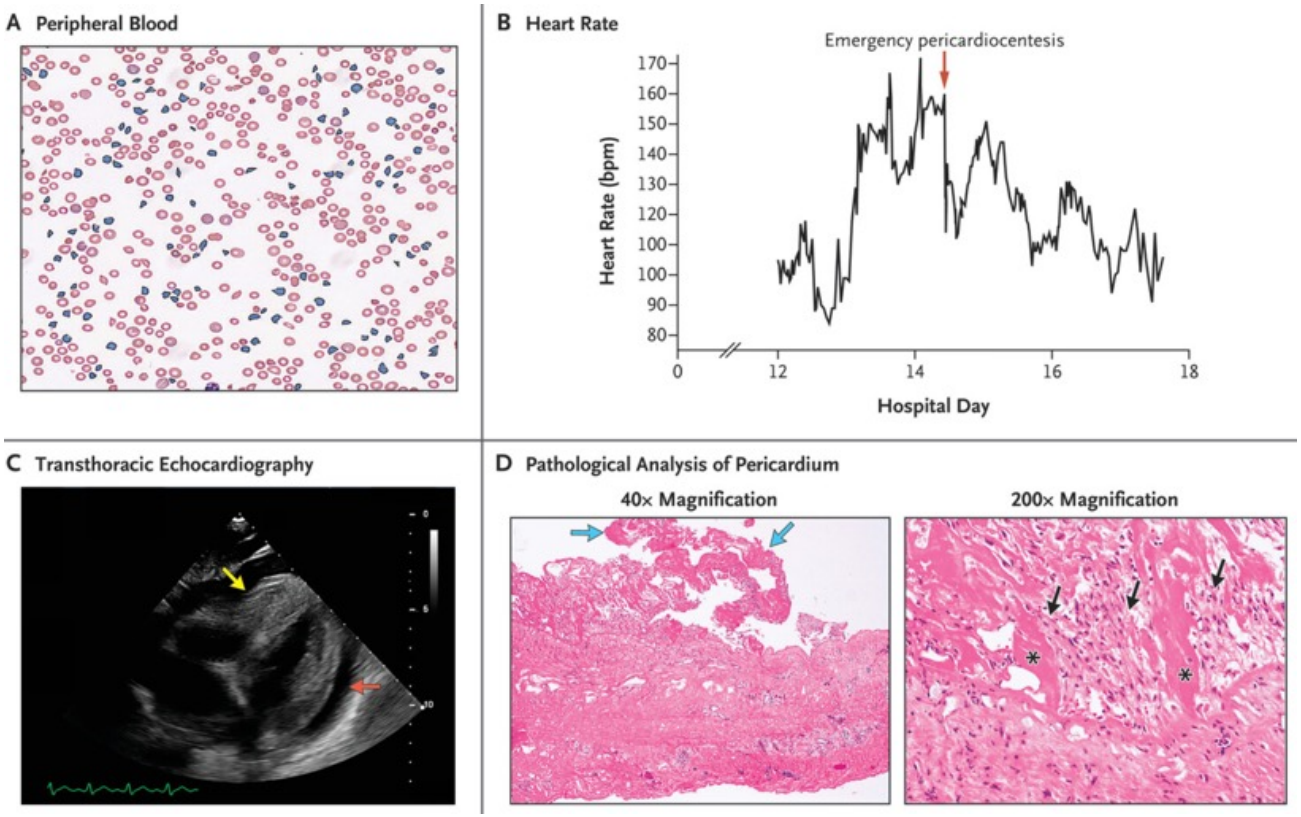

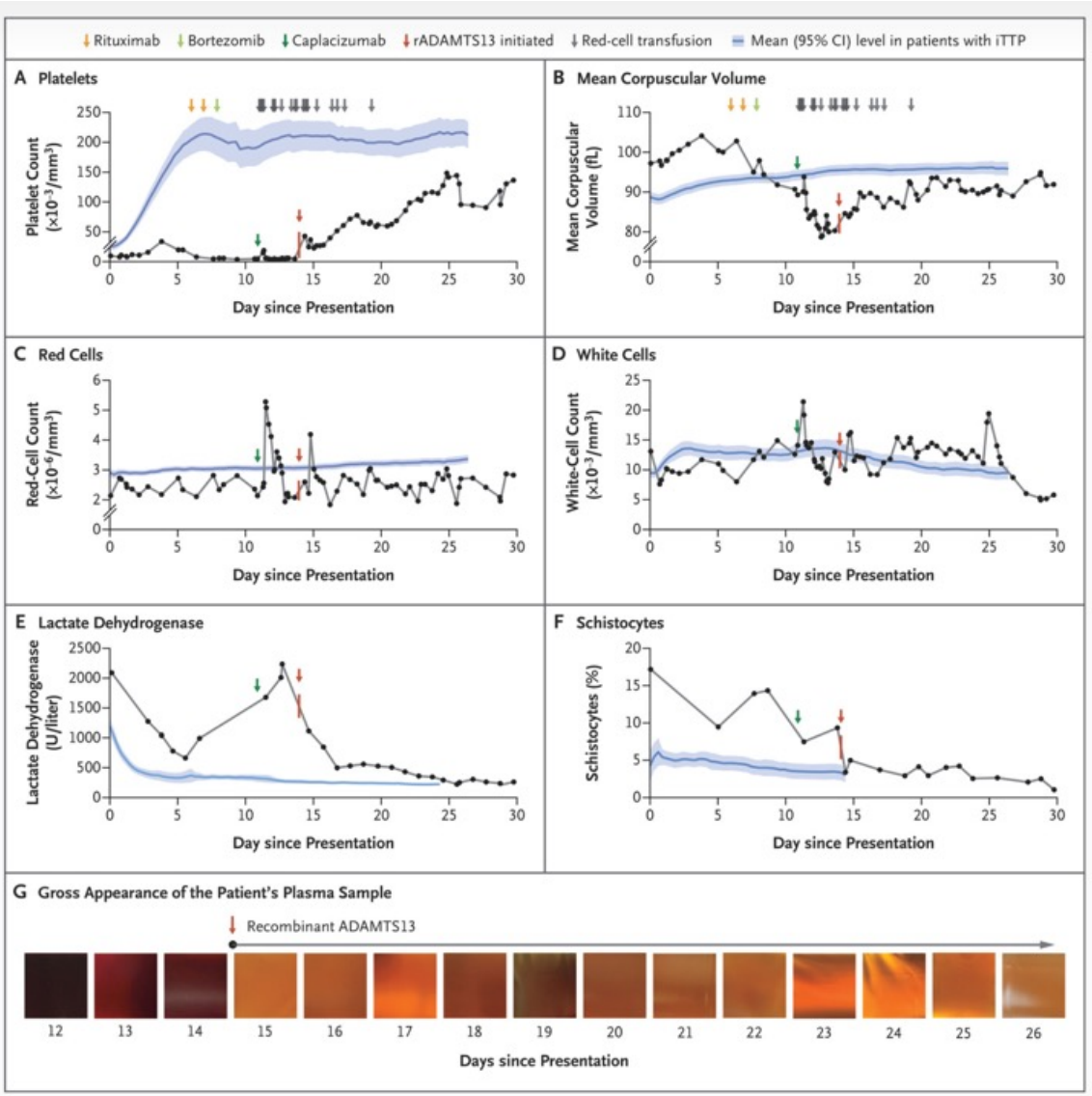
Rituximab
Bortezomib
Caplacizumab
rADAMTS13 initiated
Red-cell transfusion
Mean (95% CI) level in patients with iTTP
A Platelets
Platelet Count (×10⁻³/mm³)
Day since Presentation
B Mean Corpuscular Volume
Mean Corpuscular Volume (fL)
Day since Presentation
C Red Cells
Red-Cell Count (×10⁻⁶/mm³)
Day since Presentation
D White Cells
White-Cell Count (×10⁻³/mm³)
Day since Presentation
E Lactate Dehydrogenase
Lactate Dehydrogenase (U/liter)
Day since Presentation
F Schistocytes
Schistocytes (%)
Day since Presentation
G Gross Appearance of the Patient's Plasma Sample
Recombinant ADAMTS13
12 13 14 15 16 17 18 19 20 21 22 23 24 25 26
Days since Presentation

FIGURE S3

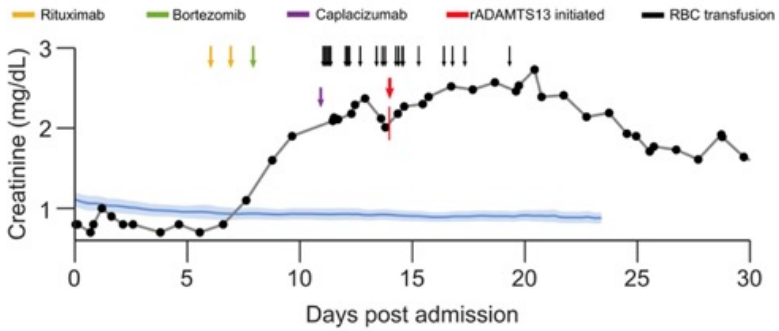

Figure S3. Creatinine Trend in our Patient. Serial daily measurements of serum creatinine in our patient are shown (black), with the timepoints of key therapies depicted as described in the legend. The blue line and shaded region represent the mean ± 95% CI creatinine trajectory for 102 consecutive iTTP cases in the Harvard TMA Research Collaborative dataset.

FIGURE S4

Days since Admission	12	16	17	18	32	36	39	46	51	72	126	193	230
On rADAMTS13	No	Yes	Yes	Yes	Yes	Yes	Yes	Yes	No	No	No	No	No
VWF Activity	49	139	104	42	163	143	143	162	158	184	167	156	136
VWF Antigen	68	159	146	82	169	144	138	167	164	175	169	149	132
Ratio	0.72	0.87	0.71	0.51	0.96	0.99	1.04	0.97	0.96	1.05	0.99	1.05	1.03

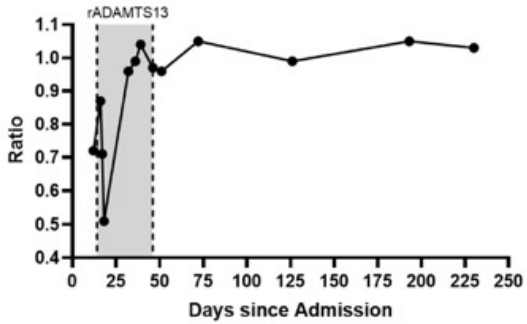

Figure S4. von Willebrand Factor (vWF) Testing in Relation to Therapy with rADAMTS13. The table (top) depicts results of vWF testing during and after therapy with rADAMTS13. The ratio of vWF activity to vWF antigen was graphed according to the day since admission, with the period of rADAMTS13 therapy shaded in gray (bottom). We measured vWF antigen and activity using the ELISA and vWF:GPIbM assays, respectively, as described in the Supplementary Methods.

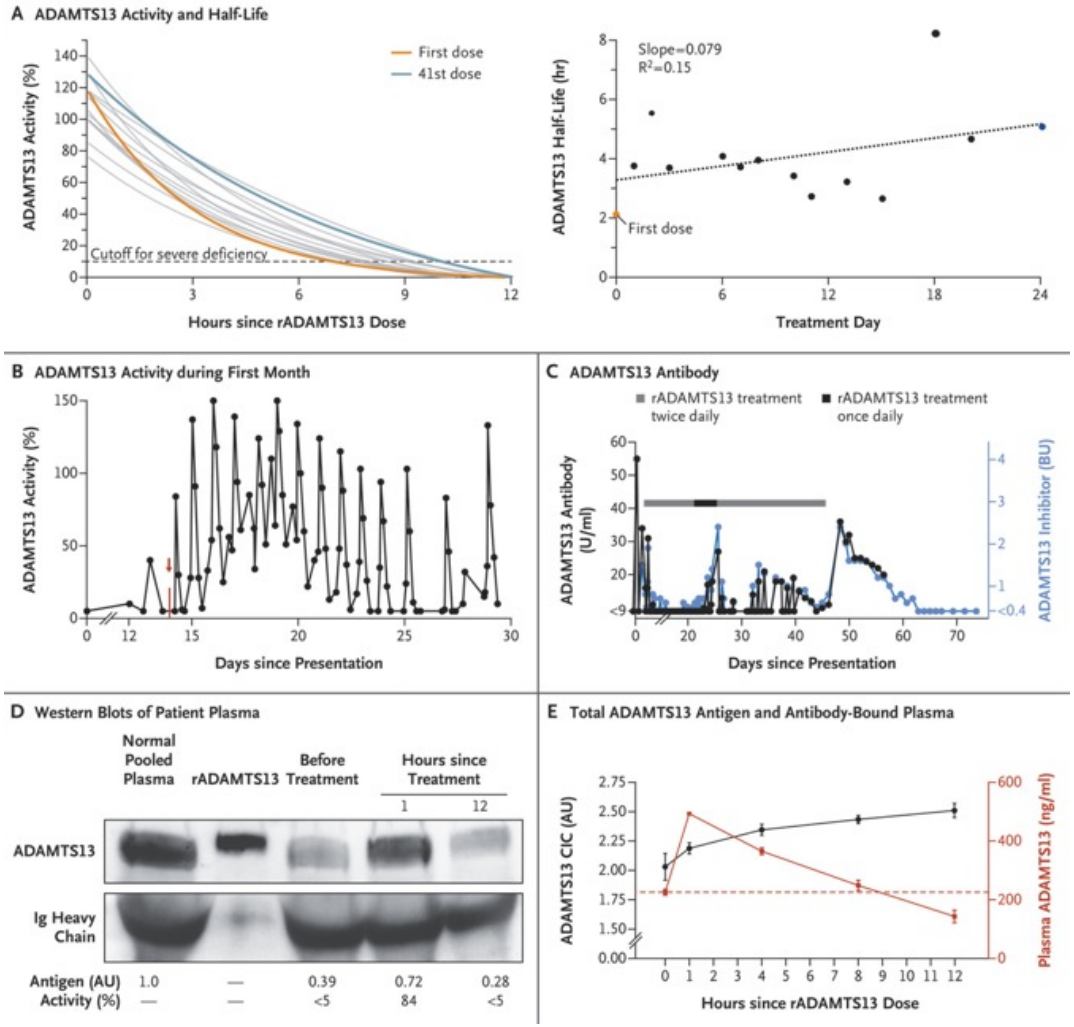

FIGURE S6

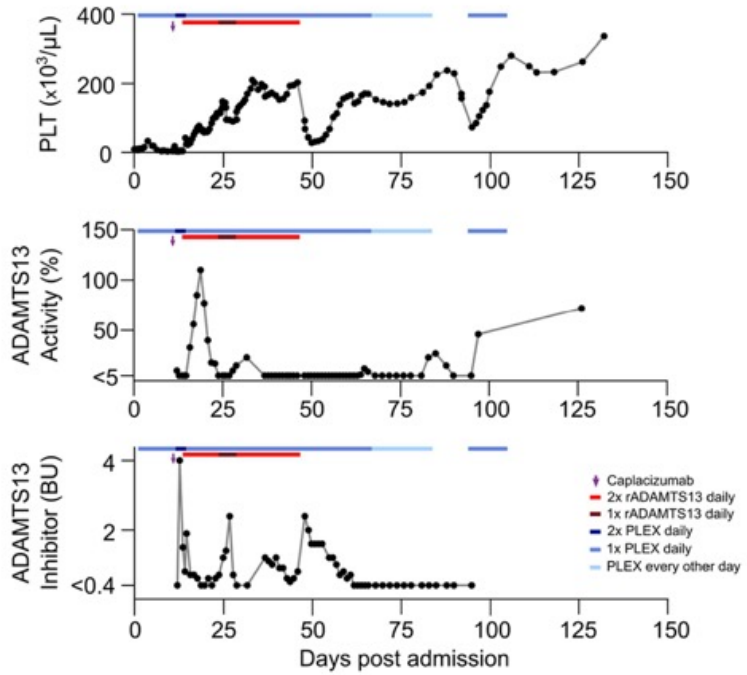

Figure S6. Relationship between ADAMTS13 Activity and Inhibitor Levels, Platelet Count, and iTTP Therapies. ADAMTS13 activity and inhibitor values represent trough levels drawn at the conclusion of a 12-hour rADAMTS13 dosing interval and immediately prior to daily plasma exchange. Once daily platelet counts drawn with morning phlebotomy are shown.

Discussion

We describe the use of rADAMTS13 as a novel salvage therapy in a patient with iTTP with multiorgan dysfunction and clinical deterioration despite daily plasma exchange. The administration of rADAMTS13 was followed by prompt improvement in our patient's clinical picture and the achievement of a full recovery.

During her acute illness, our patient had a decreased ratio of von Willebrand factor activity to antigen, which suggests the presence of a mild acquired abnormality in von Willebrand factor. Although studies have shown that rADAMTS13 may cause a temporary decrease in high-molecular-weight multimer levels in patients with congenital TTP during remission, we found that the relative loss of high-molecular-weight multimers of von Willebrand factor in plasma seemed to be primarily due to the known sequestration of high-molecular-weight forms in the microcirculation in patients with acute iTTP. Accordingly, rADAMTS13 proved to be safe under the conditions we tested, and initiation of rADAMTS13 was associated with platelet-count recovery and cessation of our patient's clinically significant vaginal and gastrointestinal hemorrhages. The apparent safety of rADAMTS13 may be due to its relative selectivity for the open form of von Willebrand factor unraveled under shear stress, conformational regulation of ADAMTS13 function, and the blunting of ADAMTS13 activity by autoantibody.

In this study, we obtained clinical, pharmacokinetic, and pharmacodynamic proof of concept that rADAMTS13 can add substantial value in the treatment of iTTP that is refractory to plasma exchange despite the presence of anti-ADAMTS13 autoantibodies. On the basis of these results, data from well-designed randomized, controlled trials may help to determine whether rADAMTS13 should serve as an adjunct to, or replacement for, the current standard of care with plasma exchange in patients with iTTP.

Physiological Integration of Taste and Metabolism

“You don’t know what you’re missing till it’s gone” is a truism that certainly applies to taste. It took a pandemic for taste to get attention. Severe acute respiratory syndrome coronavirus 2 (SARS-CoV-2) infections can cause acute loss or distortions of taste as a result of infection within taste buds and, in some cases, can result in long-term taste dysfunction. Since chemosensory disorders can substantially dampen a person’s enjoyment of life, this is an opportune time to appreciate recent advances in our understanding of taste. It is time to let go of old ideas, such as the myth of the tongue taste map (which persists in the collective consciousness despite decades of research debunking it) and the notion of taste as limited to the mouth. Research reveals that downstream signaling of extraoral taste receptors regulates our physiological balance long after conscious gustation has faded.

PHYSIOLOGICAL INTEGRATION OF TASTE AND METABOLISM

- The tongue taste map that we all learned in school is wrong; taste receptor cells responsive to each of the tastes are present in taste buds across the tongue.
- Tastant signal transduction machinery is also expressed in nontaste tissue, including enteroendocrine cells.
- Obesity may be related, in part, to disruptions in neural pathways that encourage reward-related eating and suppress homeostatic feedback that curbs hunger.
- Nonnutritive sweeteners have paradoxically been associated with an increase in obesity in the general population, possibly related to an uncoupling of sweet perception from energy sensing.
- In general, animals and people prefer nutritive sugars over nonnutritive sweeteners, a preference related, in part, to the added stimulation by sugars of sodium–glucose cotransporter 1 (SGLT1) signaling and vagal afferents that function as reward neurons.

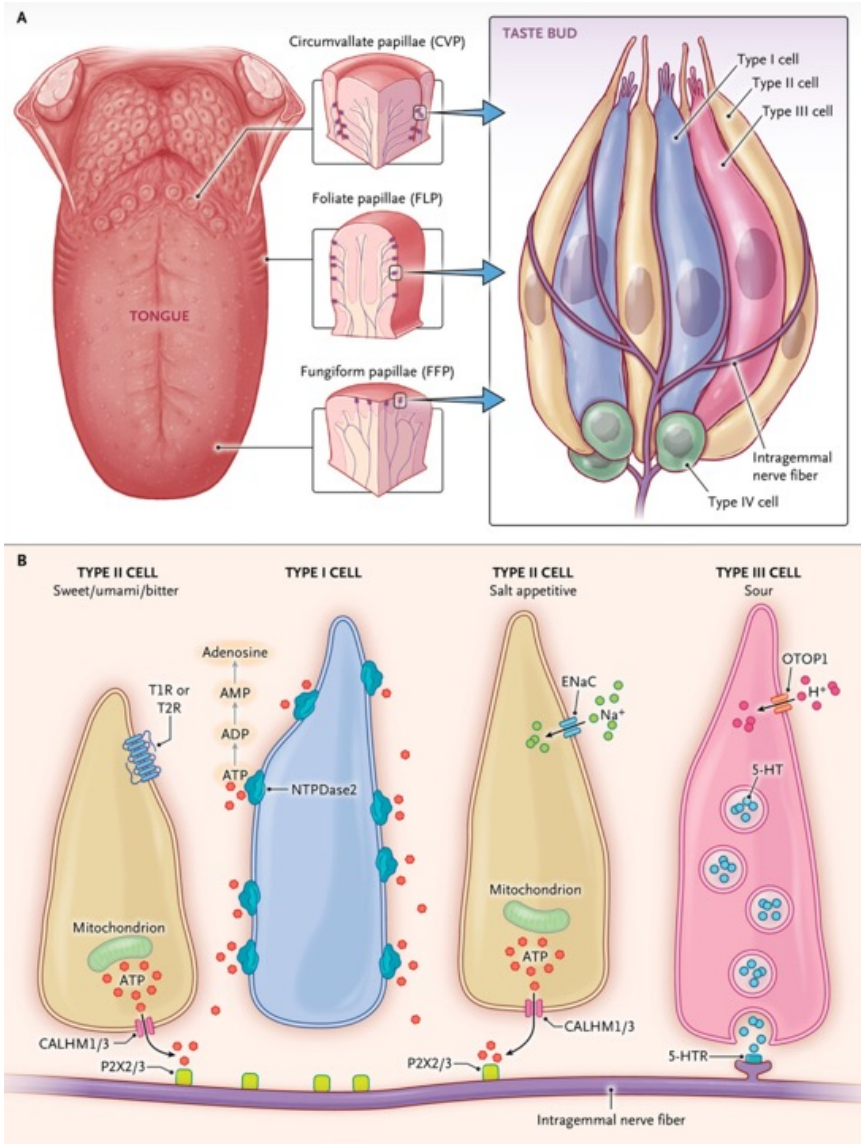

Taste receptor cells (TRCs) are morphologically classified into types I, II, and III, which can be subclassified on the basis of differences in TRC function, molecular markers, or both.

In taste buds, glial-type type I TRCs support the structure of the buds. On the plasma membranes of these cells, the enzyme NTPDase2 degrades intragemmal ATP secreted by type II cells in response to tastants. Type II TRCs detect sweet, umami, and bitter tastants through subfamilies of G protein–coupled receptors (GPCRs): the TAS1R (TAS1R1, TAS1R2, and TAS1R3) and TAS2R classes. These taste receptors initiate intracellular signal transduction by stimulating the heterotrimeric G protein α-gustducin. The resulting cascade follows a common downstream pathway, involving phospholipase $C\beta_2$, inositol triphosphate (IP_3) production, which causes Ca^{2+} release from the endoplasmic reticulum, followed by Ca^{2+}-dependent activation of transient receptor potential melastatin 5 (TRPM5) channels and culminating in cell depolarization and ATP release through specialized channels (CALHM1/3).[6] ATP is a bona fide TRC neurotransmitter that activates purinergic receptors on nerve fibers, which then transduce tastant information to the brain.

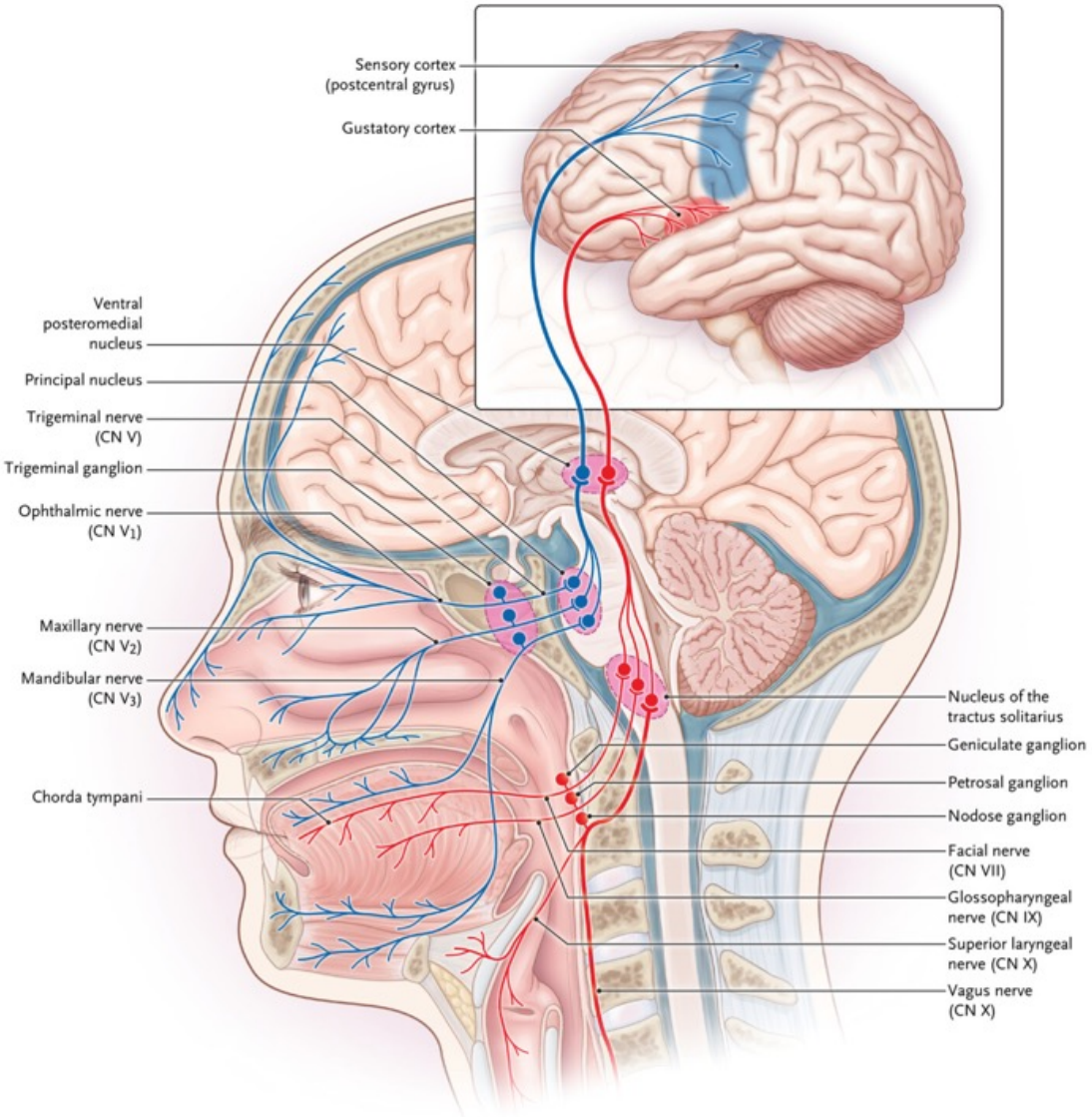

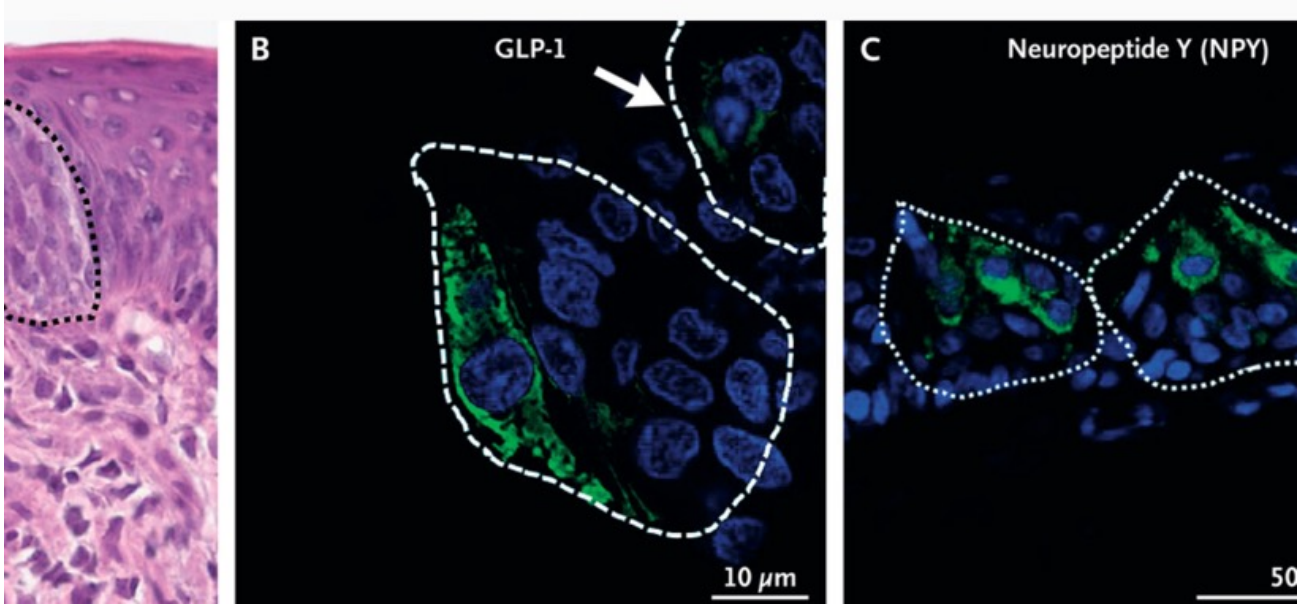

Adding to the orchestration of taste perception are the hormones produced in TRCs that modulate TRC signaling. Hormones produced by enteroendocrine cells of the gut (cholecystokinin, glucagon-like peptide 1 [GLP-1], ghrelin, peptide YY, and vasoactive intestinal peptide) and islets of Langerhans (glucagon and insulin), as well as by some central nervous system neurons (neuropeptide Y and vasoactive intestinal peptide), are also synthesized in TRCs.[25] More work is needed to uncover all their functions in taste buds, but so far we know that receptors for some of those hormones, such as GLP-1, are present on the intragemmal nerve fibers in taste buds where GLP-1 receptor (GLP-1R) activation in mice modulates sweet perception.

Role of Taste in Food Intake, Metabolism, and Obesity

Obesity and obesity-related noncommunicable diseases are at epidemic levels, with one projection forecasting that by 2030, nearly 1 in 2 adults in the United States will be obese. Although there are many contributing factors, those relevant to this review concern the ways in which the contemporary food environment, with its cornucopia of appetitive offerings, encourages overeating by stimulating our deeply ingrained reward systems. Taste, by guiding us toward gastronomic delights (i.e., tasty, energy-containing food) and away from dangerous toxins, functions as an evolutionary gatekeeper for the substances that enter our body. Sweet preference is innate, developed well before birth, and consuming sweet tastants triggers satisfaction through central reward pathways. Studies in humans have shown both immediate and delayed dopamine signaling in response to palatable food, which suggests that reward pathways respond to oral sensation and postingestive processing in the gut. There is even some evidence suggesting that sugar can be addictive in the same way that nicotine is.

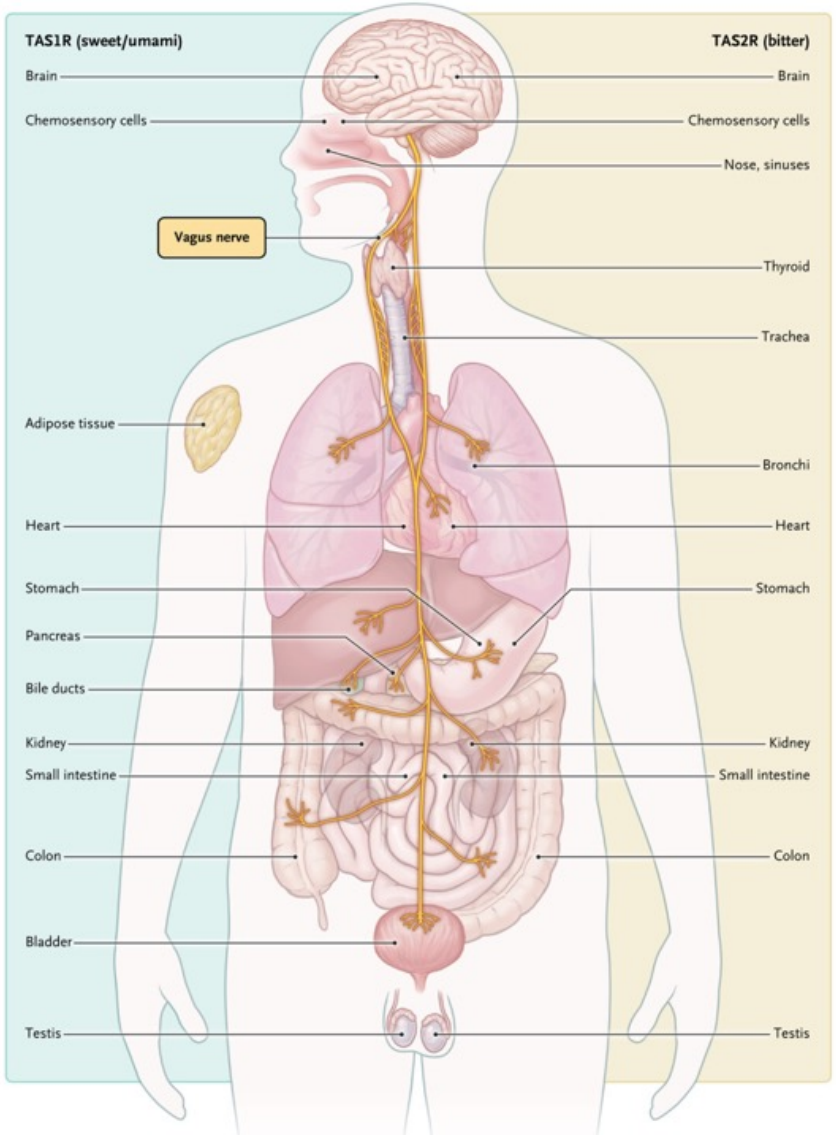

Metabolic Consequences of Nonnutritive Sweeteners

As studies implicated added sugars in the rising incidence of cardiovascular disease, diabetes, and obesity, public health messaging began recommending restrictions on sugar intake, and food manufacturers sought sugar substitutes. One proposed mechanism for how consumption of nonnutritive sweeteners induces metabolic dysfunction is an uncoupling of sweet taste from caloric value. The seminal studies on this mechanism showed that mice that had been conditioned to associate sweetness with calories gained less weight and consumed less food than mice that could not rely on sweet taste to predict caloric value.

Recent work has drawn a distinction between two glucose-sensing pathways: the traditional TAS1R sweet tasting pathway and the pathway involving SGLTs, which transport glucose but not nonnutritive sweeteners. Studies exploring differential brain responses in mice have identified distinct neural pathways for sweet sensing as compared with energy sensing and have shown how prolonged activation of reward pathways in the brain leads to compulsive sucrose consumption. Even in flies, a high-fat, high-sugar diet impairs central processing of sweet taste, weakening satiation and encouraging overeating.

Common Sugars, Sweeteners, and Amino Acids and Proteins Known to Taste Sweet to Humans.

Sugars

Glucose
Fructose
Maltose
Sucrose
Galactose

Nonnutritive and low-calorie sweeteners

Aspartame
Acesulfame potassium (Ace-K)
Sucralose
Neotame
Advantame
Saccharin
Cyclamate
Alitame
Certain steviol glycosides
Mogrosides: extracts from *Siraitia grosvenorii* (monk fruit, also known as Swingle fruit or luo han guo)

Sweet-tasting amino acids and proteins

D-phenylalanine
D-serine
D-tryptophan
Monellin
Brazzein
Thaumatin

Taste, the Vagus, and the Enteroendocrine System

Despite the competing mechanistic theories, the evidence thus far supports the notion that nonnutritive sweeteners and natural sugars elicit distinct homeostatic and hedonic responses in the body. Therefore, it is more accurate to call nonnutritive sweeteners simulacra of sugars, not sugar substitutes. TRC machinery in extraoral tissues, especially the gut, and physiological mechanisms of tastant binding have been "sweet" avenues for exploring the unique effects of sugars as compared with nonnutritive sweeteners. The latter have been linked to gut epithelial-cell death and increased gut-wall permeability and to alterations in the composition of the gastrointestinal microbiota (affecting pathways such as those involved in purine metabolism, glycolysis, and fatty acid synthesis), which have potential downstream consequences for hormone secretion, metabolic homeostasis, and obesity. More directly, rodent studies suggest that activation of the sweet taste receptors in the gut by sugars and nonnutritive sweeteners is linked to hormonal up-regulation and increased SGLT1 expression, glucose transporter 2 (GLUT2) induction, and glucose absorption.

Conclusions

The physiology of taste provides insight into our relationship with food and our metabolic well-being. Research has long dispelled the taste map myth and is now venturing into new territory, providing a complex understanding of how tastants activate hedonic and homeostatic pathways and a recognition of the gut's involvement in food intake. This knowledge may, in turn, inform updates to dietary guidelines and clinical practice guidelines for what constitutes an ideal diet.

Polyarteritis Nodosa

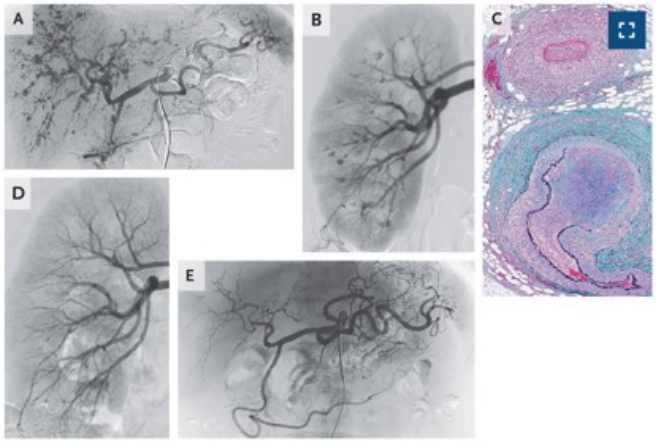

A 62-year-old man presented to the hospital with a 1-month history of muscle aches and weakness in the anterior thighs and the lower posterior aspect of both legs and weight loss of 10 kg. On physical examination, there was numbness of the anterior thighs and posterior lower legs but no skin changes or abdominal tenderness. Laboratory tests showed elevated levels of inflammatory markers. Findings on computed tomography of the chest, abdomen, and pelvis were unremarkable. Tests for antineutrophil cytoplasmic antibodies and hepatitis B were negative. Owing to concern about polyarteritis nodosa, abdominal angiography was performed and revealed aneurysms and irregularity of the vessel walls in the axes of the celiac artery (Panel A), inferior mesenteric artery, and renal arteries (Panel B, right kidney). Treatment with oral glucocorticoids and cyclophosphamide was initiated. Ten days later, a bowel perforation developed. Histopathological examination of a resected segment of the transverse colon showed neutrophilic infiltration and fibrinoid necrosis of the walls of medium-size arteries, as well as disruption of the internal elastic lamina (Panel C, elastin stain). A final diagnosis of polyarteritis nodosa was made. During a prolonged postoperative hospital course, an intraabdominal abscess was treated and immunosuppression therapy was adjusted. At follow-up 5 months after presentation, angiography showed resolution of the vascular changes (Panel D [renal artery, right kidney] and Panel E [celiac artery axis]).

Lymphatic Filariasis

A healthy 72-year-old man who had emigrated from Zimbabwe 20 years previously presented to the dermatology clinic with a 17-year history of swelling of the penis, scrotum, and left leg. During a recent hospitalization, nonpitting edema of the left leg had been noted, and a urinary catheter had been placed temporarily (Panel A). At the current presentation, there was nonpitting edema of the penis and scrotum (Panel B), as well as ongoing swelling of the left leg. Laboratory testing showed an eosinophil count of 500 per cubic millimeter (normal range, 0 to 300). Magnetic resonance imaging of the pelvis showed swelling of the scrotal tissues on both sides; no hydrocele was present. An enzyme-linked immunosorbent assay and an indirect fluorescent antibody test for *Wuchereria bancrofti* were positive. A blood smear to identify microfilariae was not obtained. A diagnosis of chronic lymphatic filariasis — a mosquito-borne parasitic infection in which nematodes invade the lymphatic system — was made. The patient was treated initially with a course of doxycycline and single-dose albendazole. Single-dose diethylcarbamazine was given later, after tests for concomitant onchocerciasis and loiasis returned negative. Diethylcarbamazine administration is contraindicated in patients with lymphatic filariasis and concomitant onchocerciasis or loiasis owing to the risk of severe adverse reactions from the rapid killing of microfilariae. At follow-up 2 months after the completion of treatment, the patient's symptoms had resolved.

CASE RECORDS OF THE MASSACHUSETTS GENERAL HOSPITAL

Case 14-2024: A 30-Year-Old Woman with Back Pain, Leg Stiffness, and Falls

A 30-year-old woman was evaluated in the neurology clinic of this hospital because of back pain and leg stiffness.

The patient had been in her usual state of health until 3 years before the current presentation, when stiffness in the back and upper legs developed abruptly while she attempted to rise from a seated position. She also began to have associated low back pain that worsened with bending the knees or climbing stairs. During the next several months, back and leg stiffness waxed and waned; at times, the patient could walk normally and engage in running for exercise, and at other times, she was unable to walk because her knees felt as though they had "locked up." Two months after the onset of symptoms, the patient fell and broke her right arm. She perceived the fall as being unusual in that after she tripped, she was unable to prevent herself from falling because of tension in her legs. After the fall, the patient underwent physical therapy for several months, but she did not resume running for exercise because of a fear of falling.

Two and a half years before the current presentation, the patient was evaluated in a rheumatology clinic of another hospital. Passive flexion of the left knee was guarded, but the knee bent when a distraction technique was used; the remainder of the examination was normal. Hip and knee radiographs were reportedly unremarkable. The knee stiffness was not thought to be due to an underlying rheumatologic disorder.

Magnetic resonance imaging (MRI) of the lumbar spine, performed without the administration of intravenous contrast material, showed normal paraspinal soft tissues and exaggeration of the normal lumbar lordosis, with preserved vertebral height. A loss of normal signal intensity was noted in the L4–L5 intervertebral disk space on T2-weighted images, a finding that was consistent with mild degeneration. Evaluation for signal abnormality in the visible portion of the spinal cord and in the cauda equina nerve roots could not be assessed owing to severe motion artifact. There was no evidence of high-grade spinal canal or foraminal stenosis.

Treatment with cyclobenzaprine, which was to be taken as needed at night for back pain, was initiated, and physical therapy was recommended. However, after 3 months of physical therapy, the back pain had not abated, and the leg stiffness had worsened. The patient sought evaluation in the neurology clinic of this hospital.

In the neurology clinic, the patient reported ongoing leg stiffness and rigidity that caused gait abnormalities. She noticed jerking movements at night as she was falling asleep. Three months before the current evaluation, she had taken lorazepam for claustrophobia before entering the MRI machine for spinal imaging, and her gait was reportedly normal for several hours after imaging.

On examination, the temporal temperature was 36.6°C, the blood pressure 141/91 mm Hg, the pulse 100 beats per minute, the respiratory rate 16 breaths per minute, and the oxygen saturation 98% while the patient was breathing ambient air. The body-mass index (the weight in kilograms divided by the square of the height in meters) was 21.7. The patient appeared anxious but was in no acute distress. Strength was assessed as normal in the arms and legs. She had mildly increased tone in the legs; no fasciculations were present. Deep-tendon reflexes were 2+ in the arms and 3+ in the legs, with nonsustained clonus in the ankles. An exaggerated startle response was present. Sensation was normal. On ambulation, there was reduced flexion of the knees and a wide-based gait.

Blood levels of electrolytes were normal, as were the results of tests of kidney function. The blood level of creatine kinase was 33 U per liter (reference range, 26 to 192), the C-reactive protein level 1 mg per liter (reference range, 0 to 10), and the erythrocyte sedimentation rate 2 mm per hour (reference range, 0 to 20). Imaging studies were obtained.

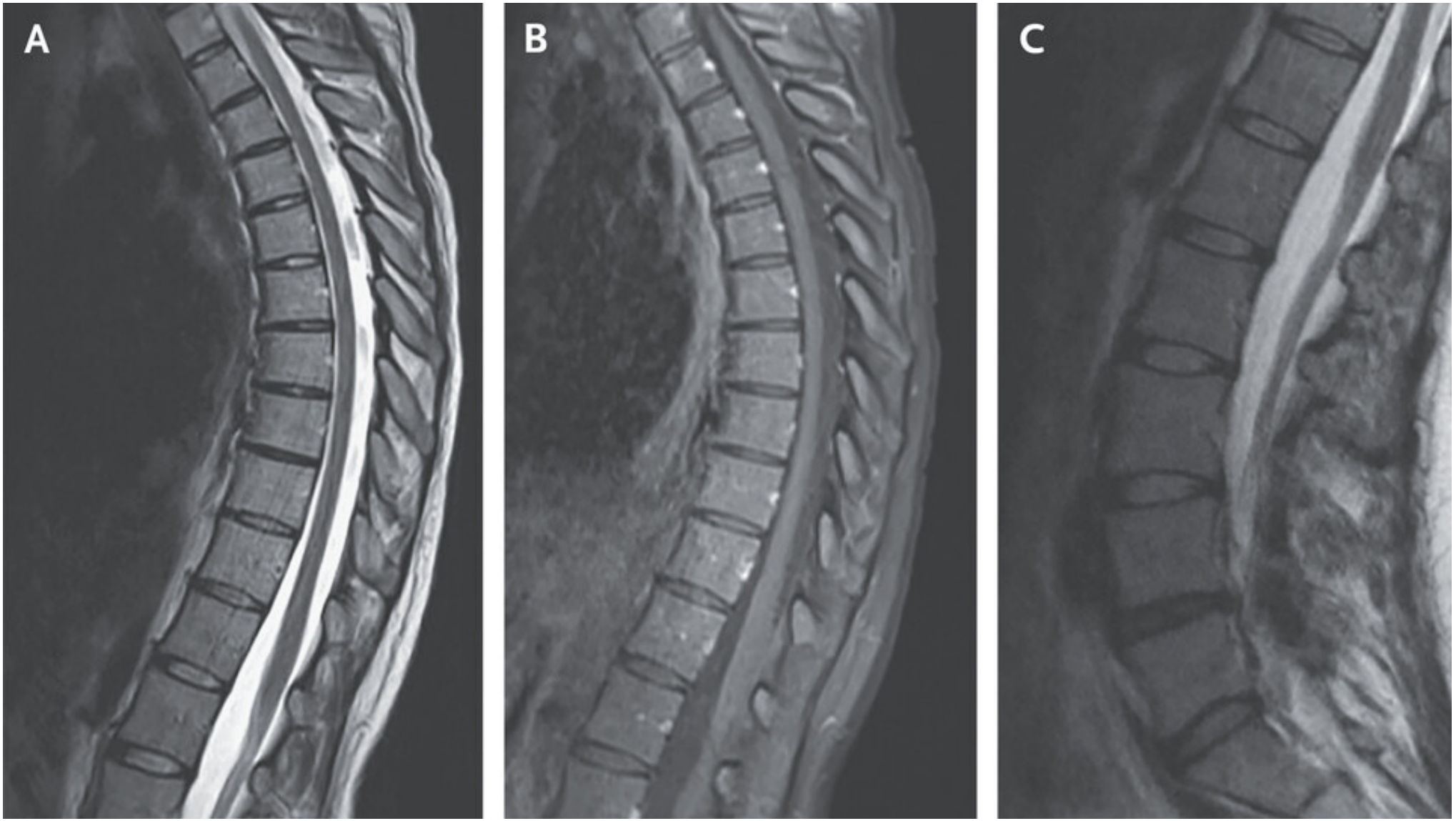
A
B
C

Disorder	Triggers for Stiffness	Alleviating Factors	Key Neurologic Examination Findings
Myotonia congenita	Prolonged rest before movement Cold temperature	Ongoing activity ("warm-up" phenomenon)	Generalized muscular hypertrophy Action myotonia Percussion myotonia
Paramyotonia congenita	Repeated exercise Cold temperature	Warm temperature	Generalized muscular hypertrophy Action myotonia
Peripheral nerve hyperexcitability	Activity	Rest	Fasciculations Myokymia
Dystonia	Varies with specific syndrome; some are task-specific (e.g., writer's cramp or musician's dystonia) and others are provoked by certain posture	A "geste antagoniste" (i.e., a sensory trick in which a simple, tactile, nonforceful action is directed toward the affected body part)	Observation of the abnormal movements or postures
Paroxysmal kinesigenic dyskinesia	Abrupt changes in movement Anxiety Stress Startle response	Aging	Observation of the abnormal movements or postures
Stiff-person syndrome	Sudden voluntary movement Physical touch Cold temperature Emotional upset Startle response	Use of benzodiazepines	Palpable rigidity of paraspinal and abdominal muscles Simultaneous contraction of agonist and antagonist muscle pairs Lumbar hyperlordosis Exaggerated startle response Increased deep-tendon reflexes

Peripheral Nervous System Disorder

Most peripheral nervous system disorders associated with muscle symptoms cause muscle weakness rather than muscle stiffness. Myotonic disorders are notable exceptions.

Central Nervous System Disorder

Stiffness is more common with central nervous system disorders than with peripheral nervous system disorders. Spasticity is a disorder that is characterized by increased muscle tone due to upper motor neuron dysfunction.

Dystonia

Dystonia describes sustained or intermittent muscle contractions that cause abnormal movements and postures that are often repetitive.

Hyperekplexia

An important clue to the patient's diagnosis may be found in the description of her falls. Her legs stiffened in response to an unexpected physical stimulus — after unexpectedly striking her leg on a coffee table, she was unable to control her leg movements and could not protect herself from falling and striking her face on the floor. Hyperekplexia is a group of genetic disorders that is characterized by an exaggerated myoclonic startle response, although rare acquired forms have been described.

Stiff-Person Syndrome

Stiff-person syndrome is an adult-onset, acquired autoimmune disorder that is associated with stiffness, gait dysfunction with falls, and an exaggerated startle response. Symptoms result from impaired γ-aminobutyric acid (GABA)–mediated inhibition of alpha motor neurons in the spinal cord and brain, which leads to hyperactivity. Stiffness and painful muscle spasms are the primary symptoms. In patients with classic stiff-person syndrome, stiffness begins in the paraspinal and abdominal muscles and progresses to involve the proximal legs. Sudden voluntary movement, physical touch, cold temperature, emotional upset, and startle response can all provoke painful spasms, which often occur in clusters. The combination of stiffness and superimposed spasms can lead to falls during which persons are unable to brace themselves.

The median age at onset of stiff-person syndrome is between 35 and 40 years, and this patient's symptoms started when she was 27 years of age. More than 50% of persons with stiff-person syndrome have a history of other autoimmune conditions, with up to 30% having type 1 diabetes mellitus. This patient had a history of vitiligo, eczema, alopecia areata, Graves' disease, and immune thrombocytopenia.

Laboratory Diagnosis

Glutamic acid decarboxylase 65 autoantibody–associated stiff-person syndrome.

Discussion of Management

If testing for GAD65 autoantibodies had been negative in this patient, I would have considered testing for autoantibodies against glycine receptor, amphiphysin, or dipeptidyl-peptidase–like protein 6, given her clinical presentation, which was characteristic of stiff-person syndrome. In addition, electromyography could have been performed to assess for the presence of continuous motor-unit activity in the paraspinal muscles or the presence of simultaneous contraction of agonist and antagonist muscle pairs.

A multidisciplinary approach is beneficial in the management of stiff-person syndrome. In this patient, physical therapy (including aqua therapy) had been recommended. Data to guide physical therapy approaches in patients with stiff-person syndrome are limited; the goals of therapy for this patient included flexibility, pain relief, and functional mobility. With regard to drug therapy, relief of symptoms can often occur after treatment with benzodiazepines or muscle relaxants, usually at high doses. In patients with severe symptoms or in those who have adverse side effects from drug therapies, immunotherapy with intravenous immune globulin may be beneficial. Anxiety or a fear of falling is typical of patients with stiff-person syndrome and can worsen the symptoms of the disease. Management includes medications, psychotherapy, and mindfulness-based approaches.

After a discussion with the patient about treatment options, the patient elected to start treatment with diazepam for relief of her symptoms, in addition to physical therapy and psychotherapy. At a follow-up visit 1 month later, she reported marked improvement in ambulation and in her ability to climb and descend stairs, as well as improvement in her ability to participate in physical activities. This improvement was sustained over the course of the next year with adjustments in the diazepam dose and in ongoing multidisciplinary care.

Approximately 2 years after diagnosis, the patient began to have worsening of symptoms with an increased fear of falling. Treatment with intravenous immune globulin was initiated, and her symptoms abated.

Der intravaskuläre Ultraschall (IVUS) erlaubt über eine invasive Untersuchung mit Einbringen eines kleinen Ultraschallkatheters in das Koronargefäß eine genaue morphologische Bilddarstellung der Gefäße bzw. auch von Engstellen.

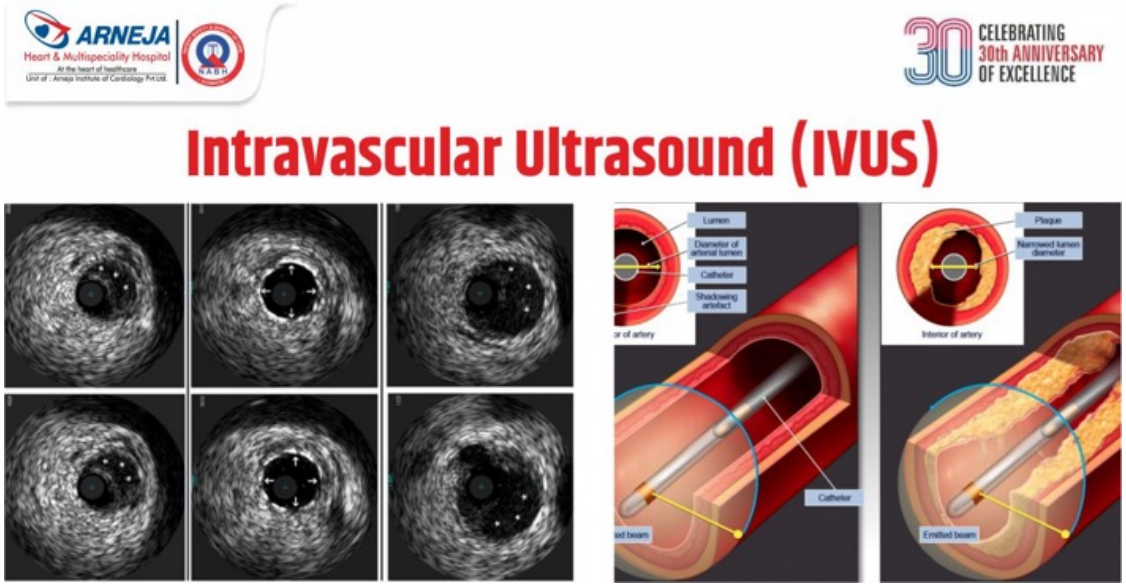

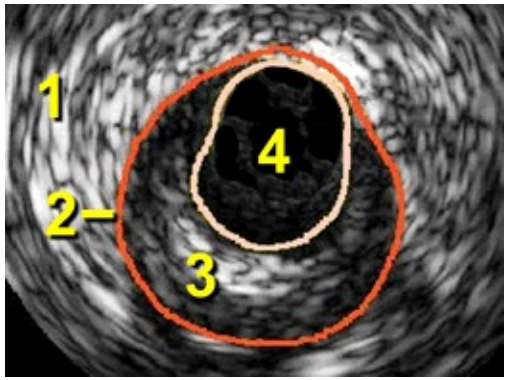

Intravascular ultrasound-guided versus angiography-guided percutaneous coronary intervention in acute coronary syndromes (IVUS-ACS): a two-stage, multicentre, randomised trial

Summary

Background Intravascular ultrasound-guided percutaneous coronary intervention has been shown to result in superior clinical outcomes compared with angiography-guided percutaneous coronary intervention. However, insufficient data are available concerning the advantages of intravascular ultrasound guidance for patients with an acute coronary syndrome. This trial aimed to investigate whether the use of intravascular ultrasound guidance, as compared with angiography guidance, improves the outcomes of percutaneous coronary intervention with contemporary drug-eluting stents in patients presenting with an acute coronary syndrome.

Methods In this two-stage, multicentre, randomised trial, patients aged 18 years or older and presenting with an acute coronary syndrome at 58 centres in China, Italy, Pakistan, and the UK were randomly assigned to intravascular ultrasound-guided percutaneous coronary intervention or angiography-guided percutaneous coronary intervention. Patients, follow-up health-care providers, and assessors were masked to random assignment; however, staff in the catheterisation laboratory were not. The primary endpoint was target vessel failure, a composite of cardiac death, target vessel myocardial infarction, or clinically driven target vessel revascularisation at 1 year after randomisation. This trial is registered at ClinicalTrials.gov, NCT03971500, and is completed.

Findings Between Aug 20, 2019 and Oct 27, 2022, 3505 patients with an acute coronary syndrome were randomly assigned to intravascular ultrasound-guided percutaneous coronary intervention (n=1753) or angiography-guided percutaneous coronary intervention (n=1752). 1-year follow-up was completed in 3504 (>99·9%) patients. The primary endpoint occurred in 70 patients in the intravascular ultrasound group and 128 patients in the angiography group (Kaplan-Meier rate 4·0% *vs* 7·3%; hazard ratio 0·55 [95% CI 0·41–0·74]; p=0·0001), driven by reductions in target vessel myocardial infarction or target vessel revascularisation. There were no significant differences in all-cause death or stent thrombosis between groups. Safety endpoints were also similar in the two groups.

Interpretation In patients with an acute coronary syndrome, intravascular ultrasound-guided implantation of contemporary drug-eluting stents resulted in a lower 1-year rate of the composite outcome of cardiac death, target vessel myocardial infarction, or clinically driven revascularisation compared with angiography guidance alone.

Introduction

Most percutaneous coronary interventions in the USA and Europe are guided by angiography. The low resolution of angiography and its inability to provide insight beyond the coronary artery lumen[1] led to the development of intravascular ultrasound and optical coherence tomography to provide more precise lesion assessment, stent size selection, and evaluation of stent expansion, vessel wall apposition, and lesion coverage.[2–5] Randomised trials and meta-analyses have shown reductions in composite adverse outcomes with intravascular imaging-guided percutaneous coronary intervention compared with angiography-guided intervention.[2–5]

Most patients with an acute coronary syndrome present with coronary thrombosis after disruption of a lipid-rich plaque,[6] and stenting such lesions entails greater procedural risks compared with chronic stable lesions.[7] Although the prognosis of patients with an acute coronary syndrome is improved by percutaneous coronary intervention,[7] adverse outcomes from the intervention, including death, myocardial infarction, and stent thrombosis, are higher in patients with an acute coronary syndrome than in patients with chronic coronary syndrome.[8] Some registry studies have suggested that major adverse cardiac events in patients with an acute coronary syndrome could be reduced by implantation of contemporary drug-eluting stents guided by intravascular ultrasound.[9–13] To date, only three small randomised trials have compared intravascular imaging-guided percutaneous coronary intervention with optical coherence tomography-guided versus angiography-guided percutaneous coronary intervention for patients with an acute coronary syndrome, all with inconclusive results;[14–16] no dedicated randomised trial of intravascular ultrasound-guided percutaneous coronary intervention has been reported in this patient population. Consequently, international guidelines do not currently recommend intravascular imaging guidance during percutaneous coronary intervention for patients with an acute coronary syndrome.[17,18] We therefore conducted this large-scale randomised trial to compare intravascular ultrasound-guided percutaneous coronary intervention versus angiography-guided intervention in this patient population.

Procedures

Percutaneous coronary intervention for lesions responsible for the acute coronary syndrome (culprit lesions) was performed during the index procedure using standard techniques as per the discretion of the operator. If other non-culprit lesions were present, their treatment was also recommended during the same procedure. If percutaneous coronary intervention for non-culprit lesions could not be completed during the index procedure, a second percutaneous coronary intervention procedure was allowed 2–3 days before discharge and followed the originally assigned intravascular ultrasound versus angiography guidance strategy.

In the group assigned to intravascular ultrasound-guided guidance, intravascular ultrasound was done with the Opticross catheter (Boston Scientific, Marlborough, MA, USA) and was recommended before percutaneous coronary intervention and mandatory after percutaneous coronary intervention for assessment of whether criteria for optimal stent implantation were achieved.[2,3,5] For lesions with a TIMI flow of 0–1 or patients with critical (ie, >90% of diameter stenosis but TIMI flow 2–3) disease and tenuous haemodynamics (ie, large infarct with hypotension), pre-dilation using a small balloon (usually 1·5–2·0 mm) was mandatory before the pre-percutaneous coronary intervention intravascular ultrasound. The target criteria for non-left main lesions were minimal stent area of more than 5·0 mm² or more than 90% of the minimal lumen area at the distal reference segment; plaque burden of less than 55% within 5 mm proximal or distal to the stent edge; and absence of medial dissection over 3 mm in length. For left main lesions, the target minimal stent area was more than 10 mm² for the left main segment, more than 7 mm² for the ostial or proximal left anterior descending artery and more than 6 mm² for the ostial or proximal left circumflex artery (if stented).[5] For both non-left main and left main lesions, all criteria had to be present to declare optimal stent implantation. Intravascular ultrasound use was not permitted in patients assigned to angiography guidance unless the operator believed it was essential for lesion selection, in which case intravascular ultrasound was used only before percutaneous coronary intervention. Use of optical coherence tomography was not permitted in either group unless the IVUS catheter could not cross the lesion. All patients received dual antiplatelet therapy consisting of oral aspirin (100 mg daily) plus oral ticagrelor (90 mg, twice daily) for 30 days after percutaneous coronary intervention and before the second-stage randomisation for the ULTIMATE-DAPT trial.

Angiograms and intravascular ultrasounds before and after percutaneous coronary intervention procedures were analysed by independent core laboratories. Measurements were assessed in the target lesion responsible for the acute coronary syndrome as assessed by the operator (appendix 2 pp 9–10). Follow-up visits were scheduled for 1, 4, 6, and 12 months after discharge. Angiographic follow-up was done only for clinical indications.

Outcomes

The primary endpoint was target vessel failure, a composite of cardiac death, target vessel myocardial infarction, or clinically driven target vessel revascularisation, assessed at 12 months after the first randomisation. Secondary endpoints consisted of the individual components of the primary endpoint (ie, cardiac death, target vessel myocardial infarction, clinically driven target vessel revascularisation), target vessel failure without procedural myocardial infarction, target lesion revascularisation, Bleeding Academic Research Consortium (BARC)-defined types 3 or 5 bleeding, and Academic Research Consortium (ARC)-defined definite or probable stent thrombosis (appendix 2 pp 11–14). In brief, cardiac death was defined as any death due to a proximate cardiac cause (eg,

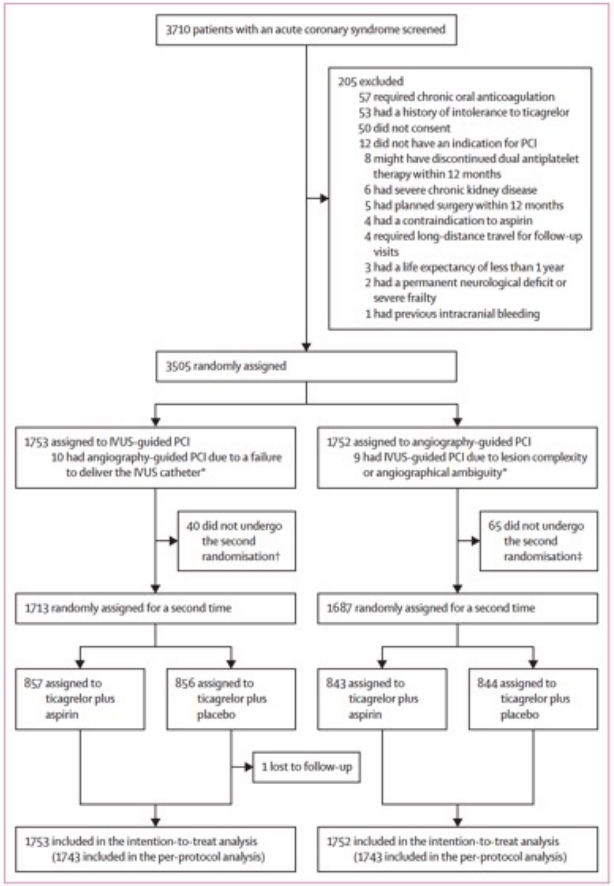

Figure 1: **Trial profile of the integrated IVUS-ACS and ULTIMATE-DAPT study programme**
All randomly assigned patients (n=3505) received open-label dual antiplatelet therapy (ticagrelor plus aspirin) for 30 days after PCI and before the second randomisation. BARC=Bleeding Academic Research Consortium. IVUS=intravascular ultrasound. PCI=percutaneous coronary intervention. *Ten patients in the intravascular ultrasound-guided percutaneous coronary intervention group had angiography-guided PCI instead, and nine patients in the angiography-guided percutaneous coronary intervention group had intravascular ultrasound-guided percutaneous coronary intervention instead; these 19 patients were included in the intention-to-treat population (all patients who underwent first randomisation) but were excluded from the per-protocol population. †40 patients did not undergo the second random assignment (two stopped DAPT for ≥48 h, nine had clinical events, five had BARC types 3 or 5 bleeding, five refused, 17 had dyspnea, one was allergic to ticagrelor, and one was lost-to follow-up). ‡65 patients did not undergo the second random assignment (six stopped DAPT for ≥48 h, ten had clinical events, nine had BARC types 3 or 5 bleeding, 12 refused, 23 had dyspnea, one was allergic to ticagrelor, and four needed chronic oral anticoagulation).

	Intravascular ultrasound-guided percutaneous coronary intervention (n=1753)	Angiography-guided percutaneous coronary intervention (n=1752)
Age (years)	62 (54–69)	63 (54–69)
Sex		
Male	1285 (73·3%)	1299 (74·1%)
Female	468 (26·7%)	453 (25·9%)
Race		
Chinese	1550 (88·4%)	1545 (88·2%)
Other	203 (11·6%)	207 (11·8%)
Initial presentation		
Unstable angina	699 (39·9%)	726 (41·4%)
Non-STEMI	570 (32·5%)	537 (30·7%)
STEMI	484 (27·6%)	489 (27·9%)
Medical history		
Hypertension	1103 (62·9%)	1089 (62·2%)
Diabetes	554 (31·6%)	551 (31·5%)
On insulin treatment	148 (8·4%)	145 (8·3%)
Dyslipidaemia	1187 (67·7%)	1222 (69·8%)
Current smoking*	499 (28·5%)	487 (27·8%)
Chronic kidney disease	132 (7·5%)	127 (7·3%)
Previous PCI	179 (10·2%)	179 (10·2%)
Previous CABG	4 (0·2%)	4 (0·2%)
Previous myocardial infarction	152 (8·7%)	154 (8·8%)
Previous stroke	142 (8·1%)	169 (9·7%)
Peripheral arterial disease	82 (4·7%)	83 (4·7%)
Heart failure	111 (6·3%)	106 (6·1%)
Left ventricular ejection fraction, %	62% (55–65)	62% (55–65)
Medications at discharge after percutaneous coronary intervention		
Aspirin	1753 (100%)	1752 (100%)
Ticagrelor	1753 (100%)	1752 (100%)
β blocker	857 (48·9%)	840 (48·0%)
ACEI or ARB	793 (45·2%)	812 (46·4%)
Calcium channel antagonist	468 (26·7%)	456 (26·0%)
Statin	1434 (81·8%)	1474 (84·1%)

Data are median (IQR), or n (%). ACEI=angiotensin converting enzyme inhibitor. ARB=angiotensin receptor blocker. CABG=coronary artery bypass graft surgery. PCI=percutaneous coronary intervention. STEMI=ST-segment elevation myocardial infarction. *Defined as ≥100 lifetime cigarettes and still smoking at the time of enrolment; other tobacco products were not included.

Table 1: **Baseline characteristics and medications at discharge**

	Intravascular ultrasound-guided percutaneous coronary intervention (n=1753)	Angiography-guided percutaneous coronary intervention (n=1752)	Hazard ratio (95% CI)	p value
Primary endpoint				
Target vessel failure*	70 (4·0%)	128 (7·3%)	0·55 (0·41–0·74)	0·0001
Secondary endpoints				
Target vessel failure without procedural myocardial infarction*	38 (2·2%)	90 (5·1%)	0·45 (0·30–0·66)	<0·0001
Cardiac death*	9 (0·5%)	20 (1·1%)	0·56 (0·24–1·29)	0·17
Target vessel myocardial infarction*	44 (2·5%)†	67 (3·8%)†	0·63 (0·43–0·92)	0·018
Procedural myocardial infarction	34 (1·9%)	42 (2·4%)	0·78 (0·50–1·22)	0·28
Non-procedural myocardial infarction	11 (0·6%)	26 (1·5%)	0·41 (0·20–0·84)	0·014
Clinically driven target vessel revascularisation*	24 (1·4%)	56 (3·2%)	0·44 (0·27–0·72)	0·0010
Clinically driven target lesion revascularisation*	22 (1·3%)	44 (2·5%)	0·52 (0·31–0·88)	0·014
Safety endpoints				
Definite or probable stent thrombosis	10 (0·6%)	16 (0·9%)	0·82 (0·35–1·90)	0·64
Definite stent thrombosis	5 (0·3%)	11 (0·6%)	0·51 (0·18–1·46)	0·21
Probable stent thrombosis	5 (0·3%)	5 (0·3%)	1·77 (0·36–8·65)	0·48
All-cause death	14 (0·8%)	26 (1·5%)	0·64 (0·32–1·27)	0·20
Major bleeding (BARC types 3 or 5)	18 (1·0%)	35 (1·9%)	0·58 (0·33–1·02)	0·06

Data are number (%) of events (Kaplan-Meier estimated percentage at 1 year), unless otherwise specified. BARC=Bleeding Academic Research Consortium. *Related to the acute coronary syndrome culprit lesion. †One patient in each group had both a procedure-related and non-procedure-related target vessel myocardial infarction.

Table 2: **Primary, secondary, and safety endpoints at 1 year**

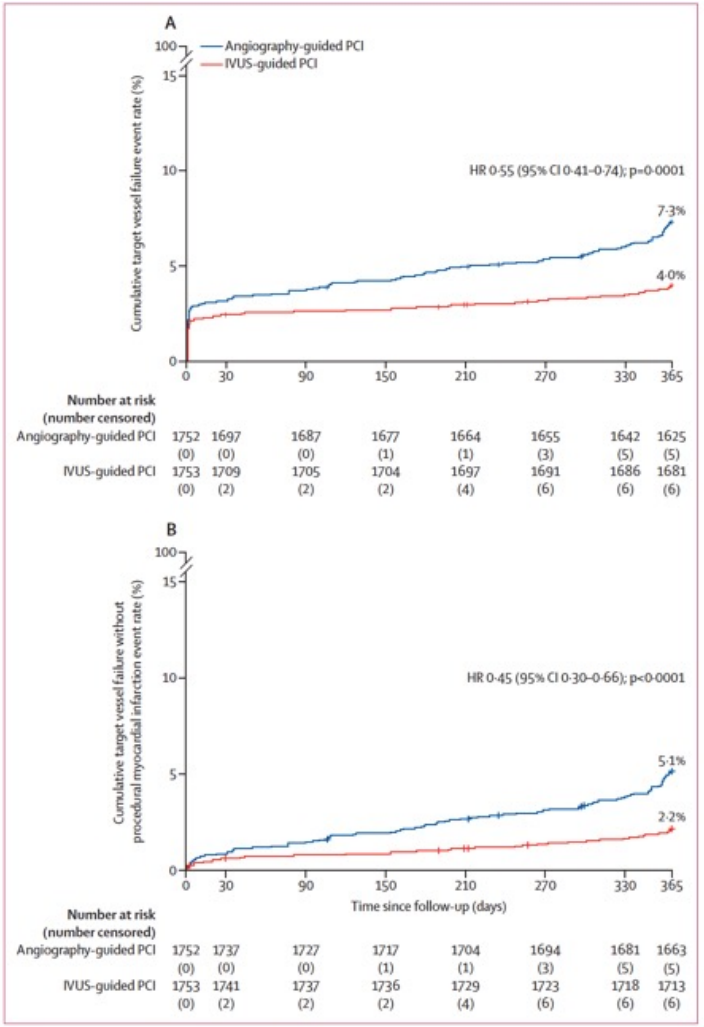

Figure 2: **Cumulative incidence of target vessel failure**
(A) The primary endpoint was target vessel failure, defined as the composite of death from cardiac causes, target vessel myocardial infarction, or clinically driven target vessel revascularisation in the intention-to-treat population through 1 year of follow-up. (B) The secondary endpoint of target vessel failure excluding procedural myocardial infarction. HR=hazard ratio. IVUS=intravascular ultrasound. PCI=percutaneous coronary intervention.

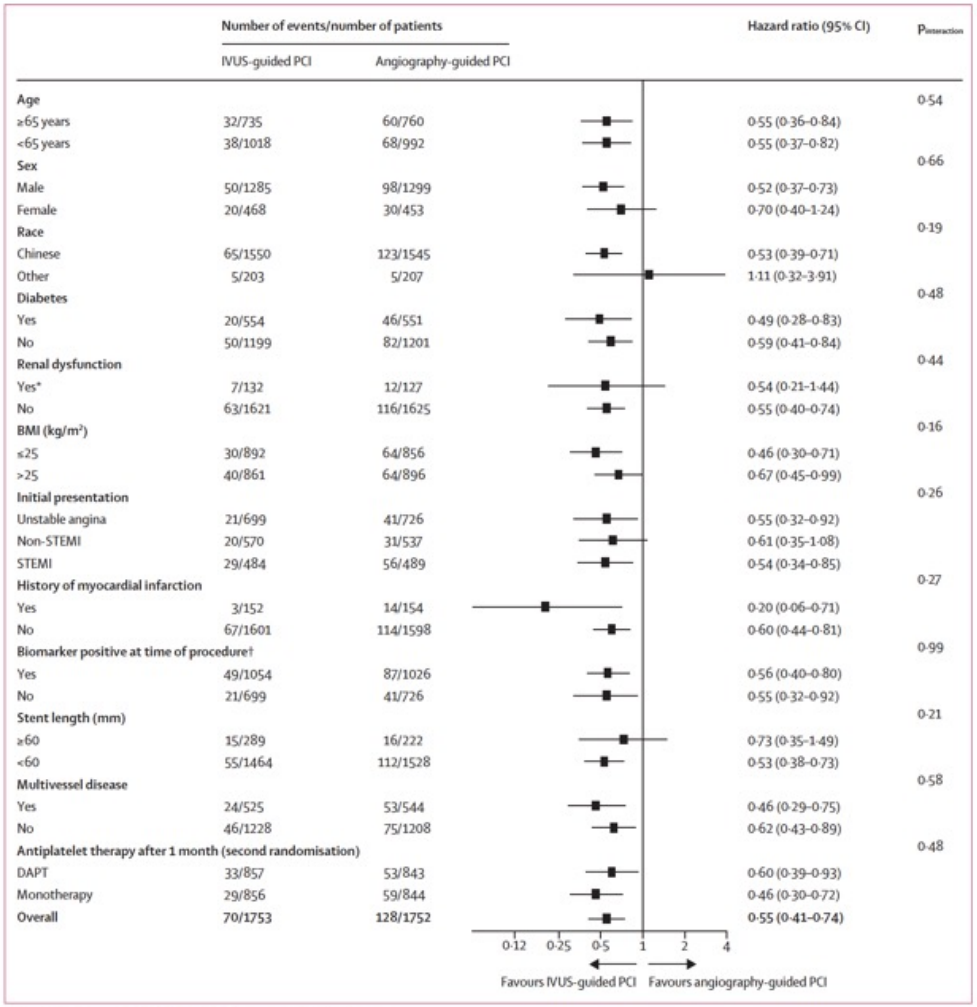

Figure 3: **Subgroup analysis for the primary endpoint at 1 year**

The hazard ratio for the primary endpoint of target vessel failure at 1 year was consistent across 12 prespecified subgroups, including acute coronary syndrome type and the second randomisation. Antiplatelet therapy between 1 month and 12 months represents the outcomes in event-free patients at 1-month after percutaneous coronary intervention who were randomised again to DAPT (ticagrelor plus aspirin) or ticagrelor plus placebo. DAPT=dual antiplatelet therapy. IVUS=intravascular ultrasound. PCI=percutaneous coronary intervention. STEMI=ST segment elevation myocardial infarction. *Defined as an estimated glomerular filtration rate <60 mL/min per 1·73 m². †Defined as either troponin or CK-NB >1 time increase.

Research in context

Evidence before this study

We searched PubMed using the search terms "intravascular ultrasound", "angiography", and "percutaneous coronary intervention" using MeSH terms and appropriate variations from Jan 1, 2010, to March 11, 2019, with no language restrictions, before designing our study. We found no previous randomised controlled trials that compared intravascular ultrasound-guided percutaneous coronary intervention with angiography-guided percutaneous coronary intervention for either an acute procedural success or clinical outcomes exclusively in patients with an acute coronary syndrome. Some, but not all, registry studies have suggested that major adverse cardiac events in patients with an acute coronary syndrome could be reduced with contemporary drug-eluting stents implanted with intravascular ultrasound guidance. Three small randomised trials of optical coherence tomography guidance compared with angiography guidance were previously done, but their results were inconclusive due to their small sample size.

Added value of this study

The present study is the first randomised controlled trial to compare intravascular ultrasound-guided versus angiography-guided percutaneous coronary intervention in a population composed exclusively of patients with an acute coronary syndrome. The study was conducted at 58 hospitals in four countries. The results show that implantation of contemporary drug-eluting stents with intravascular ultrasound guidance reduces the 1-year risk of target vessel failure compared with angiography guidance alone in these patients. The improvement was driven by fewer target vessel myocardial infarctions (especially during the follow-up period) and fewer repeat revascularisations with intravascular ultrasound guidance, with rates of survival and stent thrombosis similar between groups. Intravascular ultrasound guidance was safe, although the procedures were longer and slightly more contrast material was required—acceptable trade-offs for the lower risk of early and late major adverse cardiac events.

Implications of all the available evidence

The findings from the IVUS-ACS trial are consistent with those of previous studies in patients with a chronic coronary syndrome. Collectively, these data show that intravascular ultrasound-guided percutaneous coronary intervention improves clinical outcomes, including measures of both safety and effectiveness, across the spectrum of coronary artery disease and patient presentations (acute or non-acute coronary syndrome). Adverse events during follow-up are especially reduced in patients for whom prespecified intravascular ultrasound criteria for optimal stent implantation are achieved, including optimal stent expansion, lesion coverage, and freedom from major edge dissections.

Der Wirkstoff Ticagrelor gehört zur Gruppe der Thrombozytenaggregationshemmer und wird üblicherweise mit Acetylsalicylsäure kombiniert um atherothrombotischen Ereignissen wie einem Herzinfarkt präventiv entgegenzuwirken.

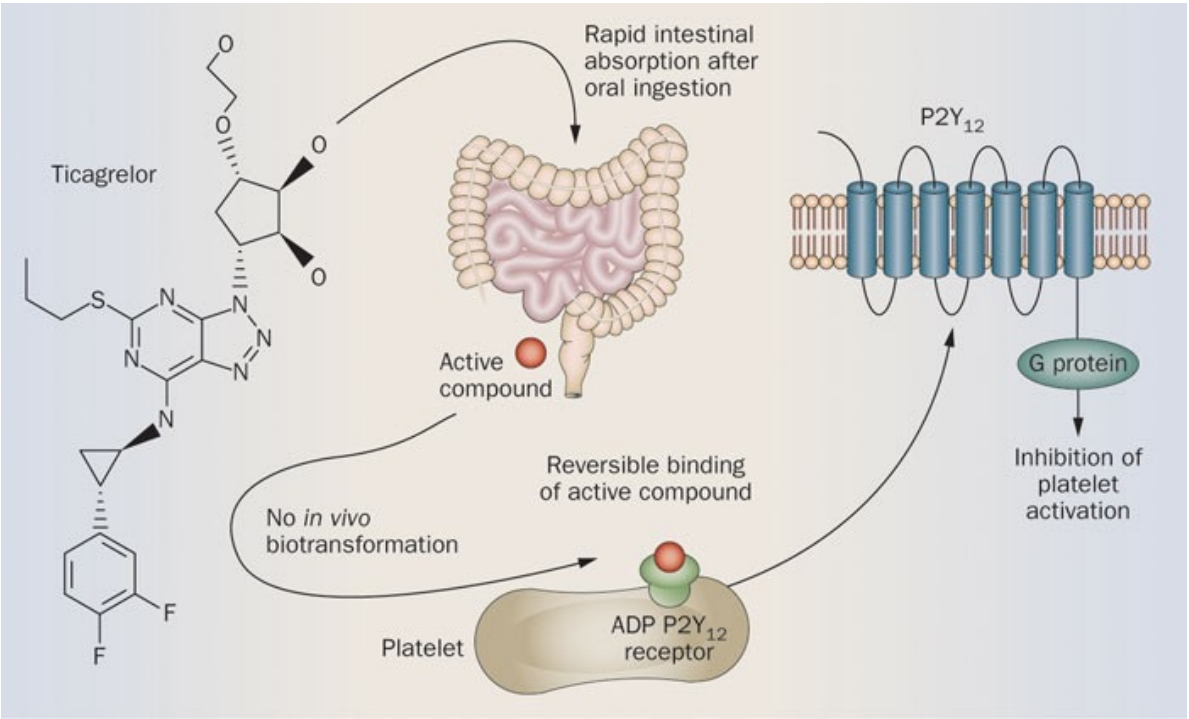

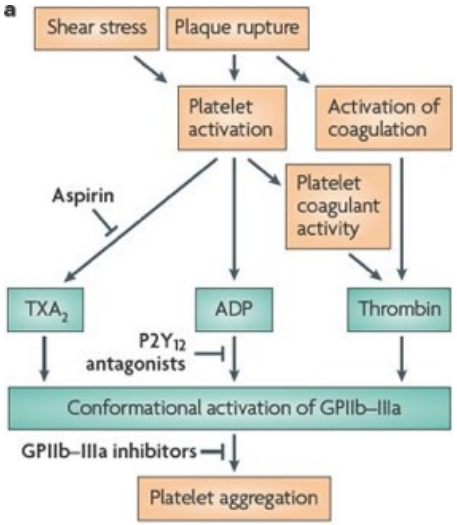

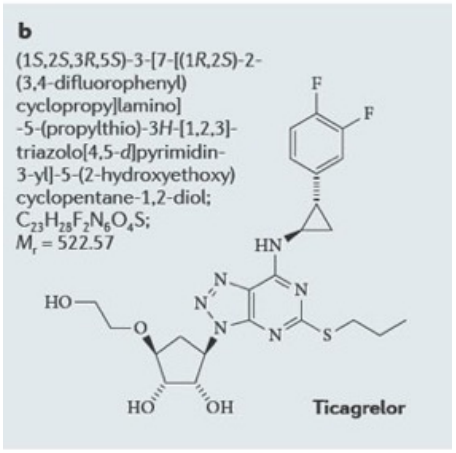

Nature Reviews | Drug Discovery

Wirkmechanismus

Ticagrelor ist ein selektiver, direkt wirkender und reversibler P2Y12-Rezeptorantagonist. Der natürliche Ligand des P2Y12-Rezeptors, Adenosindiphosphat (ADP), vermittelt über diesen die Thrombozytenaktivierung und folglich die Thrombozytenaggregation. Der Antagonismus durch Ticagrelor bewirkt demnach eine Thrombozytenaggregationshemmung. Ticagrelor verhindert allerdings nicht die Bindung von ADP an den P2Y12-Rezeptor, sondern blockiert in gebundener Form die ADP-induzierte Signalübertragung.

Ticagrelor unterscheidet sich pharmakologisch von anderen P2Y12-Rezeptorantagonisten, denn ältere Vertreter der Wirkstoffklasse wie Clopidogrel oder Prasugrel inhibieren den Rezeptor irreversibel. Eine Hemmung des equilibrativen Nukleosid-Transporters-1 (ENT-1) durch Ticagrelor erhöht zusätzlich lokale endogene Adenosin-Spiegel.

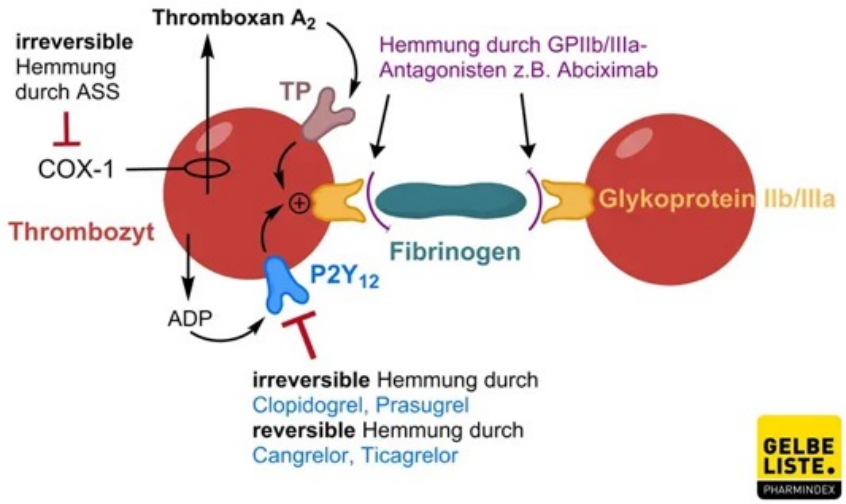

Ticagrelor alone versus ticagrelor plus aspirin from month 1 to month 12 after percutaneous coronary intervention in patients with acute coronary syndromes (ULTIMATE-DAPT): a randomised, placebo-controlled, double-blind clinical trial

Summary

Background Following percutaneous coronary intervention with stent placement to treat acute coronary syndromes, international clinical guidelines generally recommend dual antiplatelet therapy with aspirin plus a $P2Y_{12}$ receptor inhibitor for 12 months to prevent myocardial infarction and stent thrombosis. However, data on single antiplatelet therapy with a potent $P2Y_{12}$ inhibitor earlier than 12 months after percutaneous coronary intervention for patients with an acute coronary syndrome are scarce. The aim of this trial was to assess whether the use of ticagrelor alone, compared with ticagrelor plus aspirin, could reduce the incidence of clinically relevant bleeding events without an accompanying increase in major adverse cardiovascular or cerebrovascular events (MACCE).

Methods In this randomised, placebo-controlled, double-blind clinical trial, patients aged 18 years or older with an acute coronary syndrome who completed the IVUS-ACS study and who had no major ischaemic or bleeding events after 1-month treatment with dual antiplatelet therapy were randomly assigned to receive oral ticagrelor (90 mg twice daily) plus oral aspirin (100 mg once daily) or oral ticagrelor (90 mg twice daily) plus a matching oral placebo, beginning 1 month and ending at 12 months after percutaneous coronary intervention (11 months in total). Recruitment took place at 58 centres in China, Italy, Pakistan, and the UK. Patients were required to remain event-free for 1 month on dual antiplatelet therapy following percutaneous coronary intervention with contemporary drug-eluting stents. Randomisation was done using a web-based system, stratified by acute coronary syndrome type, diabetes, IVUS-ACS randomisation, and site, using dynamic minimisation. The primary superiority endpoint was clinically relevant bleeding (Bleeding Academic Research Consortium [known as BARC] types 2, 3, or 5). The primary non-inferiority endpoint was MACCE (defined as the composite of cardiac death, myocardial infarction, ischaemic stroke, definite stent thrombosis, or clinically driven target vessel revascularisation), with an expected event rate of 6·2% in the ticagrelor plus aspirin group and an absolute non-inferiority margin of 2·5 percentage points between 1 month and 12 months after percutaneous coronary intervention. The two co-primary endpoints were tested sequentially; the primary superiority endpoint had to be met for hypothesis testing of the MACCE outcome to proceed. All principal analyses were assessed in the intention-to-treat population. This trial is registered with ClinicalTrials.gov, NCT03971500, and is completed.

Findings Between Sept 21, 2019, and Oct 27, 2022, 3400 (97·0%) of the 3505 participants in the IVUS-ACS study were randomly assigned (1700 patients to ticagrelor plus aspirin and 1700 patients to ticagrelor plus placebo). 12-month follow-up was completed by 3399 (>99·9%) patients. Between month 1 and month 12 after percutaneous coronary intervention, clinically relevant bleeding occurred in 35 patients (2·1%) in the ticagrelor plus placebo group and in 78 patients (4·6%) in the ticagrelor plus aspirin group (hazard ratio [HR] 0·45 [95% CI 0·30 to 0·66]; p<0·0001). MACCE occurred in 61 patients (3·6%) in the ticagrelor plus placebo group and in 63 patients (3·7%) in the ticagrelor plus aspirin group (absolute difference –0·1% [95% CI –1·4% to 1·2%]; HR 0·98 [95% CI 0·69 to 1·39]; $p_{non\text{-}inferiority}<0·0001$, $p_{superiority}=0·89$).

Interpretation In patients with an acute coronary syndrome who had percutaneous coronary intervention with contemporary drug-eluting stents and remained event-free for 1 month on dual antiplatelet therapy, treatment with ticagrelor alone between month 1 and month 12 after the intervention resulted in a lower rate of clinically relevant bleeding and a similar rate of MACCE compared with ticagrelor plus aspirin. Along with the results from previous studies, these findings show that most patients in this population can benefit from superior clinical outcomes with aspirin discontinuation and maintenance on ticagrelor monotherapy after 1 month of dual antiplatelet therapy.

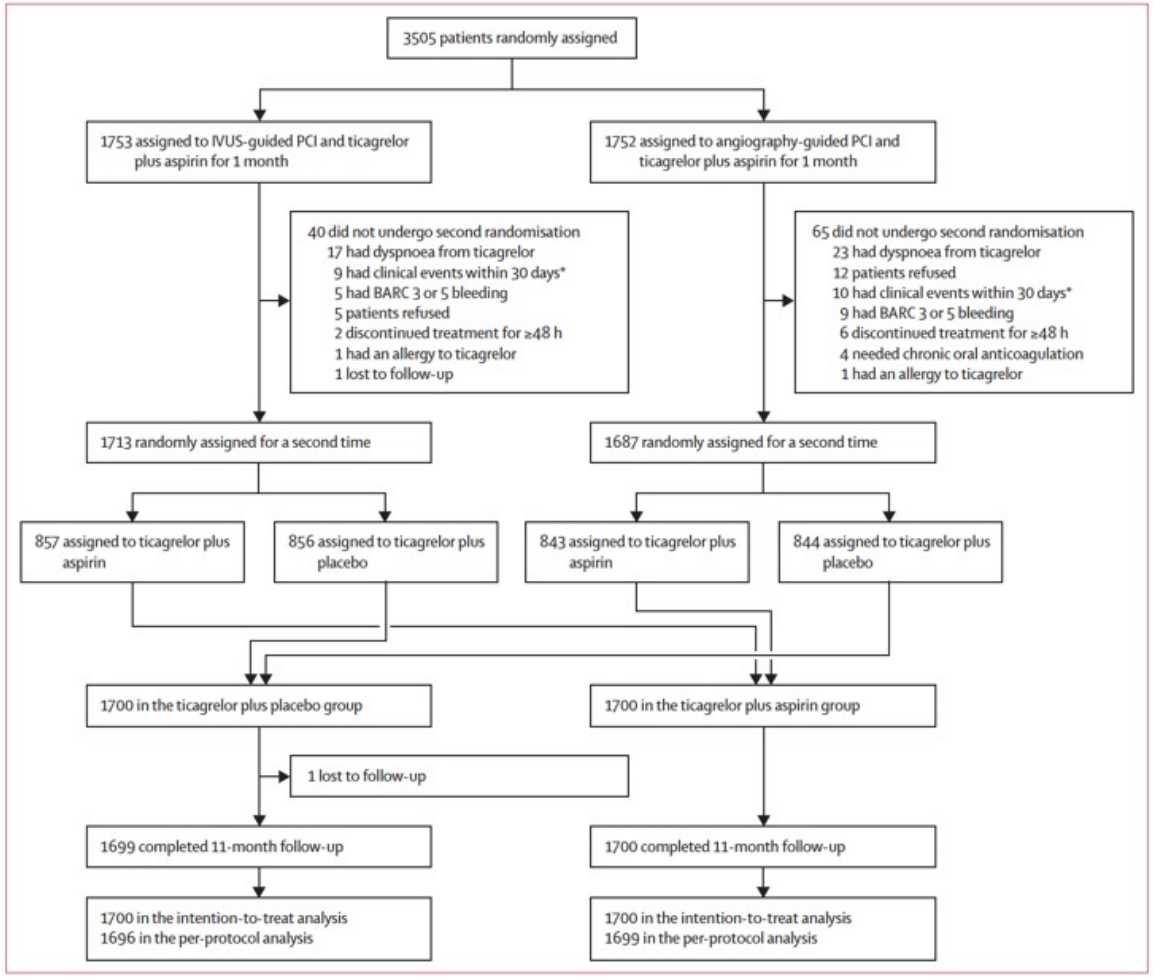

Figure 1: **Trial profile**

The intention-to-treat population included all randomly assigned patients, regardless of therapy received. The per-protocol population consists of all patients as randomised, excluding those who did not take their assigned treatment for at least 7 days (unless medication interruption or discontinuation was required for adverse events), or who did not comply with the medication schedule. BARC=Bleeding Academic Research Consortium. IVUS=intravascular ultrasound. PCI=percutaneous coronary intervention. *Clinically driven target vessel revascularisation, definite stent thrombosis, stroke, ST-segment elevation myocardial infarction, BARC 3 or 5 major bleeding, or death.

	Ticagrelor plus placebo (n=1700)	Ticagrelor plus aspirin (n=1700)
Age, years		
Median (IQR)	62 (54-70)	63 (54-69)
Sex		
Male	1264 (74·4%)	1257 (73·9%)
Female	436 (25·7%)	443 (26·1%)
Race		
Chinese	1476 (86·8%)	1519 (89·4%)
Other	224 (13·2%)	181 (10·7%)
Country of enrolment		
China	1476 (86·8%)	1519 (89·4%)
Pakistan	202 (11·9%)	159 (9·4%)
UK	12 (0·7%)	11 (0·7%)
Italy	10 (0·6%)	11 (0·7%)
Initial presentation		
Unstable angina	668 (39·3%)	708 (41·7%)
With ischaemic changes on electrocardiogram	650/668 (97·3%)	685/708 (96·8%)
Acute myocardial infarction	1032 (60·7%)	992 (58·4%)
Non-STEMI	545 (32·1%)	531 (31·2%)
STEMI	487 (28·7%)	461 (27·1%)
Killip class		
1	475/1032 (46·0%)	442/992 (44·6%)
2	457/1032 (44·3%)	468/992 (47·2%)
3	100/1032 (9·7%)	82/992 (8·3%)
Medical history		
Hypertension	1058 (62·2%)	1063 (62·5%)
Diabetes	540 (31·8%)	535 (31·5%)
Insulin-treated diabetes	136 (8·0%)	144 (8·5%)
Dyslipidaemia	1178 (69·3%)	1157 (68·1%)
Current smoking*	486 (28·6%)	482 (28·4%)
Chronic renal insufficiency†	119 (7·0%)	129 (7·6%)
Previous percutaneous coronary intervention	171 (10·1%)	174 (10·2%)
Previous coronary artery bypass graft surgery	2 (0·1%)	4 (0·2%)
Previous myocardial infarction	143 (8·4%)	156 (9·2%)
Previous stroke	154 (9·1%)	147 (8·7%)
Peripheral arterial disease	76 (4·5%)	79 (4·7%)
Heart failure	109 (6·4%)	101 (5·9%)
Left ventricular ejection fraction (%)‡		
Median (IQR)	62% (55–65)	63% (56–65)
Medication use at 1 month (the time of the second randomisation)		
Aspirin	1700 (100%)	1700 (100%)
Ticagrelor	1700 (100%)	1700 (100%)
β blocker	838 (49·3%)	802 (47·2%)
Angiotensin converting enzyme inhibitor or angiotensin receptor blocker	774 (45·5%)	788 (46·4%)
Calcium antagonist	430 (25·3%)	463 (27·2%)
Statin	1417 (83·4%)	1404 (82·6%)

Data are n (%) unless otherwise specified. STEMI=ST-segment elevation myocardial infarction. *Defined as ≥100 lifetime cigarettes and still smoking at the time of enrolment; other tobacco products were not included. †Defined as an estimated glomerular filtration rate of <60 mL/min per 1·73 m². ‡Includes baseline transthoracic echocardiographic measurements from 1496 patients in the ticagrelor plus placebo group and 1504 patients in the ticagrelor plus aspirin group.

Table 1: **Baseline characteristics and medication use**

	Ticagrelor plus placebo (n=1700)	Ticagrelor plus aspirin (n=1700)	Hazard ratio(95% CI)	p value
Primary endpoints				
Clinically relevant bleeding (BARC types 2, 3, or 5)	35 (2·1%)	78 (4·6%)	0·45 (0·30 to 0·66)	<0·0001
Major adverse cardiovascular or cerebrovascular events*	61 (3·6%)	63 (3·7%)	0·98 (0·69 to 1·39)	0·89†
Key secondary endpoint				
Net adverse clinical events	97 (5·7%)	140 (8·2%)	0·68 (0·53 to 0·88)	0·0066
Secondary bleeding endpoints				
Major bleeding (BARC types 3 or 5)	11 (0·7%)	28 (1·7%)	0·39 (0·19 to 0·79)	0·0087
TIMI major or minor bleeding	11 (0·7%)	27 (1·6%)	0·41 (0·20 to 0·82)	0·012
GUSTO moderate, severe, or life-threatening bleeding	8 (0·5%)	19 (1·1%)	0·42 (0·18 to 0·96)	0·041
ISTH major bleeding	8 (0·5%)	21 (1·2%)	0·38 (0·17 to 0·86)	0·020
Patients with any of the four secondary bleeding endpoints	11 (0·7%)	28 (1·7%)	0·39 (0·19 to 0·79)	0·0087
Patients with all four secondary bleeding endpoints	8 (0·5%)	19 (1·1%)	0·42 (0·18 to 0·96)	0·041
Secondary ischaemic events and mortality				
All-cause death	12 (0·7%)	13 (0·8%)	0·93 (0·42 to 2·03)	0·84
Cardiac death	8 (0·5%)	7 (0·4%)	1·15 (0·42 to 3·18)	0·46
Any stroke	20 (1·2%)	24 (1·4%)	0·83 (0·46 to 1·50)	0·54
Ischaemic	11 (0·7%)	15 (0·9%)	0·74 (0·34 to 1·61)	0·58
Haemorrhagic	4 (0·2%)	3 (0·2%)	1·33 (0·29 to 3·71)	0·71
Uncertain	5 (0·3%)	6 (0·4%)	0·97 (0·49 to 1·92)	0·94
Myocardial infarction	17 (1·0%)	11 (0·7%)	1·45 (0·67 to 3·23)	0·27
Procedural myocardial infarction	1 (0·1%)	1 (0·1%)	0·00 (–0·28 to 0·28)	0·88
Non-procedural myocardial infarction	16 (0·9%)	11 (0·7%)	1·42 (0·66 to 3·03)	0·29
Stent thrombosis	5 (0·3%)	5 (0·3%)	0·97 (0·28 to 3·40)	0·96
Definite	3 (0·2%)	5 (0·3%)	0·59 (0·14 to 2·51)	0·47
Probable	2 (0·1%)	0	..	..
Clinically driven revascularisation‡	40 (2·4%)	41 (2·4%)	0·99 (0·64 to 1·53)	0·95
Target vessel revascularisation	33 (2·0%)	36 (2·1%)	0·93 (0·58 to 1·49)	0·75
Target lesion revascularisation	27 (1·6%)	28 (1·7%)	0·97 (0·57 to 1·65)	0·92
Cardiac death, non-fatal myocardial infarction, or ischaemic stroke	31 (1·8%)	32 (1·9%)	0·98 (0·63 to 1·67)	0·91

Data are n (%) unless otherwise specified. Rates are number of events occurring between month 1 and month 12 after percutaneous coronary intervention (the second randomisation period), with Kaplan-Meier estimated percentages. BARC=Bleeding Academic Research Consortium. GUSTO=Global Utilization of Streptokinase and Tissue Plasminogen Activator for Occluded Arteries. ISTH=International Society on Thrombosis and Haemostasis. TIMI=Thrombolysis in Myocardial Infarction flow grading system. *The composite of cardiac death, myocardial infarction, ischaemic stroke, definite stent thrombosis, and clinically driven target vessel revascularisation. †p<0·0001 for non-inferiority for major adverse cardiovascular or cerebrovascular events. ‡For patients who had revascularisation, oral ticagrelor (90 mg twice daily) plus oral open-labelled aspirin (100 mg once daily) were prescribed after procedure.

Table 2: **Primary and secondary endpoints**

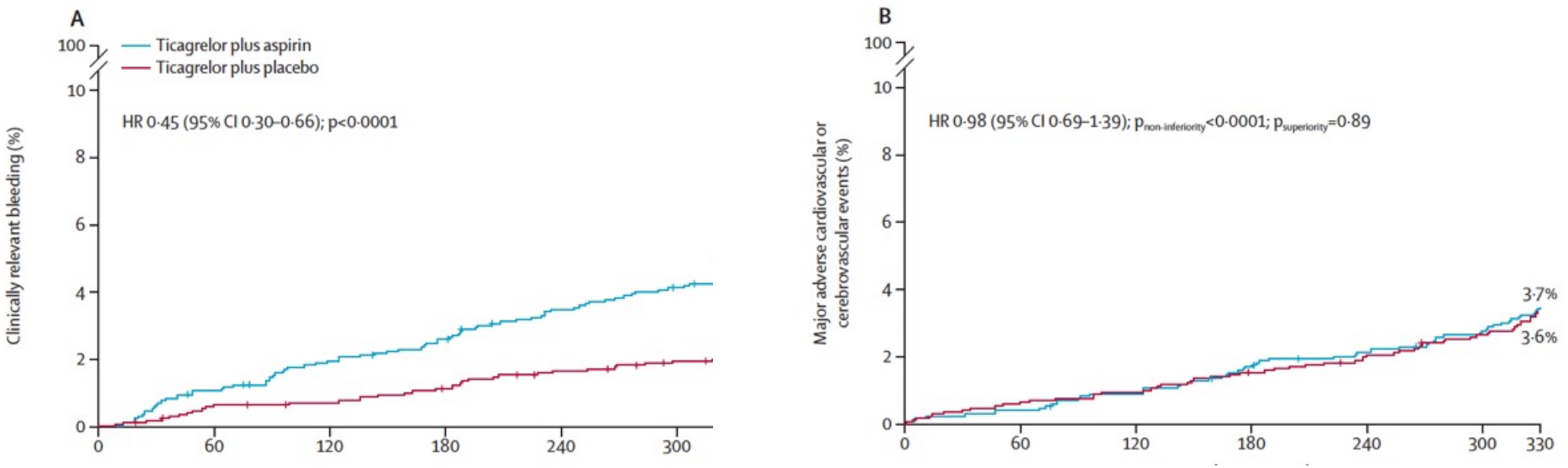

Figure 2: **Primary efficacy and safety outcomes during follow-up between 1 month and 12 months after percutaneous coronary intervention**

(A) The primary efficacy endpoint of clinically relevant bleeding, defined as BARC types 2, 3, or 5 bleeding, was assessed in the intention-to-treat population between 1 month and 12 months after percutaneous coronary intervention in patients who were event-free after 1 month of ticagrelor and aspirin. (B) The primary safety endpoint of major adverse cardiovascular or cerebrovascular events, which comprised cardiac death, myocardial infarction, ischaemic stroke, definite stent thrombosis, and clinically driven target vessel revascularisation, was assessed in the intention-to-treat population between 1 month and 12 months after percutaneous coronary intervention in patients who were event-free after 1 month of ticagrelor and aspirin. Patients treated with ticagrelor monotherapy from month 1 had similar rates of adverse ischaemic events as patients who were maintained on ticagrelor plus aspirin. BARC=Bleeding Academic Research Consortium. HR=hazard ratio.

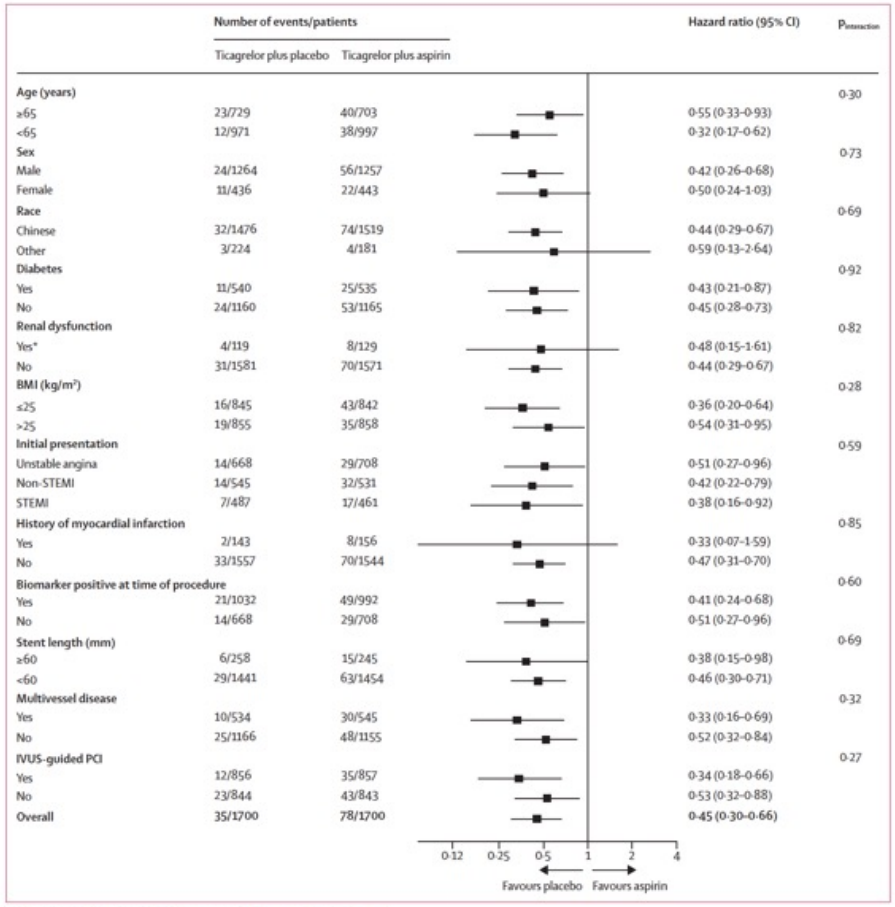

Figure 3: **Clinically relevant bleeding events in prespecified subgroups**
IVUS=intravascular ultrasound. PCI=percutaneous coronary intervention. STEMI=ST-segment elevation myocardial infarction. *Defined as an estimated glomerular filtration rate <60 mL/min per 1·73 m².

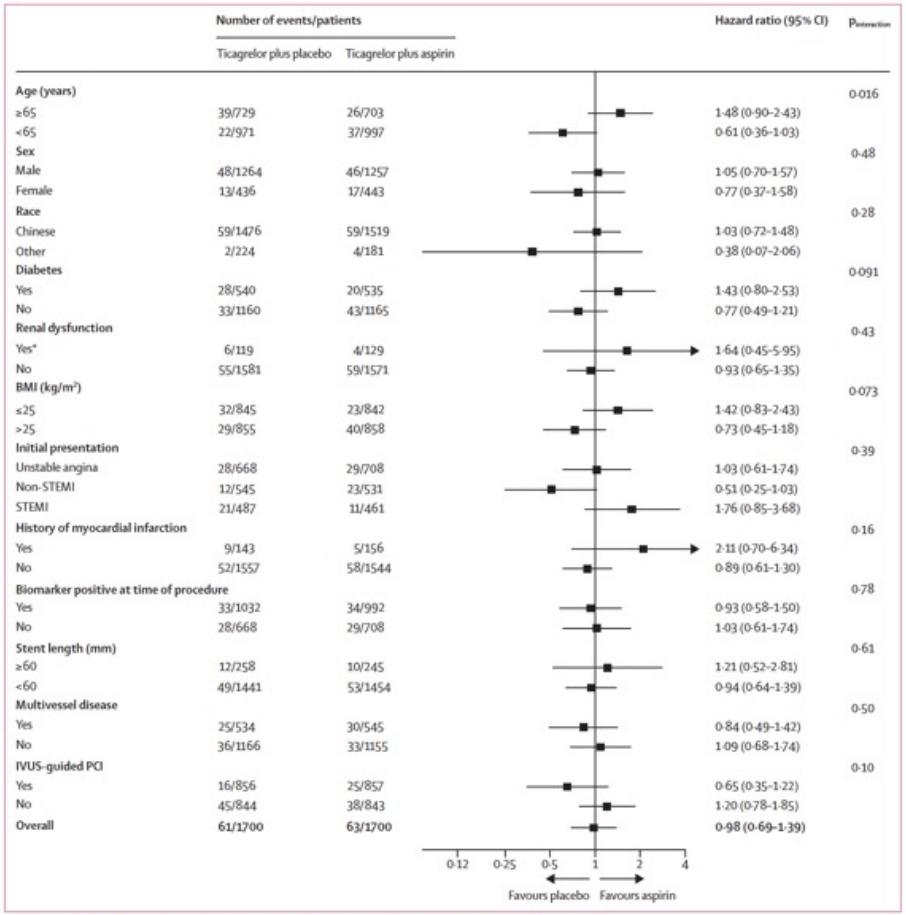

Figure 4: **Composite major adverse cardiovascular or cerebrovascular events in prespecified subgroups**
IVUS=intravascular ultrasound. PCI=percutaneous coronary intervention. STEMI=ST-segment elevation myocardial infarction. *Defined as an estimated glomerular filtration rate <60 mL/min per 1·73 m².

Research in context

Evidence before this study

We searched PubMed on March 11, 2019, using the search terms "intravascular ultrasound", "angiography", "percutaneous coronary intervention", "antiplatelet therapy", and "acute coronary syndrome (ACS)" using MeSH terms and appropriate variations, with no language or date restrictions, before designing our study. Subgroup analyses from several randomised trials suggested that a course of dual antiplatelet therapy lasting 1–3 months using different $P2Y_{12}$ inhibitors might safely reduce bleeding events in patients with an acute coronary syndrome after implantation of drug-eluting stents. We found no previous randomised, placebo-controlled trials in patients with an acute coronary syndrome who remained event-free after 1 month of dual antiplatelet therapy that compared ticagrelor alone with ticagrelor plus aspirin between month 1 and month 12 of follow-up.

Added value of this study

ULTIMATE-DAPT is the first randomised controlled trial to compare dual antiplatelet therapy with a potent platelet $P2Y_{12}$ inhibitor plus aspirin versus a potent $P2Y_{12}$ inhibitor plus placebo in patients with an acute coronary syndrome treated with percutaneous coronary intervention and who remained event-free after only 1 month of dual antiplatelet therapy. The results of this study show that patients with an acute coronary syndrome treated with contemporary drug-eluting stents and who are event-free after a 1-month course of dual antiplatelet therapy can be safely maintained on ticagrelor monotherapy from 1 month after to 12 months after percutaneous coronary intervention, and that this regimen will substantially reduce major and minor bleeding compared with standard ongoing treatment with ticagrelor plus aspirin. In addition, no increase in ischaemic events such as myocardial infarction, stent thrombosis, or cardiac death was observed with the ticagrelor monotherapy regimen in patients with a high-risk acute coronary syndrome, and net adverse clinical events occurred less frequently with ticagrelor monotherapy than with ticagrelor plus aspirin.

Implications of all the available evidence

The data from ULTIMATE-DAPT (along with that of previous studies) provide strong evidence that, in patients with an acute coronary syndrome treated with percutaneous coronary intervention with contemporary drug-eluting stents and who are event-free after 1 month of post-procedural dual antiplatelet therapy, ticagrelor monotherapy can safely reduce major and minor bleeding during follow-up.

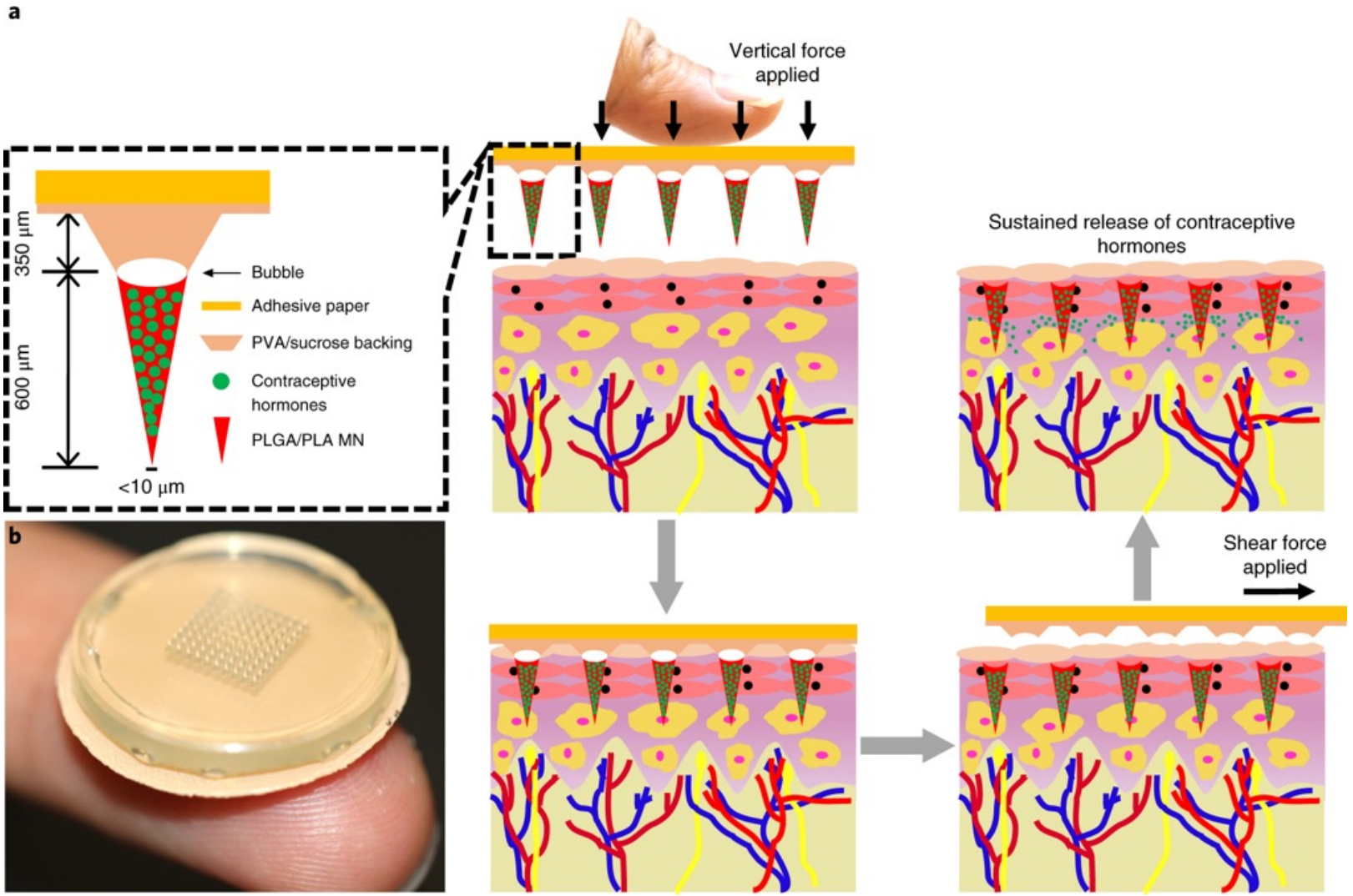
a
Vertical force applied
350 µm
600 µm
<10 µm
Bubble
Adhesive paper
PVA/sucrose backing
Contraceptive hormones
PLGA/PLA MN
Sustained release of contraceptive hormones
Shear force applied
b

A measles and rubella vaccine microneedle patch in The Gambia: a phase 1/2, double-blind, double-dummy, randomised, active-controlled, age de-escalation trial

Summary

Background Microneedle patches (MNPs) have been ranked as the highest global priority innovation for overcoming immunisation barriers in low-income and middle-income countries. This trial aimed to provide the first data on the tolerability, safety, and immunogenicity of a measles and rubella vaccine (MRV)-MNP in children.

Methods This single-centre, phase 1/2, double-blind, double-dummy, randomised, active-controlled, age de-escalation trial was conducted in The Gambia. To be eligible, all participants had to be healthy according to prespecified criteria, aged 18–40 years for the adult cohort, 15–18 months for toddlers, or 9–10 months for infants, and to be available for visits throughout the follow-up period. The three age cohorts were randomly assigned in a 2:1 ratio (adults) or 1:1 ratio (toddlers and infants) to receive either an MRV-MNP (Micron Biomedical, Atlanta, GA, USA) and a placebo (0·9% sodium chloride) subcutaneous injection, or a placebo-MNP and an MRV subcutaneous injection (MRV-SC; Serum Institute of India, Pune, India). Unmasked staff ransomly assigned the participants using an online application, and they prepared visually identical preparations of the MRV-MNP or placebo-MNP and MRV-SC or placebo-SC, but were not involved in collecting endpoint data. Staff administering the study interventions, participants, parents, and study staff assessing trial endpoints were masked to treatment allocation. The safety population consists of all vaccinated participants, and analysis was conducted according to route of MRV administration, irrespective of subsequent protocol deviations. The immunogenicity population consisted of all vaccinated participants who had a baseline and day 42 visit result available, and who had no protocol deviations considered to substantially affect the immunogenicity endpoints. Solicited local and systemic adverse events were collected for 14 days following vaccination. Unsolicited adverse events were collected to day 180. Age de-escalation between cohorts was based on the review of the safety data to day 14 by an independent data monitoring committee. Serum neutralising antibodies to measles and rubella were measured at baseline, day 42, and day 180. Analysis was descriptive and included safety events, seroprotection and seroconversion rates, and geometric mean antibody concentrations. The trial was registered with the Pan African Clinical Trials Registry PACTR202008836432905, and is complete.

Findings Recruitment took place between May 18, 2021, and May 27, 2022. 45 adults, 120 toddlers, and 120 infants were randomly allocated and vaccinated. There were no safety concerns in the first 14 days following vaccination in either adults or toddlers, and age de-escalation proceeded accordingly. In infants, 93% (52/56; 95% CI 83·0–97·2) seroconverted to measles and 100% (58/58; 93·8–100) seroconverted to rubella following MRV-MNP administration, while 90% (52/58; 79·2–95·2) and 100% (59/59; 93·9–100) seroconverted to measles and rubella respectively, following MRV-SC. Induration at the MRV-MNP application site was the most frequent local reaction occurring in 46 (77%) of 60 toddlers and 39 (65%) of 60 infants. Related unsolicited adverse events, most commonly discolouration at the application site, were reported in 35 (58%) of 60 toddlers and 57 (95%) of 60 infants that had received the MRV-MNP. All local reactions were mild. There were no related severe or serious adverse events.

Interpretation The safety and immunogenicity data support the accelerated development of the MRV-MNP.

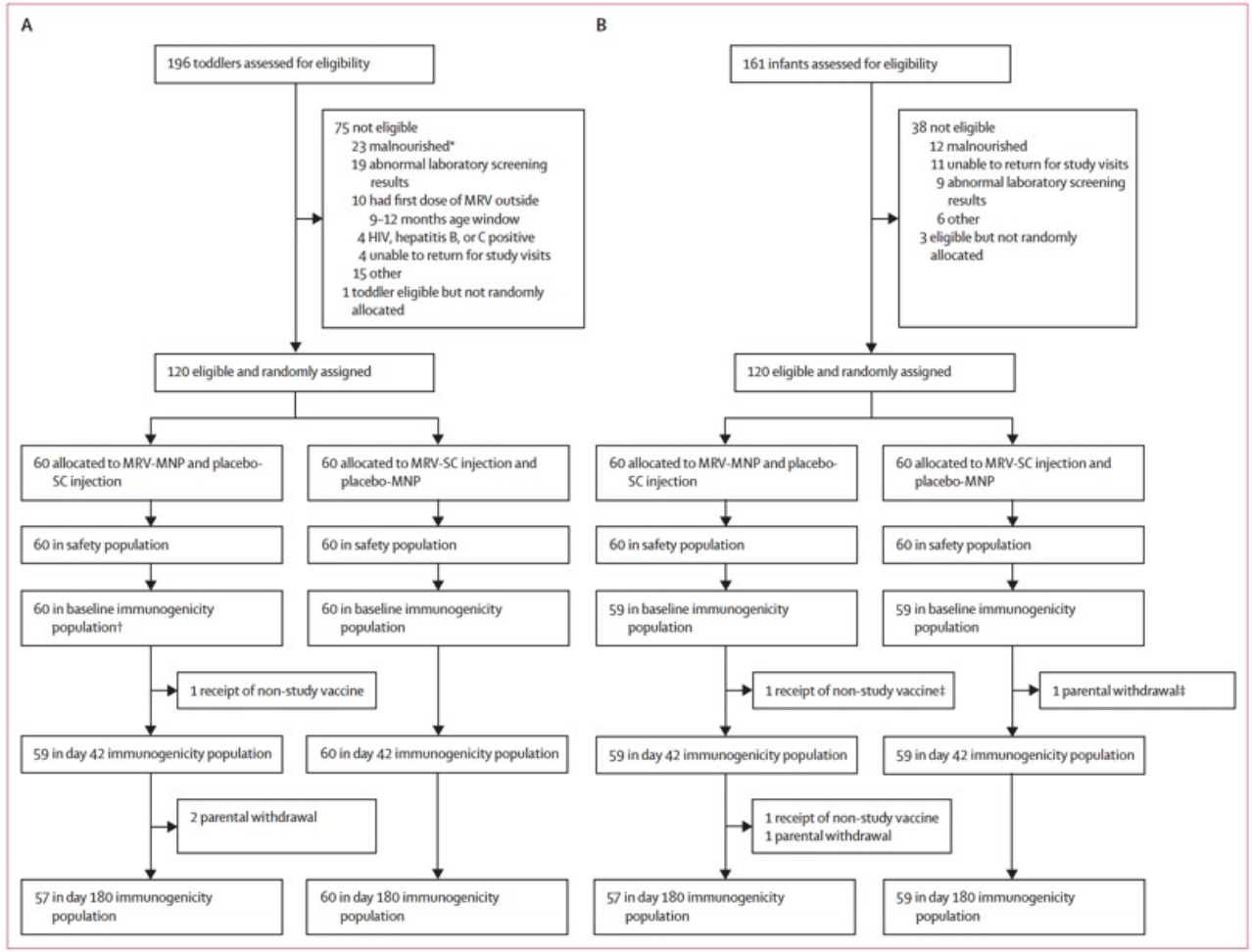

Figure 1: **Trial profile—toddler and infant cohorts**

(A) Toddler cohort (B) Infant cohort. MNP=microneedle patch. MRV=measles and rubella vaccine. SC=subcutaneous. *Defined as weight-for-length Z score of <2 SDs below the mean. †In the toddler MRV-MNP group the baseline immunogenicity sample was analysed for the toddler who received a non-study vaccine between baseline and day 42, thus 60 baseline sample results were available. ‡One infant in the MRV-MNP group and one infant in the MRV-SC group were withdrawn between baseline and day 42. The baseline samples for these two infants were not analysed, hence 59 infants were included in the immunogenicity population at baseline as well as day 42.

	Toddlers		Infants	
	MRV-MNP and placebo SC (n=60)	MRV-SC and placebo MNP (n=60)	MRV-MNP and placebo SC (n=60)	MRV-SC and placebo MNP (n=60)
Age, months*				
Median (IQR)	15 (15 to 16)	15 (15 to 16)	9 (9 to 9)	9 (9 to 9)
Sex				
Male	30 (50%)	30 (50%)	26 (43%)	25 (42%)
Female	30 (50%)	30 (50%)	34 (57%)	35 (58%)
Ethnicity				
African	60 (100%)	60 (100%)	60 (100%)	60 (100%)
Tribe†				
Mandinka	39 (65%)	27 (45%)	35 (58%)	28 (47%)
Wolof	6 (10%)	7 (12%)	4 (7%)	7 (12%)
Fula	4 (7%)	9 (15%)	6 (10%)	3 (5%)
Jola	4 (7%)	12 (20%)	10 (17%)	7 (12%)
Other	7 (12%)	5 (8%)	5 (8%)	15 (25%)
Weight, kg‡				
Median (IQR)	8·9 (8·4 to 9·7)	9·0 (8·7 to 9·8)	8·2 (7·5 to 9·1)	8·0 (7·3 to 8·8)
Length, cm‡				
Median (IQR)	77·4 (75·5 to 79·4)	77·0 (75·4 to 79·5)	70·5 (69·3 to 72·5)	70·0 (68·7 to 72·0)
Weight-for-length Z score‡				
Median (IQR)	−0·9 (−1·6 to −0·5)	−1·0 (−1·4 to −0·2)	−0·3 (−0·8 to 0·5)	0·0 (−1·0 to 0·1)

Data are n (%) unless otherwise stated. MNP=microneedle patch. MRV=measles and rubella combined vaccines. SC=subcutaneous. *On the day of consent. †Some percentages might not add up to 100% owing to rounding. ‡On the day of random allocation and vaccination.

Table 1: **Demographic and baseline data for the toddler and infant cohorts**

	Toddlers		Infants	
	MRV-MNP and placebo-SC, n=60	MRV-SC and placebo-MNP, n=60	MRV-MNP and placebo-SC, n=60	MRV-SC and placebo-MNP, n=60
Acute allergic reaction	0	0	0	0
Local solicited adverse events				
MNP application site				
Any local solicited event*				
Total	50 (83%)	18 (30%)	46 (77%)	18 (30%)
Mild (grade 1)	50 (83%)	18 (30%)	46 (77%)	18 (30%)
Tenderness				
Total	1 (2%)	1 (2%)	0	0
Mild (grade 1)	1 (2%)	1 (2%)	0	0
Erythema				
Total	10 (17%)	9 (15%)	18 (30%)	14 (23%)
Mild (grade 1)	10 (17%)	9 (15%)	18 (30%)	14 (23%)
Induration				
Total	46 (77%)	9 (15%)	39 (65%)	6 (10%)
Mild (grade 1)	46 (77%)	9 (15%)	39 (65%)	6 (10%)
SC injection site				
Any local solicited event*				
Any reaction	8 (13%)	5 (8%)	2 (3%)	4 (7%)
Mild (grade 1)	6 (10%)	5 (8%)	2 (3%)	4 (7%)
Moderate (grade 2)	2 (3%)	0	0	0
Systemic solicited adverse events				
Fever				
Total	5 (8%)	11 (18%)	8 (13%)	4 (7%)
Mild (grade 1)	1 (2%)	9 (15%)	5 (8%)	4 (7%)
Moderate (grade 2)	4 (7%)	1 (2%)	3 (5%)	0
Severe (grade 3)	0	1 (2%)	0	0
Any systemic solicited event†				
Total	27 (45%)	30 (50%)	31 (52%)	24 (40%)
Mild (grade 1)	24 (40%)	23 (38%)	28 (47%)	23 (38%)
Moderate (grade 2)	3 (5%)	7 (12%)	3 (5%)	1 (2%)

Data are n (%), where n=number of participants experiencing event by maximum severity grading. MRV=measles and rubella vaccine. MNP=microneedle patch. SC=subcutaneous. *Tenderness, erythema, and induration. †Vomiting, diarrhoea, irritability, drowsiness, reduced feeding, and rash.

Table 2: **Solicited safety events from days 0 to 13—toddler and infant cohorts**

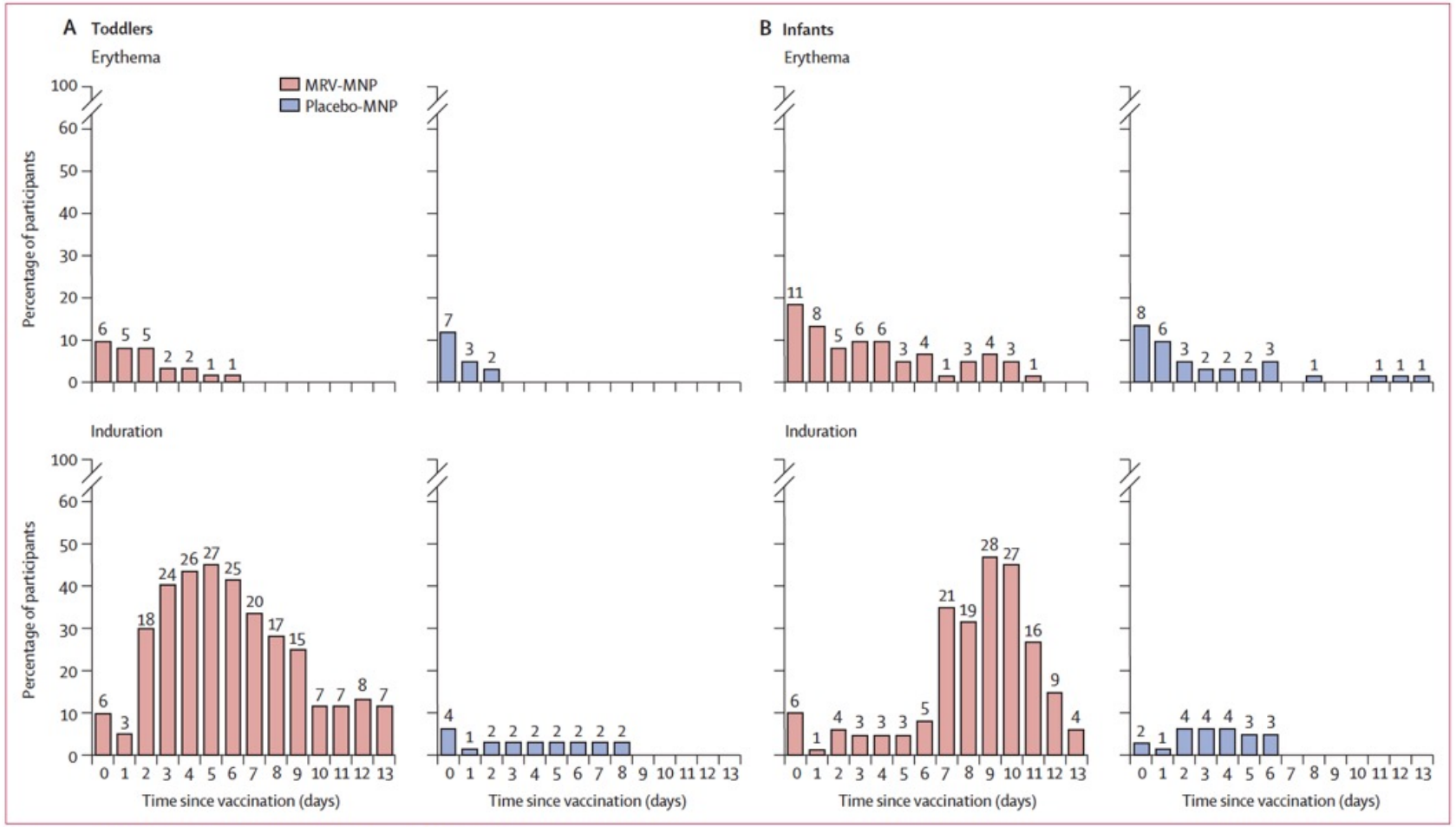

Figure 2: **Local solicited adverse events—toddler and infant cohorts**

(A) Toddler cohort (B) Infant cohort. Numbers represent the absolute number of participants, from among the 60 in each randomisation group and cohort, affected on each day. All local reactions were mild in severity. In addition, one toddler had mild tenderness on day 8 following MRV-MNP and one toddler had mild tenderness on day 1 following placebo-MNP (data not shown graphically). MNP=microneedle patch. MRV=measles and rubella vaccine. SC=subcutaneous.

	Toddlers				Infants			
	MRV-MNP and placebo-SC, n=60		MRV-SC and placebo-MNP, n=60		MRV-MNP and placebo-SC, n=60		MRV-SC and placebo-MNP, n=60	
	n (%)	E	n (%)	E	n (%)	E	n (%)	E
Adverse events								
Total	59 (98%)	203	56 (93%)	187	60 (100%)	347	59 (98%)	285
Mild (grade 1)	47 (78%)	190	38 (63%)	162	39 (65%)	315	44 (73%)	267
Moderate (grade 2)	11 (18%)	12	13 (22%)	20	21 (35%)	32	14 (23%)	17
Severe (grade 3)	1 (2%)	1	5 (8%)	5	0	0	1 (2%)	1
Serious adverse events	1 (2%)	1	7 (12%)	8	1 (2%)	1	1 (2%)	1
Adverse events resulting in discontinuation from the study	0	0	0	0	0	0	0	0
Related adverse events								
Total	35 (58%)	43	16 (27%)	16	57 (95%)	75	38 (63%)	41
Mild (grade 1)	35 (58%)	42	16 (27%)	16	57 (95%)	75	38 (63%)	41
MNP site discolouration	29 (48%)	29	12 (20%)	12	50 (83%)	50	32 (53%)	32
MNP site exfoliation	5 (8%)	5	1 (2%)	1	14 (23%)	14	6 (10%)	6
MNP site induration	3 (5%)	3	0	0	7 (12%)	7	1 (2%)	1
Other	5 (8%)	5*	3 (5%)	3†	4 (7%)	4‡	2 (3%)	2§
Moderate (grade 2)	1 (2%)	1¶	0	0	0	0	0	0
Related serious adverse events	0	0	0	0	0	0	0	0

Data are n (%), where n=number of participants experiencing event by maximum severity grading, unless otherwise stated. MRV=measles and rubella vaccine. MNP=microneedle patch. SC=subcutaneous. E=number of events by maximum severity grade. *Two MNP site papules, one MNP site pruritus, two SC injection site induration. †One MNP site papules, two generalised maculopapular rash. ‡One MNP site macule, one generalised rash, one generalised papular rash; one poor infant feeding. §One MNP site papules, one diarrhoea. ¶One generalised papular rash.

Table 3: **Unsolicited adverse events—toddler and infant cohorts**

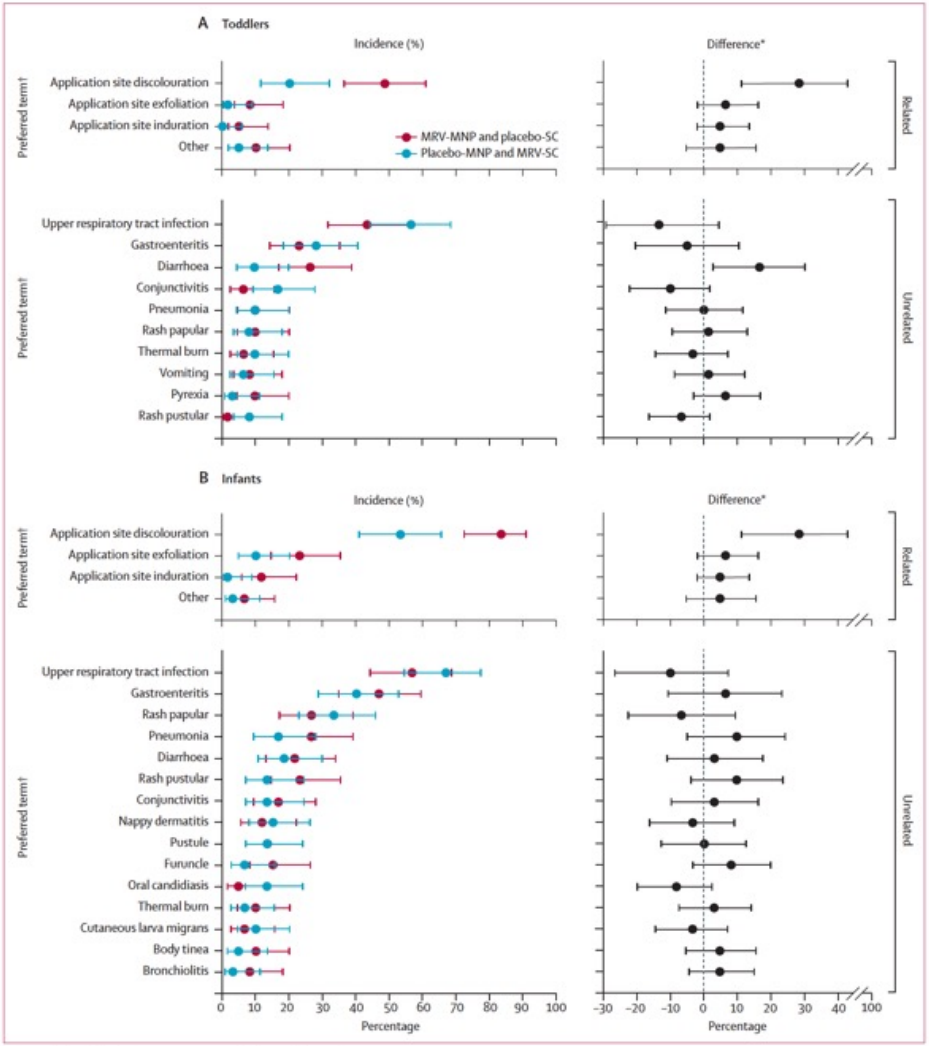

Figure 3: **Unsolicited adverse events—toddler and infant cohorts**

(A) Toddler cohort (B) Infant cohort. Incidence or incidence difference and 95% CIs are shown. Only events which occurred in at least three participants in a given age cohort are included in the figure. MNP=microneedle patch. MRV=measles and rubella vaccine. SC=subcutaneous. *Percentage prevalence in MRV-MNP group minus percentage prevalence in placebo-MNP group. †Preferred term based on the Medical Dictionary for Regulatory Affairs.

	Measles			Rubella		
	MRV-MNP and placebo-SC	MRV-SC and placebo-MNP	Ratio* or difference†	MRV-MNP and placebo-SC	MRV-SC and placebo-MNP	Ratio* or difference†
Toddlers						
Baseline						
Median (IQR)	489 (279 to 1159)	591 (319 to 961)	NA	152 (85 to 275)	151 (73 to 241)	NA
GMC (95% CI)	572·8 (450·1 to 729·1)	566·9 (448·8 to 716·1)	1·01* (0·73 to 1·41)	151·6 (126·2 to 182·2)	126·4 (101·2 to 157·9)	1·20* (0·90 to 1·59)
Seroprotection, n/N (%; 95% CI)	54/59 (92%; 81·7 to 96·3)	55/60 (92%; 81·9 to 96·4)	0·0† (−11·1 to 10·7)	59/59 (100%; 93·9 to 100·0)	60/60 (100%; 94·0 to 100·0)	0·0† (−6·1 to 6·0)
Visit 4 (day 42)						
Median (IQR)	2222 (1678 to 3447)	1791 (1284 to 2807)	NA	278 (182 to 406)	247 (174 to 338)	NA
GMC (95% CI)	2182·9 (1905·6 to 2500·5)	1811·5 (1480·6 to 2216·4)	1·21* (0·95 to 1·53)	268·2 (228·3 to 315·0)	234·3 (199·6 to 274·9)	1·14* (0·91 to 1·43)
GMFR (95% CI)	3·8 (3·0 to 4·9)	3·2 (2·5 to 4·1)	1·19* (0·85 to 1·68)	1·8 (1·4 to 2·2)	1·9 (1·5 to 2·9)	0·96* (0·71 to 1·28)
Seroprotection, n (%; 95% CI)	59/59 (100%; 94·0 to 100·0)	59/60 (98%; 91·1 to 99·7)	1·7† (−4·6 to 8·9)	59/59 (100%; 93·9 to 100)	60/60 (100%; 94·0 to 100)	0·0† (−6·1 to 6·0)
Baseline seronegative, n	5	5	NA	0	0	NA
Seroconversion, n/N (%; 95% CI)	5/5 (100%; 56·6 to 100·0)	4/5 (80%; 37·6 to 96·4)	20·0† (−26·4 to 62·5)	NA	NA	NA
Baseline seropositive, n	54	55	NA	59	60	NA
Four-fold rise, n/N (%; 95% CI)	23/54 (43%; 30·3 to 55·8)	21/55 (38%; 26·5 to 51·4)	4·4† (−13·6 to 22·1)	5/59 (8%; 3·7 to 18·4)	8/60 (13%; 6·9 to 24·2)	−4·9† (−16·7 to 6·9)
Immune response n/N (%; 95% CI)	28/59 (47%; 35·3 to 60·0)	25/60 (42%; 30·1 to 54·3)	5·8† (−11·8 to 22·9)	5/59 (8%; 3·7 to 18·4)	8/60 (13%; 6·9 to 24·2)	−4·9† (−16·7 to 6·9)
Visit 5 (day 180)						
Median (IQR)	1311 (654 to 2048)	1203 (844 to 1961)	NA	181 (110 to 261)	141 (98 to 224)	NA
GMC (95% CI)	1195·2 (958·7 to 1489·9)	1290·8 (1086·9 to 1532·8)	0·93* (0·70 to 1·22)	183·3 (154·9 to 216·9)	142·2 (121·8 to 166·1)	1·29* (1·03 to 1·62)
Seroprotection n/N (%; 95% CI)	56/57 (98%; 90·7 to 99·7)	60/60 (100%; 94·0 to 100·0)	−1·8† (−9·3 to 4·4)	57/57 (100%; 93·7 to 100·0)	60/60 (100%; 94·0 to 100·0)	0·0† (−6·3 to 6·0)

(Table 4 continues on next page)

(Continued from previous page)

	Measles			Rubella		
	MRV-MNP and placebo-SC	MRV-SC and placebo-MNP	Ratio* or difference†	MRV-MNP and placebo-SC	MRV-SC and placebo-MNP	Ratio* or difference†
Infants						
Baseline						
Median (IQR)	8 (7 to 12)	7 (6 to 9)	NA	6 (5 to 6)	5 (5 to 6)	NA
GMC (95% CI)	12·8 (9·5 to 17·2)	11·3 (8·5 to 15·1)	1·13* (0·75 to 1·70)	6·9 (6·4 to 7·4)	6·5 (6·2 to 6·9)	1·05* (0·96 to 1·15)
Seroprotection n (%; 95% CI)	3/59 (5%; 1·7 to 13·9)	1/59 (2%; 0·3 to 9·0)	3·4† (−4·6 to 12·3)	1/59 (2%; 0·3 to 9·0)	0/59 (0·0 to 6·1)	1·7† (−4·6 to 9·0)
Visit 4 (day 42)						
Median (IQR)	505 (309 to 716)	494 (311 to 671)	NA	123 (74 to 176)	156 (113 to 201)	NA
GMC (95% CI)	520·9 (420·8 to 644·9)	495·2 (402·5 to 609·3)	1·05* (0·78 to 1·41)	120·3 (99·9 to 144·9)	140·3 (120·9 to 162·7)	0·86* (0·68 to 1·09)
GMFR (95% CI)	40·8 (32·3 to 51·5)	43·7 (34·8 to 54·8)	0·93* (0·68 to 1·29)	17·5 (14·2 to 21·5)	21·4 (18·5 to 24·9)	0·82* (0·63 to 1·05)
Seroprotection n/N (%; 95% CI)	55/59 (93%; 83·8 to 97·3)	53/59 (90%; 79·5 to 95·3)	3·4† (−7·5 to 14·5)	59/59 (100%; 93·9 to 100·0)	59/59 (100%; 93·9 to 100·0)	0·0† (−6·1 to 6·1)
Baseline seronegative, n	56	58	NA	56	59	NA
Seroconversion n (%; 95% CI)	52/56 (93%; 83·0 to 97·2)	52/58 (90%; 79·2 to 95·2)	3·2† (−8·1 to 14·5)	58/58 (100%; 93·8 to 100·0)	59/59 (100%; 93·9 to 100·0)	0·0† (−6·2 to 6·1)
Baseline seropositive, n	3	1	NA	1	0	NA
Four-fold rise n/N (%; 95% CI)	1/3 (33%; 6·2 to 79·2)	0/1 (0·0 to 79·4)	33·3† (−50·5 to 79·2)	0/1 (0·0 to 79·4)	NA	NA
Immune response n/N (%; 95% CI)	53/59 (90%; 79·5 to 95·3)	52/59 (88%; 77·5 to 94·1)	1·7† (−10·2 to 13·7)	58/59 (98%; 91·0 to 99·7)	59/59 (100%; 93·9 to 100·0)	−1·7† (−9·0 to 4·6)
Visit 5 (day 180)						
Median (IQR)	654 (347 to 1100)	706 (329 to 985)	NA	125 (89 to 178)	139 (94 to 216)	NA
GMC (95% CI)	661·2 (501·5 to 871·9)	629·0 (498·7 to 793·5)	1·05* (0·74 to 1·50)	125·1 (109·0 to 143·6)	140·7 (122·1 to 161·9)	0·89* (0·73 to 1·08)
Seroprotection n/N (%; 95% CI)	52/57 (91%; 81·1 to 96·2)	55/59 (93%; 83·8 to 97·3)	−2·0† (−13·0 to 8·6)	57/57 (100%; 93·7 to 100·0)	59/59 (100%; 93·9 to 100·0)	0·0† (−6·3 to 6·1)

Baseline and visit 4 (day 42) analysis are in the primary immunogenicity population; visit 5 (day 180) analysis is in the day 180 secondary immunogenicity population; seroconversion is defined as a change from seronegative at baseline to seropositive at day 42; four-fold rise is defined as a four-fold rise in antibody concentrations between baseline and day 42 among individuals who were seropositive at baseline; immune response includes all those who were seronegative at baseline and seroconverted on day 42 or who were seropositive at baseline and had a four-fold rise in antibody concentrations; for measles, seronegative is defined as an antibody concentration of <200 mIU/mL, seropositive or seroprotection is defined as an antibody concentration of ≥200 mIU/mL; for rubella, seronegative is defined as an antibody concentration of <10 IU/mL and seropositive or seroprotection is defined as an antibody concentration of ≥10 IU/mL. MRV=measles and rubella vaccine. MNP=microneedle patch. SC=subcutaneous. NA=not applicable. IU=international unit. GMC=geometric mean antibody concentrations reported in mIU/mL for measles and IU/mL for rubella. GMFR=geometric mean fold rise. *Ratio [MNP]/[SC injection]. †Difference [MNP]−[SC injection]. Estimates are presented with 95% CIs. CIs for the log, transformed means assume a Student's t test. CIs for seroprotection and seroconversion were calculated using the Wilson score method without continuity correction. CIs for differences between proportions were calculated using the Newcombe method without continuity correction.

Table 4: **Measles and rubella serum neutralising antibodies—toddler and infant primary immunogenicity populations**

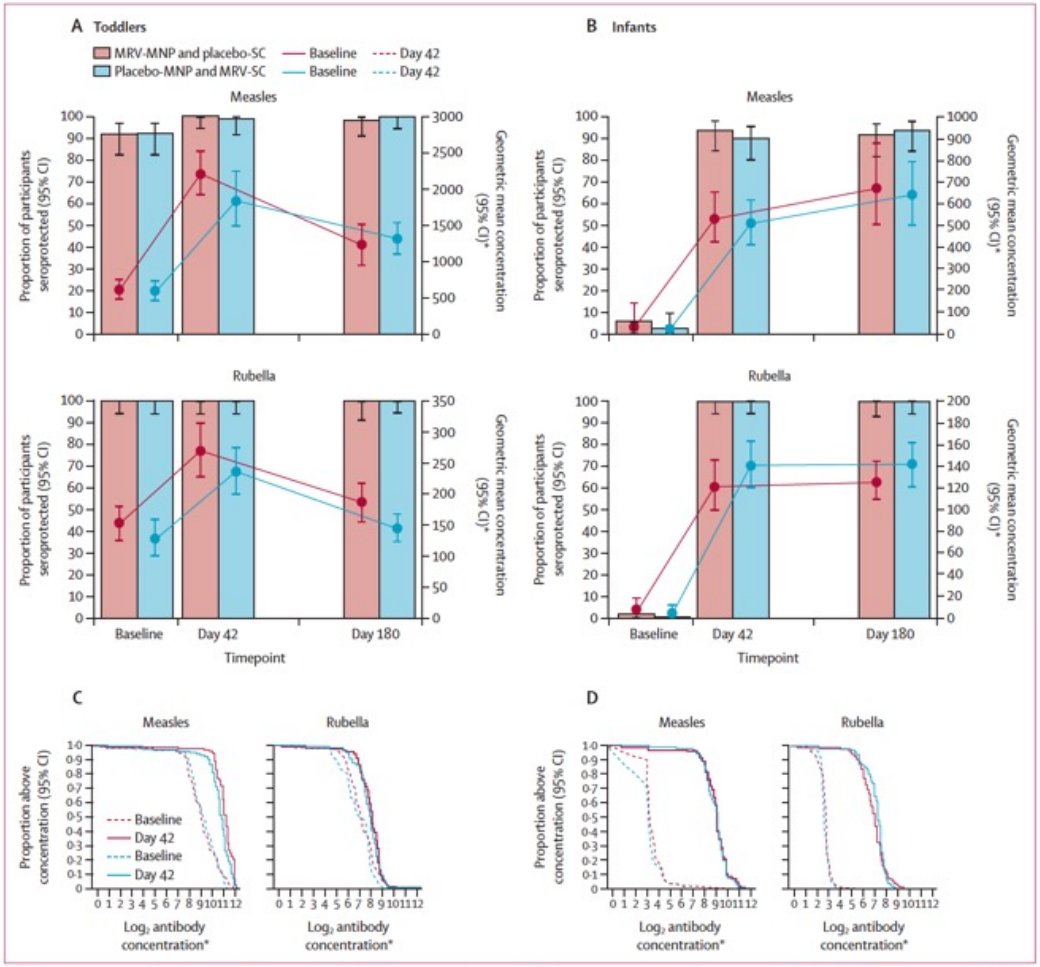

Figure 4: **Serum neutralising antibody seroprotection levels, geometric mean antibody concentrations, and reverse cumulative distribution curves—toddler and infant cohorts**

Toddler cohort (A) and infant cohort (B) measles and rubella serum neutralising antibody seroprotection rates (solid bars) and 95% CIs. Seroprotection rates are defined as the percentage of evaluable participants with an antibody concentration higher than 200 mIU/mL for measles and higher than 10 IU/mL for rubella. Toddler cohort (C) and infant cohort (D) measles and rubella serum neutralising antibody baseline and day 42 reverse cumulative distributions curves. MNP=microneedle patch. MRV=measles and rubella vaccine. SC=subcutaneous. IU=international unit. *Measles geometric mean concentrations are measured in mIU/mL. Rubella geometric mean concentrations are reported in IU/mL

Research in context

Evidence before this study

We searched PubMed to identify articles published from database inception to July 1, 2023, using the following search terms with appropriate Boolean operators: "microneedle patch", "microarray patch", "measles", "rubella", "vaccin*", "immun*", "safety", "clinical trial", and "systematic review". We additionally identified relevant publications in the grey literature through search engines and links with key organisations working in the field. The Vaccine Innovation Prioritization Strategy, developed through a partnership between WHO, UNICEF, Gavi, the Vaccine Alliance, PATH, and the Bill & Melinda Gates Foundation, has recently defined microneedle patch (MNP) development as the number one global priority for overcoming barriers to vaccination in low-income and middle-income countries (LMICs) and for attaining coverage targets and vaccine equity. The technology is considered to be key to achieving measles and rubella elimination, for which all WHO regions now have goals that have been consistently missed due to the exceptionally high coverage required to interrupt transmission. To this end, a Target Product Profile has been published by WHO and UNICEF that defines what are seen as the key attributes for measles and rubella MNPs if elimination goals are to be met. Five studies have been conducted in adults examining the administration of the inactivated influenza vaccine by dissolvable (n=2) or solid (n=3) microneedle patches. The studies confirmed the tolerability and safety of the patches and reported similar immunogenicity to vaccines delivered subcutaneously or intramuscularly, and in some cases included antigen dose sparing. One study has been conducted using dissolvable MNPs to administer a Japanese encephalitis vaccine. Tolerability, safety, and dose sparing was demonstrated. There are no published data on the use of MNPs to deliver vaccines to children or infants (the key target group) or on the use of the technology to administer the measles and rubella vaccine (MRV). Preclinical data on the measles and rubella MNP supported the initiation of this trial.

Added value of this study

This trial provides the first data on the use of MNPs to deliver vaccines to children and infants, and the first data on dissolving measles and rubella MNPs. In adults, MRV-primed toddlers aged 15–18 months, and MRV-naive infants aged 9–10 months, the MRV-MNPs were well tolerated and safe. Induration at the application site was common, occurring in nearly half of all toddlers and infants but was mild in all cases and resolved without treatment. None of the local reactions were of any safety concern. Discolouration at the application site, almost exclusively hyperpigmentation, was also common, occurring in nearly 50% of toddlers and over 80% of infants. Over half of these reactions resolved within 42 days, and almost all by day 180. There were no severe or serious adverse events considered to be related to the MNP. The immunogenicity of the MRV when administered by MNP was similar to its immunogenicity when administered subcutaneously by needle and syringe in all three age groups. Based on serum neutralising antibodies, the gold-standard correlates of protection for measles and rubella, 93% of infants who were measles seronegative at baseline seroconverted following the MRV-MNP, compared with 90% of infants who had the vaccine administered subcutaneously. All rubella seronegative infants in both groups seroconverted. Over 90% of infants remained seropositive for measles and 100% of infants remained seropositive for rubella at day 180. Despite high baseline antibody concentrations in the toddlers, reflecting their previous measles and rubella vaccination, increases in the antibody concentrations to both antigens occurred and were similar across the two methods of administration. These are the first data demonstrating directly that MNPs are viable for the delivery of vaccines to children and infants.

Implications of all the available evidence

MRV administration by MNP is well tolerated and safe in adults, toddlers, and infants. The immunogenicity of the vaccine delivered by MNP is similar to the immunogenicity of the vaccine when administered subcutaneously by needle and syringe. MNPs are considered to be of highest priority for overcoming barriers to immunisation in LMICs and to achieving measles and rubella elimination. This phase 1/2 trial data supports their accelerated development for this purpose as well as ongoing work to apply the technology for the delivery of other priority vaccines.

Progressive ankylosis protein homolog (ANK ilosis H omolog) is a protein that in humans is encoded by the ANKH gene. This gene encodes a multipass transmembrane protein that is expressed in joints and other tissues and controls pyrophosphate levels in cultured cells. Mutation at the mouse 'progressive ankylosis' (ank) locus causes a generalized, progressive form of arthritis accompanied by mineral deposition, formation of bony outgrowths, and joint destruction. The human homolog is virtually identical to the mouse protein and ANKH-mediated control of pyrophosphate levels has been suggested as a possible mechanism regulating tissue calcification and susceptibility to arthritis in higher animals.

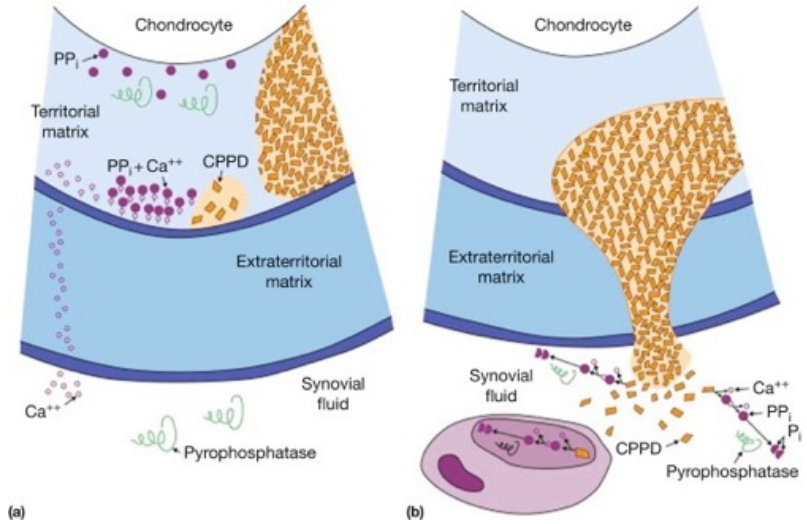

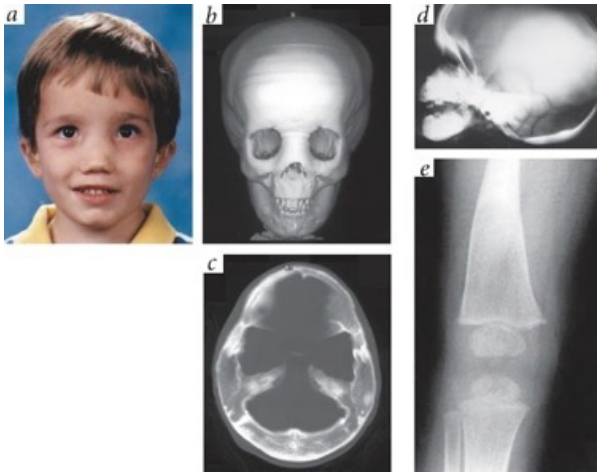

Heterozygous mutations in *ANKH*, the human ortholog of the mouse progressive ankylosis gene, result in craniometaphyseal dysplasia

Allogeneic bone marrow transplantation in craniometaphyseal dysplasia

A 30-month-old girl attended our clinic for exploration of optic nerve atrophy after she initially presented with respiratory difficulties at 20 months of age. The patient, who had been born at 39 weeks of gestation, also had feeding difficulties, nasal obstruction, and a reduced ability to open her mouth; she had developed progressive macrocephaly in the first few months of life (appendix).

On examination, she had dysmorphic facial features—a bulging forehead, a wide nasal bridge, and hypertelorism; she also had macroglossia, divergent strabismus, nasal obstruction, reduced mouth opening, and mastication and swallowing difficulties. Additionally, the patient had mixed hearing loss due to blockage of the ossicular chain with ossification of the petrous bone and cochlear nerve compression. She did not pronounce words and could only make hissing sounds.

A CT scan of the patient's head showed excessive condensation in facial and cranial bones and the progressive macrocephaly (figure 1).

A next-generation sequencing panel of bone density disorders identified a heterozygous *de novo* mutation in the human homolog (*ANKH*) of the mouse progressive ankylosis (*Ank*) gene establishing the diagnosis of autosomal dominant craniometaphyseal dysplasia (CMD).

At 38 months of age, after discussion with the patient's parents, we undertook haematopoietic stem-cell transplantation (HSCT) from her HLA 3/6-matched—haploidentical—father after conditioning with 375 mg/m² rituximab, 0·5 mg/kg alemtuzumab, busulfan (calculated total area under the curve of 85·9 mg*h/L), and 160 mg/m² fludarabine. Prophylaxis against graft-versus-host disease consisted of cyclophosphamide at a daily dose of 50 mg/kg on days 3 and 4 post HSCT; and cyclosporine and mycophenolate mofetil from day 5 post HSCT.

After HSCT, we observed a halt in disease progression and a significant improvement in the patient's condition; no additional procedures or surgical interventions were required.

Imaging showed a significant reduction in hyperostosis and no novel bone thickening (figure 2), and slowing down of macrocephaly progression (figure 3). Furthermore, the patient's neurosensory status remained stable; her respiration improved significantly, and nocturnal polysomnography was normal. No progression of the optic nerve atrophy or the facial nerve paralysis, as evidenced by normal electromyography, occurred.

At the last clinical assessment, 5 years and 6 months post HSCT, the patient aged 8 years and 8 months had neither abnormal fractures, arthropathies, bone pain, nor headaches—the common features of autosomal dominant CMD. She had acquired speech and was attending school; her parents described an overall significant improvement in her quality of life.

Autosomal dominant CMD is a rare skeletal disorder characterised by progressive thickening of craniofacial bones leading to dysmorphic features and severe visual and hearing impairment due to compression of cranial nerves.

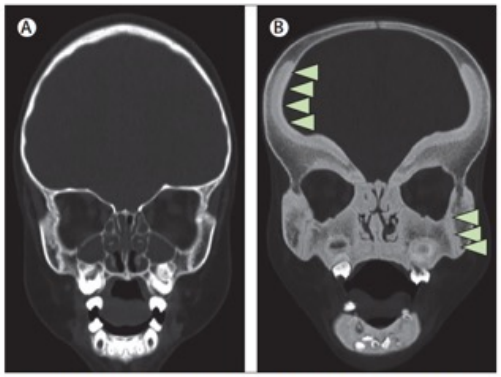

Figure 1: **Allogeneic bone marrow transplantation in craniometaphyseal dysplasia: CT scans**
Cranial CTs show an age-matched healthy girl (A), at age 30 months, compared with baseline evaluation of the patient's cranial bone density and morphology with bone thickening (arrows; B).

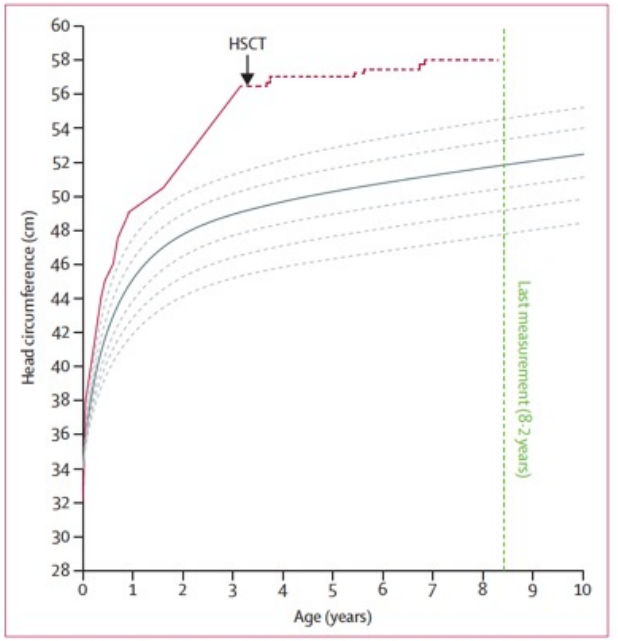

Figure 3: **Allogeneic bone marrow transplantation in craniometaphyseal dysplasia: graph**
Graph shows progressive macrocephaly with cessation of the abnormal increase in head circumference after haematopoietic stem-cell transplantation (HSCT).

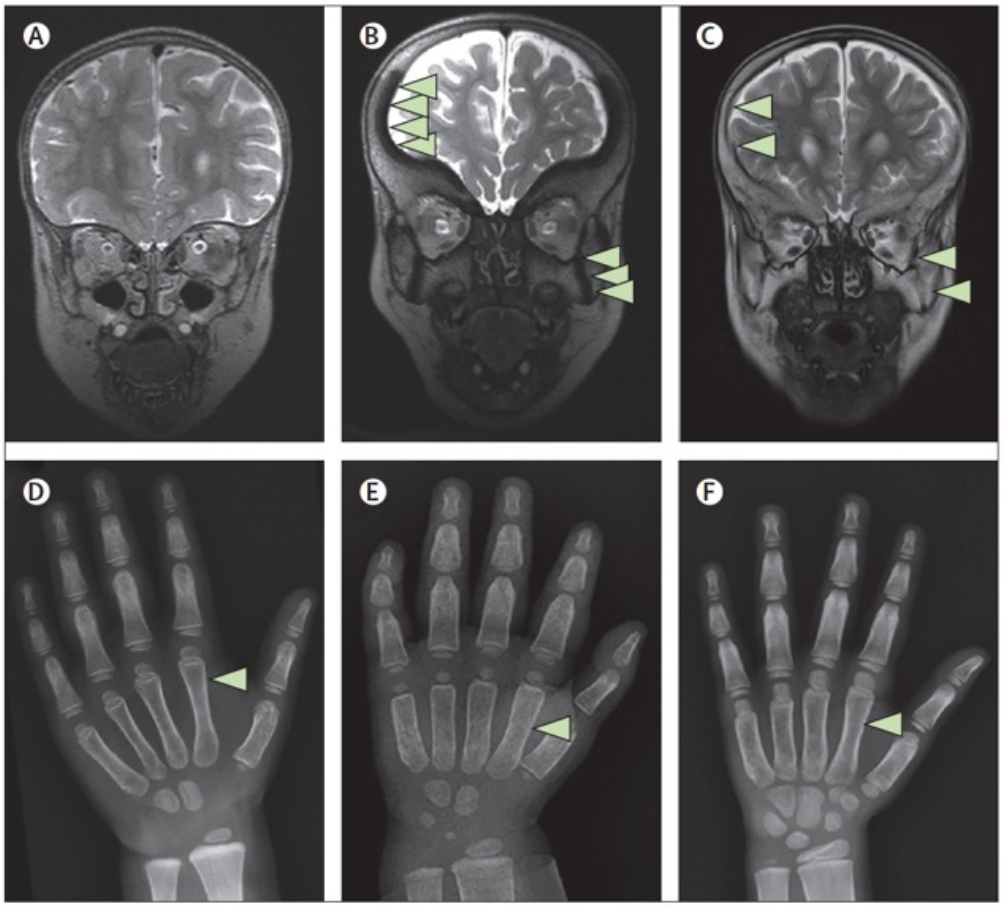

Figure 2: **Allogeneic bone marrow transplantation in craniometaphyseal dysplasia: MRIs**
T-2 weighted cranial MRIs show an age-matched healthy girl (A) at age 30 months, compared with patient (B) with hypointensity corresponding to hyperdensity areas on CT. (C) Cranial MRI at 42 months post haematopoietic stem-cell transplantation (HSCT) shows significant decrease of the pre-existing condensation in facial and cranial bones (arrows). Hand x-rays show an age-matched healthy girl (D) compared with the patient with diaphysis enlargement of the phalanges and metacarpals (E; arrows) prior to HSCT. (F) X-ray 45 months post HSCT shows bone remodelling with reduction of diaphyseal enlargement of the left hand.

To date, medical management had been limited to symptomatic measures—including invasive decompressive surgeries of obstructed cranial foramina to relieve symptoms. Additionally, as osteoblasts, unlike osteoclasts, are not derived from the haematopoietic stem cell, it was unclear whether allogeneic HSCT could restore the bone phenotype (appendix).

However, it has been suggested that as ANK protein plays a regulatory role in bone formation and resorption, it may directly affect osteoblast and osteoclast differentiation and function. Furthermore, experimental bone marrow transplantation has been shown to reduce hyperossification in homozygous *Ank* knockin mice with a CMD phenotype, implying that allogeneic HSCT may also be beneficial in human autosomal dominant CMD; our results are proof of concept that allogeneic HSCT may mitigate osteocondensation, thereby preserving neurosensory function and improving quality of life. Prompt diagnosis and management—before onset of skull hyperostosis and cranial nerve compression—may further improve outcomes.

The *Lancet* Breast Cancer Commission

Panel 1: Summary of the *Lancet* Breast Cancer Commission key messages

The *Lancet* Breast Cancer Commission report shows inequities in prevention, detection, treatment, and supportive care, with many groups of people with breast cancer being systematically left behind and forgotten. This is a global error as people with breast cancer are indispensable to our culture and socioeconomic system.

New findings

- The number of people living with metastatic breast cancer is unknown and many do not receive appropriate care. With adequate resources and a shift in attitudes, it might be possible to cure some people, treat most, alleviate the suffering of all, and abandon no one.
- Hidden breast cancer costs and suffering can be financial, physical, psychological, emotional, and social, affecting children, families, communities, and wider society. Exposing and reducing costs and suffering provides incentives for policy makers to invest in prevention, early detection, cost-effective therapies, and optimal management of breast cancer.
- Improving patient communication in breast cancer improves not only quality of life and body image, but also adherence to therapy, which can affect survival outcomes. Breast cancer can be seen as robbing many patients of power, but through good communication and facilitating patient autonomy, there could be an opportunity to regain power and exercise empowerment in other areas of their lives.

Roadmap for change

Our inclusive roadmap addresses urgent breast cancer challenges through six themes:

- Society should prevent as many as possible of the 3 million new diagnoses of breast cancers that are predicted to occur per year by 2040, through global national policy changes to minimise modifiable risk factors and coordinated, systematic personalised risk prevention programmes.
- Health-care systems and clinicians should personalise the right treatment at the right time for individuals while respecting their personal needs and preferences.
- We call for high-quality cancer registry data on cancer relapses to be collected worldwide and include not just those with metastatic breast cancer, but also with other metastatic cancers.
- Collaboration is key to close the equity gap through global early diagnosis, treatment frameworks, and innovative technologies.
- We should identify the value that society places on relief of the hidden costs and suffering related to breast cancer and measure the benefits of addressing these costs.
- Placing patients at the centre of clinical communication and empowering them to exercise their voices about their breast cancer care is an achievable and necessary global goal.

***Panel 28:* Summary of the *Lancet* Breast Cancer Commission suggested targets for change**

Breast cancer prevention

- 95% of countries should fully legislate the UNICEF Code for Advertising and Promotion of Commercial Milk Formula Products and adhere to WHO's Best Buys with respect to alcohol advertising
- Statutory access to at least 18 weeks, and preferably 26 weeks, of parental leave at 100% pay
- Mandatory provision of paid breaks and nursing expressing facilities on return to work
- Tax sugar-sweetened beverages to raise the retail price by at least 20%

Personalising breast cancer treatment

- More than 80% (aiming for 95%) of patients have access to accurate tumour subtyping
- More than 80% (aiming for 95%) of patients with a new diagnosis to be discussed at multidisciplinary meetings
- 100% of patients with breast cancer to have access to a full range of treatment modalities
- At least 10% (aiming for >25%) of participants of international breast cancer trials should be from low-income and middle-income countries (LMICs)
- At least 10% (aiming for >25%) of all breast cancer trials to be led or co-led by researchers from LMICs

Optimal inclusive management of metastatic breast cancer

- Minimum of 70% (aiming at 100%) of cancer registries to record cancer stage and relapses
- Minimum of 50%, aiming at 95%, of people with newly diagnosed metastatic breast cancer to be discussed at multidisciplinary meetings
- Record the number of people with metastatic breast cancer and aim to double the median overall survival in a decade
- Aiming for less than 5% of patients at the end of their life to not have access to morphine
- 100% of people with metastatic breast cancer to have access to life-saving cancer medicines

Tackling breast cancer gaps and inequities though global collaboration

- 60% of all invasive cancers to be diagnosed at stage I–II
- Evaluation, imaging, tissue sampling, and pathology within 60 days of presentation
- 80% of patients to undergo multimodal treatment without abandonment
- Time from drug approval to availability to the patient of less than 6 months for high-priority agents and less than 1 year for intermediate-priority agents

Identifying the hidden costs of breast cancer

- Upward trajectory year on year for universal health coverage of breast cancer across the continuum of care—aiming at 100%—to eliminate financial catastrophe and impoverishment for all families experiencing breast cancer
- Screening for serious health-related suffering at diagnosis and key milestones throughout the breast cancer pathway as a research tool with an aim for widespread implementation after validation
- Minimum of 20% (aiming at 100%) of the patients and families with the lowest incomes to receive public financing and provision of an essential package of supportive and palliative care across the breast cancer pathway

Communication and empowerment in breast cancer

- 100% of health-care professionals in every country should receive communication skills training
- 100% of breast cancer clinical research in every country should partner with patients from research concept to reporting and translation into practice

Conclusion

The *Lancet* Breast Cancer Commission has produced an evidence-based inclusive roadmap to address urgent global breast cancer challenges. However, we call society to action to scrutinise approaches to breast cancer, challenge the status quo, and expose practices that create inequity in every country of the world or waste scarce resources. We implore all stakeholders in breast cancer care to disseminate, implement, and adapt our roadmap to facilitate changes to practice and outcomes.

We have shown throughout this Commission report that data are powerful promoters for change. Therefore, it is imperative that our breast cancer targets (panel 28) are measured, used to hold policy makers and communities to account, and used to lobby for better, equitable approaches to breast cancer. We anticipate a united, collaborative, and evidence-based approach that empowers patients, families, communities, health-care providers, and policy makers to evolve and improve this roadmap. We believe that this approach will prevent the inevitability of the anticipated 3 million new diagnoses of breast cancer per year, that breast cancer will no longer be the leading cause of cancer death, and will provide better visibility and treatment for everyone affected by breast cancer, regardless of who they are or where they live.

Whole-body magnetic resonance imaging at 0.05 Tesla

Yujiao Zhao, Ye Ding, Vick Lau, Christopher Man, Shi Su, Linfang Xiao, Alex T. L. Leong, Ed X. Wu*

INTRODUCTION: Magnetic resonance imaging (MRI) has revolutionized healthcare with its nonionizing, noninvasive, multicontrast, and quantitative capabilities. It also presents a promising platformfor future artificial intelligence–driven medical diagnoses. However, after five decades of development, MRI accessibility—especially in low and middle-income countries—remains low and highly uneven due to high costs and specialized settings required for standard superconducting MRI scanners. These scanners are mostly found in specialized radiology departments and large imaging centers, restricting their availability in other medical settings. The need for radio frequency (RF)-shielded rooms and high power consumption further adds to hardware cost and compromises mobility and patient-friendliness.

RATIONALE: We developed a highly simplified whole-body ultra-low-field (ULF) MRI scanner that operates on a standard wall power outlet without RF or magnetic shielding cages. This scanner uses a compact 0.05 Tesla permanent magnet and incorporates active sensing and deep learning to address electromagnetic interference (EMI) signals. We deployed EMI sensing coils positioned around the scanner and implemented a deep learning method to directly predict EMI-free nuclear magnetic resonance signals from acquired data. To enhance image quality and reduce scan time, we also developed a data-driven deep learning image formation method, which integrates image reconstruction and three-dimensional (3D) multiscale super-resolution and leverages the homogeneous human anatomy and image contrasts available in large-scale, high-field, high-resolution MRI data.

RESULTS: We implemented commonly used clinical protocols at 0.05 Tesla, including T1-weighted, T2-weighted, and diffusion-weighted imaging, and optimized their contrasts for different anatomical structures. Each protocol was designed to have a scan time of 8minutes or less with an image resolution of approximately 2×2×8 mm^3. The scanner power consumption during scanning was under 1800W and around 300W when idle. We conducted imaging on healthy volunteers, capturing brain, spine, abdomen, lung, musculoskeletal, and cardiac images. Deep learning signal prediction effectively eliminated EMI signals, enabling clear imaging without shielding. The brain images showed various brain tissues whereas the spine images revealed intervertebral disks, spinal cord, and cerebrospinal fluid. Abdominal images displayed major structures like the liver, kidneys, and spleen. Lung images showed pulmonary vessels and parenchyma. Knee images identified knee structures such as cartilage and meniscus. Cardiac cine images depicted the left ventricle contraction and neck angiography revealed carotid arteries. Furthermore, deep learning image formation greatly improved the 0.05 Tesla image quality for various anatomical structures, including the brain, spine, abdomen, and knee; it also effectively suppressed noise and artifacts and increased image spatial resolution.

CONCLUSION: To address MRI accessibility challenges, we developed a low-power and simplified whole-body 0.05 Tesla MRI scanner that operates without the need for RF or magnetic shielding and that can be manufactured, maintained, and operated at a low cost. We experimentally demonstrated the general utility of this scanner for imaging various human anatomical structures at a whole-body level, even in the presence of strong EMI signals, with acceptable scan time. Moreover, we demonstrated the potential of deep learning image formation to substantially augment 0.05 Tesla image quality by exploiting computing and extensive high-field MRI data. These advances pave the way for affordable, patient-centric, and deep learning–powered ULF MRI scanners, addressing unmet clinical needs in diverse healthcare settings worldwide.

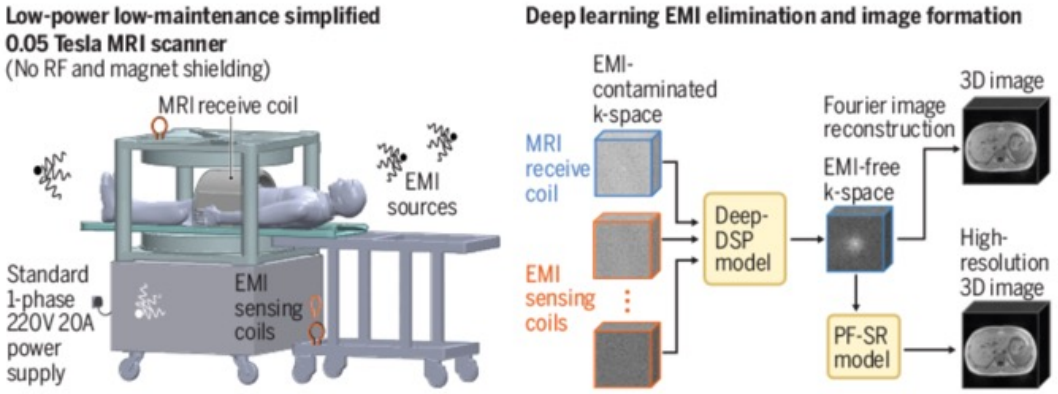

External electromagnetic interference (EMI)

Computing-powered whole-body MRI at 0.05 Tesla. (Top) Prototype of a low-cost, low-power, compact, and shielding-free imaging system using an open 0.05 Tesla permanent magnet. It incorporates active sensing and deep learning to address EMI signals. (Middle) Typical images of various anatomical structures using conventional image reconstruction. (Bottom) High-resolution images using deep learning image formation by harnessing large-scale high-field MRI data.

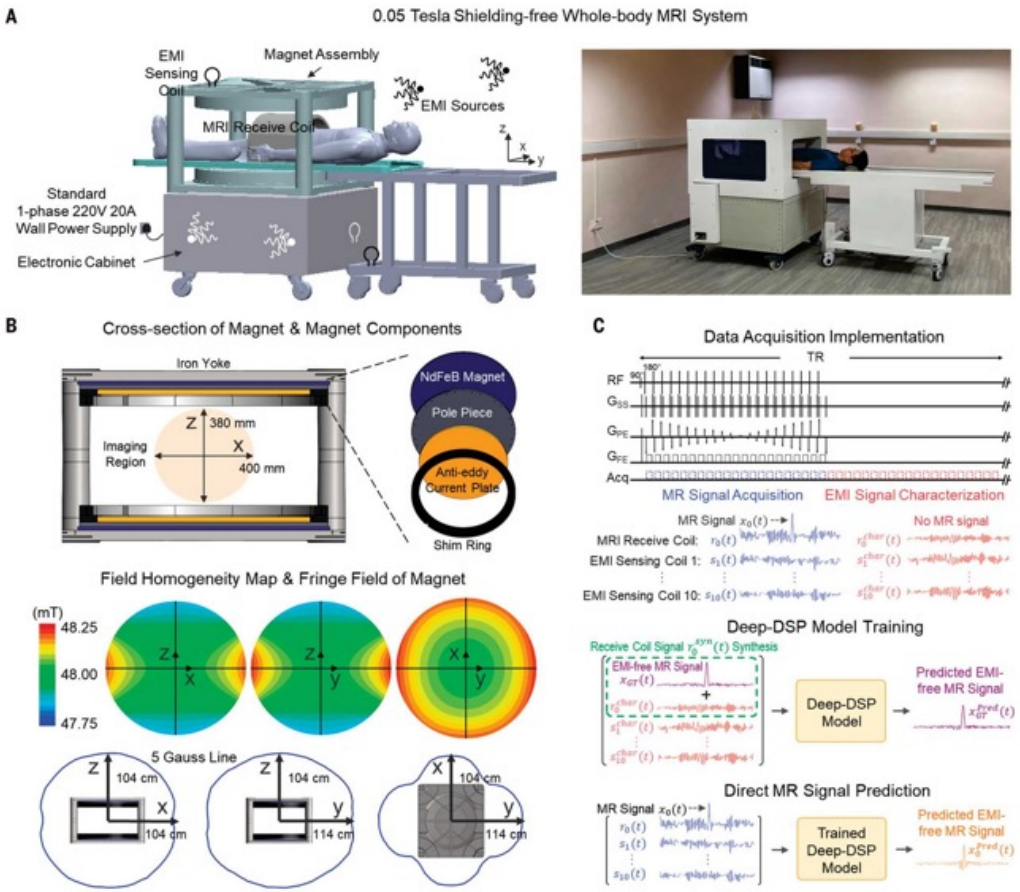

Fig. 1. Prototype of a low-cost, low-power, and shielding-free whole-body ULF MRI scanner with a homogeneous 0.05 Tesla NdFeB magnet and small 5 Gauss fringe field. (**A**) The scanner is designed to operate solely on a standard AC wall power outlet. It incorporates 10 small EMI sensing coils to actively detect EMI signal during scanning, has a compact footprint of ~1.3 m^2 (excluding the detachable patient bed), and requires neither magnetic nor RF shielding cages. (**B**) The magnet assembly includes iron yokes, pillars, NdFeB plates, poles, anti-eddy current plates, and shimming rings, with a vertical gap of 40 cm and a width of 92 cm. It has a homogeneity of <200 ppm peak-to-peak over a 40 cm diameter and 38 cm height oblate ellipsoid volume, and weighs ~1300 kg. (**C**) The scanner uses active EMI sensing and a deep learning Deep-DSP method to retrospectively eliminate EMI in MR k-space data by directly predicting EMI-free MR signals. A 3D FSE sequence is illustrated with MR signal collection and EMI signal characterization windows. Following each scan, data collected during the EMI characterization window, along with synthetic EMI-contaminated MR receive coil data, were used to train a Deep-DSP model. This model was subsequently applied to predict EMI-free MR data using data acquired during the MR signal acquisition window. Note that the EMI signal characterization window is not always necessary because the outer k-space data collected during MR signal acquisition window may be used for training.

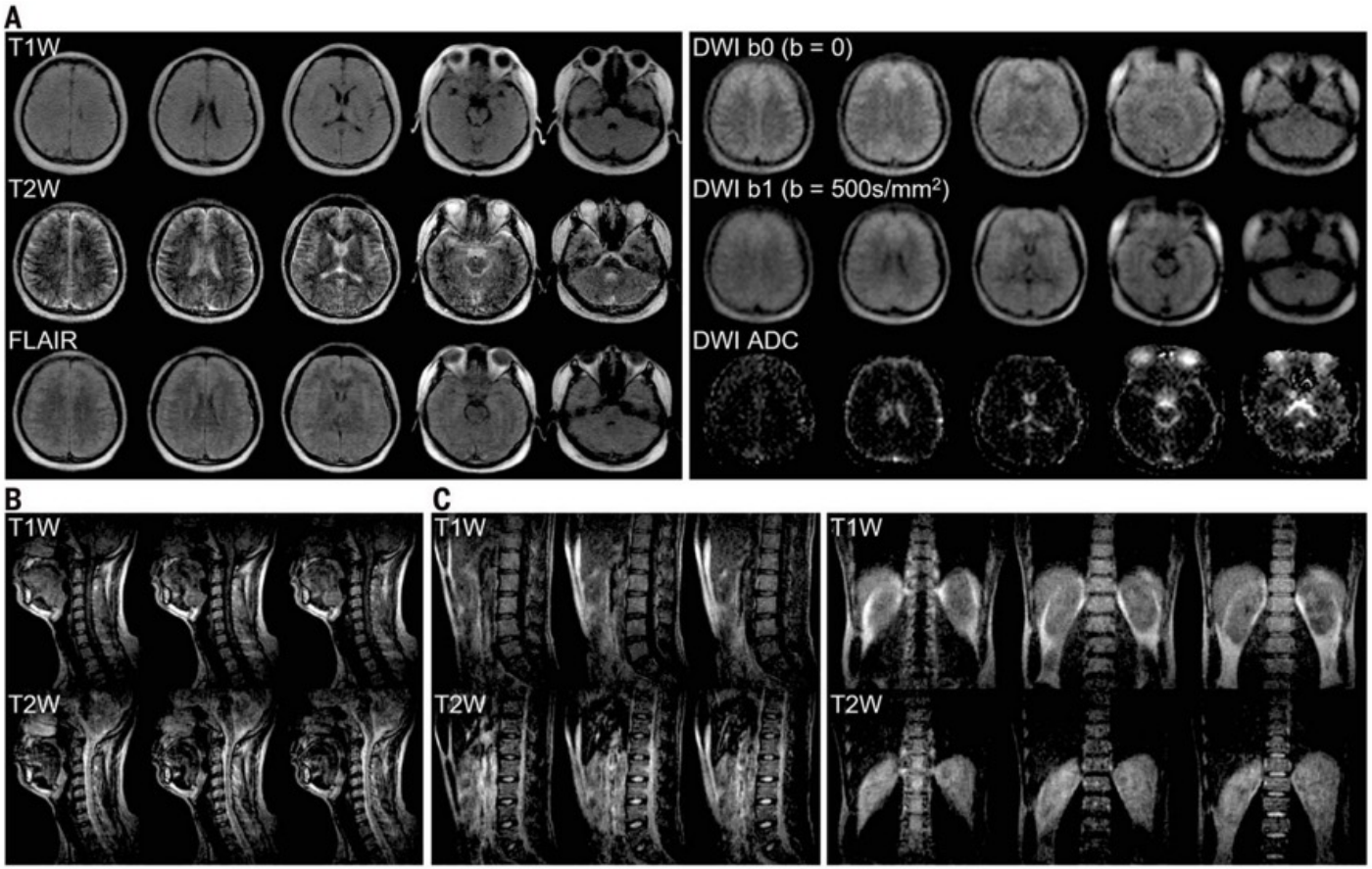

Fig. 2. Typical brain and spine images from healthy adults produced by the shielding-free whole-body 0.05 T MRI scanner. (**A**) Axial brain T1W, T2W, FLAIR, and DWI images from a healthy volunteer (23 years old; male) using 3D GRE (TR/TE/α° = 48 ms/6.6 ms/40°; resolution 2×2×8 mm^3), long-TR 3D FSE (TR/TE/ETL = 1500 ms/200 ms/21), short-TR 3D FSE (TR/TE/ETL = 500 ms/127 ms/13), and 2D EPI DWI (TR/TE = 1400 ms/104 ms), respectively. (**B**) Sagittal C-spine T1W and T2W images from a healthy volunteer (28 years old; male) using 3D FSE with TR/TE/ETL = 210 ms/76 ms/9 and 2300 ms/136 ms/25, respectively. (**C**) Coronal and sagittal L-spine images acquired using 3D FSE sequences (27 years old; male). Coronal T1W and T2W images were acquired with TR/TE/ETL = 190 ms/57 ms/7 and 1800 ms/170 ms/27, respectively. Sagittal T1W and T2W images were acquired with TR/TE/ETL = 190 ms/63 ms/7 and 1800 ms/172 ms/31, respectively. For each imaging protocol, scan time was 8 min or less. Image resolution was ~2×2×8 mm^3 by acquisition and 1×1×4 mm^3 by reconstruction for display. See table S2 for protocol details.

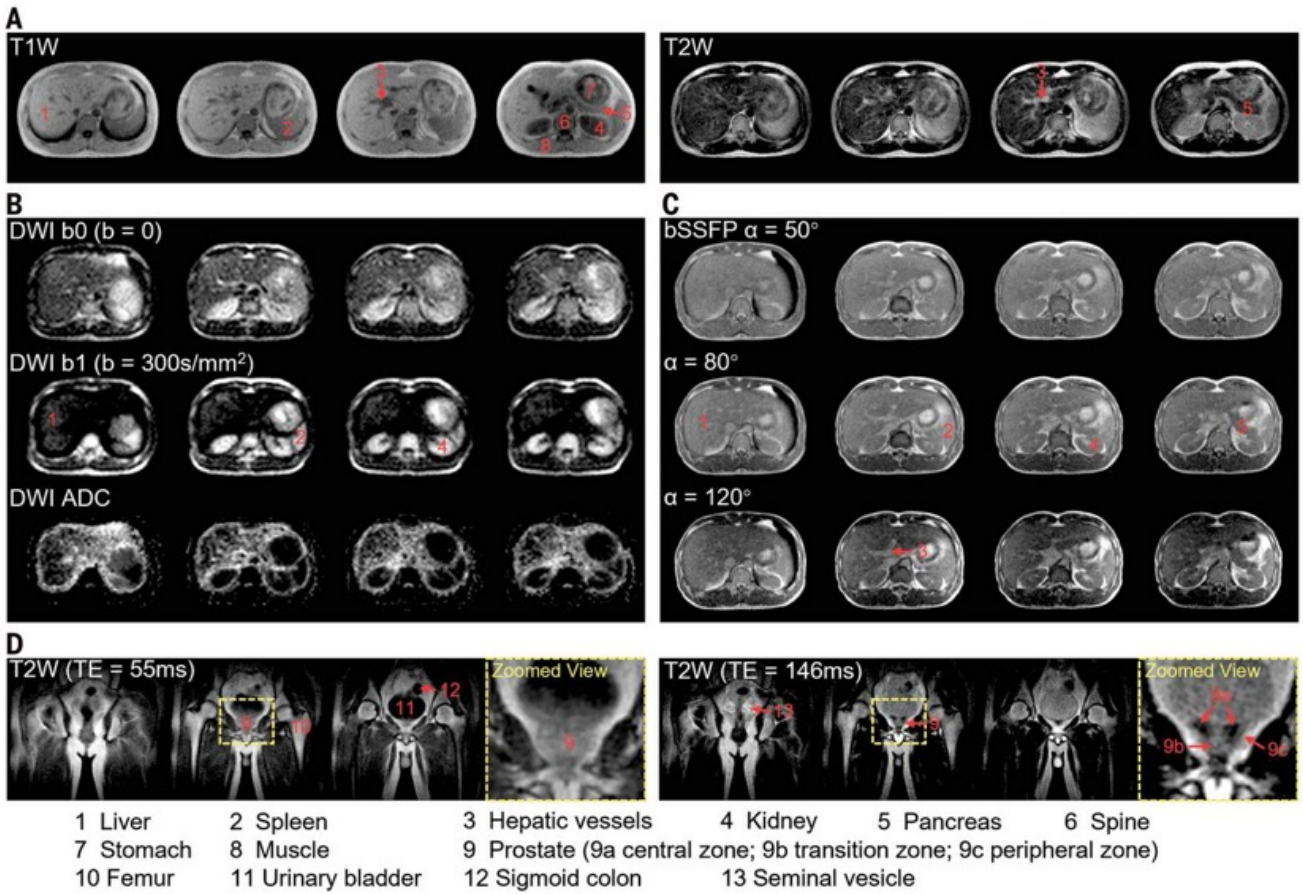

Fig. 3. Typical abdominal and pelvic images from healthy adults produced by the shielding-free whole-body 0.05 T MRI scanner. (**A**) Axial abdominal T1W and T2W images from a healthy volunteer (28 years old; male) using 3D SoS GRE (TR/TE/α° = 35 ms/5 ms/70°), and 3D SoS FSE (TR/TE/ETL = 700 ms/111 ms/18), respectively. (**B**) Axial abdominal DWI image set from a healthy volunteer (27 years old; male) using 2D EPI DWI (TR/TE = 1250 ms/84 ms). Images with b = 0 and 300 s/mm^2 are shown, together with computed apparent diffusivity coefficient (ADC) map. (**C**) Axial abdominal 3D bSSFP images with varying tissue contrasts from the same volunteer as (B) using different flip angles (α = 50°, 80°, and 120° with TR = 8 ms). (**D**) Coronal pelvis T1W and T2W images from a healthy volunteer (28 years old; male) acquired using 3D FSE with TR/TE/ETL = 450 ms/55 ms/7 and 1500 ms/146 ms/23, respectively. For each imaging protocol, scan time was 8 min or less. Image resolution was ~2.3×2.3×8.0 mm^3 (~2.3 mm in-plane resolution and 8.0 mm slice thickness) for T1W, T2W, and bSSFP images, ~5.0×5.0×8.0 mm^3 for DWI images by acquisition. All images are displayed at reconstruction resolution 1×1×4 mm^3.

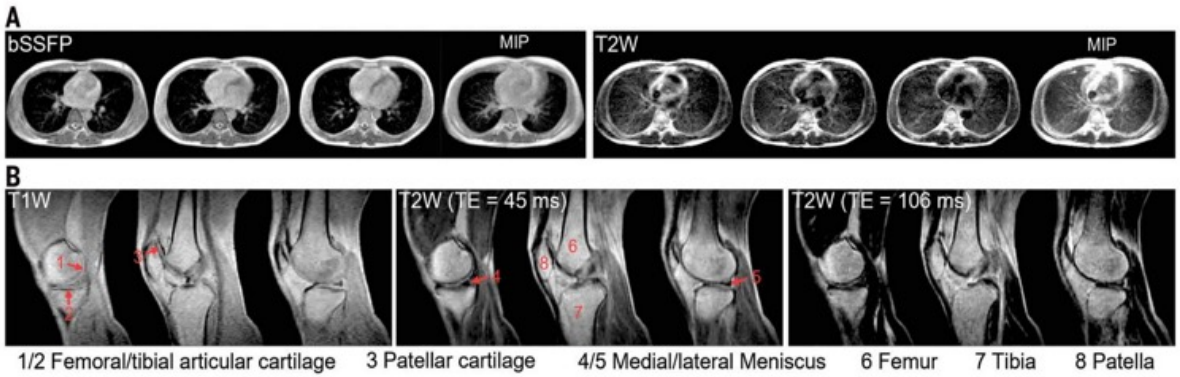

Fig. 4. Typical 0.05 T lung and knee images from healthy adults. (**A**) Axial lung bSSFP and T2W images from a healthy volunteer (25 years old; male) using 3D bSSFP (TR/α° = 8ms/50°; resolution 2.5×2.5×8.0 mm^3) and 3D SoS FSE (TR/TE/ETL = 1000ms/90ms/13; resolution 2.4×2.4×8.0 mm^3), respectively. The corresponding MIP images from 5 consecutive slices are also shown. (**B**) Sagittal knee T1W and T2W images from a healthy volunteer (34 years old; male) using 3D GRE (TR/TE = 60 ms/6 ms/70°; resolution 1.4×1.9×7.0 mm^3) and 3D FSE (TR/TE/ETL = 420 ms/45 ms/7 and 1500 ms/106 ms/17; resolution 1.9×2.0×7.0 mm^3). Scan time was 8 min or less for each protocol.

In conclusion, we addressed the challenge of limited MRI accessibility by developing an affordable, simple, and computing-powered whole-body 0.05 T MRI scanner. Our low-power, compact scanner was designed to operate from a standard AC wall power outlet, without the need for RF or magnetic shielding. We demonstrated the versatility of the ULF MRI for imaging various human anatomical structures. Moreover, we demonstrated the potential of 3D deep learning reconstruction to substantially augment ULF image quality by exploiting computing power and extensive high-field MRI data. These advancements will pave the way for affordable, patient-centric, and site-agnostic MRI scanners, addressing unmet clinical needs in various health care settings globally.

Why Highway 1 is the climate challenge that California can't fix

A fragile foundation for a highway

The most landslide prone stretch of Highway 1, from around Hearst Castle in San Simeon to Carmel-by-the-Sea and the Monterey Peninsula, has for decades epitomized California's reputation for scenic and rugged landscapes. It's where road trippers can get a view of dense redwoods out of one window and crashing waves out of the other, often at the edge of cliffs as much as 500 feet above the beach.